5-27-2016

Graphene Quantum Dots-Based Drug Delivery for Ovarian Cancer Therapy

Yiru Qin
University of South Florida, yiru@mail.usf.edu

Scholar Commons Citation
Qin, Yiru, "Graphene Quantum Dots-Based Drug Delivery for Ovarian Cancer Therapy" (2016). *Graduate Theses and Dissertations.*
http://scholarcommons.usf.edu/etd/6358

Graphene Quantum Dots-Based Drug Delivery for Ovarian Cancer Therapy

by

Yiru Qin

A dissertation submitted in fulfillment
of the requirement for the degree of
Doctor of Philosophy
Department of Molecular Medicine
Morsani College of Medicine
University of South Florida

Major Professor: Robert Deschenes, Ph.D., M.D.
Gloria C. Ferreira, Ph.D.
Eric Bennett, Ph.D.
Yu Chen, Ph.D.
Yashwant Pathak, Ph.D.

Date of Approval:
April 27, 2016

Keywords: graphene quantum dots, nanoparticles, theranostics, ovarian cancer, toxicity

DEDICATION

To my beloved parents and husband, who have been unconditionally supporting me and loving me.

ACKNOWLEDGMENTS

First, I would like to thank my major professor and co-major professor, Drs. Robert Deschenes and Gloria C. Ferreira, for their continual guidance and training throughout the process of my research, which have been instrumental in my overall achievement overmy graduate study period. Their mentorship, care and support were extremely valuable and critical to my graduate student life. To them I am truly grateful.

I gratefully and sincerely acknowledge my committee members: Drs. Eric Bennett, Yu Chen, and Matthias Batzill. Theirpatience, expertise, and efforts that they devoted throughout my study and my research are very much appreciated.

I would also like to acknowledge my previous and present lab members and collaborators: I could always count on the help of Drs. Shuting Pan, Chengbin Hu, Ruijuan Luo, Julie Yin, George Zhou, Guilong Li, Byeong Cha, Charles Szekeres, Amanda Garces and many others who have provided tremendous assistance.

Moreover, I would like to acknowledge University of South Florida College of Medicine and College of Pharmacy. They provided such a great environment that I enjoyed so much. The helped and supported me in many aspects including academically, financially, and mentally.

Finally, and most importantly, I would like to thank my family for their unconditional love and unwavering support, especially my father Xiaolin Qin, my mother Wanling Li, and my husband Wei Wei for always being there to support and encourage me. Thanks to all of my friends as well for what they have done for me.

TABLE OF CONTENTS

LIST OF TABLES

LIST OF FIGURES

LIST OF ABBREVIATIONS

AFM	Atomic force microscopy
ANOVA	Analysis of variance
APO	Apocynin
CAS	Cas 213546-53-3 (A NF-κB inhibitor)
CM-H2DCFDA	5-(and 6)-chloromethyl-2’,7’-dichlorodihy-drofluorescein diacetate
DCF	2',7'-dichlorofluorescein
DDS	Drug delivery systems
DIC	Differential interference contrast
DMSO	Dimethyl sulfoxide
DOX	Doxorubicin
DPI	Diphenyleneiodonium
EDC	1-(3-Dimethylaminopropyl)-3-ethylcarbodiimide hydrochloride
ELISA	Enzyme-linked immunosorbent assay
EPR	Enhanced permeation and retention
FA	Folic acid
FBS	Fetal bovine serum
FDA	Food and Drug Administration
FR	Folic receptor
FTIR	Fourier transform infrared Spectroscopy
GAPDH	Glyceraldehyde-3-phosphate dehydrogenase
GO	Graphene oxide
GQDs	Graphene quantum dots
HOMO	Highest occupied molecular orbital
HRTEM	High-resolution transmission electron microscopy
IL-1β	Interleukin-1β
L-Name	Nω-nitro-L-arginine methyl ester hydrochloride
LDH	Lactate dehydrogenase
LHRH	Luteinizing-hormone-releasing hormone
LPS	Lipopolysaccharide
LUMO	Lowest unoccupied molecular orbital

MAPK	Mitogen-activated protein kinase
MDR	Multidrug resistance
MTT	Methylthiazolyldiphenyl-tetrazolium bromide
NAC	N-acetyl-L-cysteine
NF-κB	Nuclear translocation of nuclear factor-κB
NHS	N-hydroxysuccinimide
NIR	Near-infrared
NO	Nitric oxide
PARP	poly(ADP-ribose) polymerase
PBS	Phosphate buffered saline
PI	Propidium iodide
PMA	Phorbol myristate acetate
PVDF	Polyvinylidene difluoride
QDs	Quantum dots
QY	Quantum yield
RAP	Rapamycin
RIPA	Radioimmunoprecipitation
ROS	Radical oxygen species
RT-PCR	Reverse transcription polymerase chain reaction
SAED	Selected area electron diffraction
SB	SB202190 [4-(4-fluorophenyl)-2-(4-hydroxyphenyl)-5-(4-pyridyl)1*H*-imidazole
SDS-PAGE	Sodium dodecyl sulfate polyacrylamide gel electrophoresis
TBST	Tris-buffered saline Tween-20
TEM	Transmission electron microscopy
TNF-α	Tumor necrosis factor-α
VEGF	Vascular endothelial growth factor

ABSTRACT

Ovarian cancer, one of the most dreadful malignancies of the female reproductive system, poses a lethal threat to women worldwide. In this dissertation, the objective was to introduce a novel type of graphene quantum dots (GQDs) based nano-sized drug delivery systems (DDS) for ovarian cancer treatment. As a starting point, the facile synthesis method of the GQDs was established. Subsequently, the targeting ligand,folic acid (FA), was conjugated to GQDs. Next, a FDA approved chemotherapeutic drug, Doxorubicin (DOX), was loaded to form the GQDs-FA-DOX nano-conjugation as the DDS. Moreover, the uptake profile and anti-cancer effect of the GQDs-FA-DOX were validated in ovarian cancer cells. Finally, the immunotoxicity of GQDs and its mechanism were investigated and elucidated. Taken together, the findings described in this dissertation provide a novel and powerful strategy of targeted treatment for ovarian cancer.

CHAPTER 1: INTRODUCTION

1.1 Ovarian Cancer

Ovaries are the main female reproductive glands, two oval-shaped organs located at the upper left and right of the uterus. They play a critical role in regulating female reproductive system, secreting the hormones estrogen and progesterone, and producing egg cells. Ovarian cancer begins in the ovaries and ranks fifth in cancer death among women according to the latest statistics from the American Cancer Society[1, 2]. In 2015, approximately 21,290 women in the United States were diagnosed with ovarian cancer and approximately 14,180 would die from it[3-5]. Although ovarian cancer only accounts for 3% of cancers in female, it actually causes in more deaths than any other cancer. Ovarian cancer is also known as a silent killer since it is often unable to be detected until it metastasizes within the pelvis and abdomen. Staging refers to the process of finding out how widespread a cancer is. It is of great significance because ovarian cancers have different prognoses and treatment strategies at different stages (Table 1. 1).

Stage I: Cancer is only found in one or both ovaries.

Stage II: Cancer is present in one or both ovaries and has developed to other parts within the pelvis.

Stage III: The cancer is discovered in one or both ovaries, and has developed outside the pelvis to other parts of the abdomen and/or to nearby lymph nodes.

Stage IV: This is the most advanced stage. Cancer has spread to other organs or tissues beyond the abdomen.

Table 1. 1 A description of the International Federation of Gynecology and Obstetrics staging system for the diagnosis of ovarian cancer.

	Stage	Description
Early stages	I	Cancer growth is confined to the ovaries.
	II	Cancer growth is confined to the pelvic region.
Late stages	III	Metastasis to the organs and the peritoneal cavity and/or regional lymph nodes.
	IV	Distant metastasis beyond the peritoneal cavity

Early-stage ovarian cancer rarely causes signs or symptoms. Patients are more likely to have symptoms if the disease has metastasis to organs beyond the ovaries. The most common signs or symptoms may include: abdominal bloating or swelling, trouble eating or feeling full fast, discomfort in the pelvis area, urinary symptoms such as urgency or frequency, and weight loss[6]. Once diagnosed, it is more difficult to treat and is frequently fatal in its advanced stage. When it is found at its early stage, it is more likely to be treated successfully. Near 80% of ovarian cancer patients were diagnosed with stage III-IV diseases[7, 8]. The mainstay of treating ovarian cancer is surgery followed by chemotherapy, which works for early stage ovarian cancer patients. However, for 70% of advanced stages patients, relapse will occur within 18

months [8, 9].

1.2 Current Therapies for Ovarian Cancer

Different treatment options are available for patients who are diagnosed with ovarian cancer. At present, the most common treatment strategies for ovarian cancer include radiation therapy[10, 11],chemotherapy[10, 12-14],surgery[15, 16],and targeted therapy[17-19]. Other treatment options available or being tested in clinical trials may include hormone therapy[20, 21]and biologic therapy[22, 23]. As a matter of fact, treatment of ovarian cancer usually involves a combination of two or more options mentioned above.

1.2.1 Surgery

Generally, doctors will give most patients an operation to remove the tumor as much as possible. The types of surgery depend on how far the tumor has spread. They may involve the removal of one or both ovaries, fallopian tubes, the uterus, the lymph nodes, and fatty tissue in abdomen where tumors often develop[24].

1.2.2 Chemotherapy

After surgery, patients are usually required to be treated with chemotherapy, using drugs to kill remaining tumor cells or to keep them from dividing[25]. The drugs can be either given orally or injected into muscle or a vein, most of the time determined by the type and stage of cancer being treated. Chemotherapy is a systemic treatment in most cases, so the drugs will enter the bloodstream and are likely to be distributed among the entire body. The following is a list of common anticancer drugs approved for ovarian cancer by the Food and Drug Administration

(FDA): Cisplatin, Carboplatin, Altretamine, Paclitaxel, Topotecan, Liposomal doxorubicin, and Combination gemcitabine–carboplatin[26].

However, chemotherapy drugs simultaneously can cause a number of unwanted side effects. They are also deleterious to normal cells while killing cancer cells[27]. Some common temporary side effects of chemotherapy drugs may include: loss of hair, loss of appetite, nausea and vomiting, mouth sores, and rashes on skins [28-30].

Most of the above symptoms are able to gradually fade away when stop taking chemotherapy drugs. But some of the drugs are likely to cause long-term or even permanent damages to bone marrow[31]or kidney[32].

1.2.3 Radiation Therapy

Radiation therapy is a type of treatment employing radiations, such as high-energy x-rays, to kill tumor cells. There are several means of radiation therapy, such as internal radiation therapy[33],external radiation therapy[34], and radioactive phosphorus[35]. Basically, the radiation therapy adopted depends on the stages of the cancer.

External radiation therapy utilizes an instrument outside the body to generate radiation to kill cancer cells. This is the most commonly used radiation therapy for ovarian cancer. The radiation beam, like X-ray, passes through patients' skin and tissue and then is focused on the cancer. Patients are actually exposed to the radiation for a short time, and the radiation can be precisely positioned and accurately aimed at the tumor cells. Internal radiation therapy uses a radioactive substance in needles, catheters, seeds, or wires which are directly sent into or near the tumor[36]. It is relatively less adopted for ovarian cancer treatment. It should be noted that there are some side effects associated with radiation therapy, including fatigue, diarrhea, skin changes, nausea, and vomiting.

Radioactive phosphorus is a treatment that instills the solution of radioactive phosphorus into the abdomen[37]. The radioactive phosphorus solution flows into the cells lining the surface of the abdomen and kills them. It was once used in the past, but it is not considered as a standard treatment for ovarian cancer anymore. Although it incurs few instant side effects, it leads to intestine injury and digestive problems, including bowel obstruction[38, 39].

1.2.4 Targeted Therapy

A comparatively new and promising type of treatment called targeted therapy has been paid more and more attention lately. In this procedure, drugs or substances have the ability to identify and kill specific cancer cells, e.g. ovarian cancer cells, without or with extremely little damage to normal cells.

Monoclonal antibody therapy[40]is a well-known targeted therapy by means of the antibodies developed from immune system cell in the laboratory. Such antibodies direct attach to certain receptors on cancer cells, and mark cancer cells to be recognized by immune system. Monoclonal antibodies can work alone or in combination with the toxins, drugs, or radioactive substances to attack tumor cells[41].

Bevacizumab[42] is a monoclonal antibody, also known as an angiogenesis inhibitor, that has been demonstrated to shrink and decelerate the growth of advanced epithelial ovarian cancers. This drug binds to vascular endothelial growth factor (VEGF) that signals new blood vessels to form[43]. This can minimize the growth of cancer cells. Bevacizumab also leads to side effects including high blood pressure, low white blood cell counts, mouth sores or even serious problems as, for example, blood clots [42].

Olaparib[44]is an orally active poly(ADP-ribose) polymerase (PARP) inhibitors. PARP enzymes usually take part in DNA repair pathways. Olaparib can effectively thwart the repair of DNA and lead cancer cells to death[45]. It is normally given by mouth, and its side effects are relatively mild, which may include nausea, fatigue and diarrhea.

1.2.5 Hormone Therapy

The utilization of hormones or hormone-blocking drug to treat cancer is called hormone therapy. Tamoxifen[46], luteinizing-hormone-releasing hormone (LHRH) agonists[47], and aromatase inhibitors[48] are some examples of anticancer drugs associated with hormone therapy.

1.2.6 Biologic Therapy

New types of treatments are still being developed to fight and conquer ovarian cancer, and some of them are being evaluated in clinical trials. Biologic therapy, also known as biotherapy or immunotherapy, is a treatment that makes use of the patients' immune system to attack cancer[49]. Substances, such as growth factors, cytokines, and, cellular adhesion molecules, produced by the human body or designed and synthesized in the laboratory are employed to improve, guide, and/or restore the body’s immune system and natural defenses against diseases[50].

1.3 Drug Delivery Strategies of Ovarian Cancer Treatment

Drug delivery systems (DDS) for ovarian cancer treatment are being developed in an attempt to attain higher drug concentrations at the location of cancer cells. In contrast to current standard treatment, i.e. surgery and systemic chemotherapy, DDS present a couple of new merits which may overcome the limitations facing current standard treatment. For instance, DDS have exhibited promise in avoiding the emergence of multidrug resistance, improving drug solubility, increasing drug concentrations in targeted tumor sites, minimizing toxicities and eventual disease relapse associated with conventional systemic chemotherapy drugs[51]. Fortunately, more and more drugs based on DDS are being tested in clinical trials for the treatment of ovarian cancer, and some of them even are available as a second-line therapy (Table **1.2**).

A summary of recent advances in DDS strategies for the treatment of ovarian cancer is given below. The DDS can be categorized into nano-sized systems, including nanoparticles, micelles, liposomes, and drug conjugates; microspheres; implants and injectable depots. The advantages, disadvantages, as well as clinical potential of the above strategies are also briefly introduced in Table 1.3.

Table 1.2 DDS that have entered clinical trials for ovarian cancer treatment. Reprinted with permission [51].

Name	Delivery System	Compound	Clinical Stage
DOXIL	Liposome	Doxorubicin	Approved
OPAXIO	Drug conjugate	Paclitaxel	Phase III
CT-2106	Drug conjugate	Camptothecin	Phase II
Genexol-PM	Block polymer micelle	Paclitaxel	Phase II (recruiting)
Paclimer	Microsphere	Paclitaxel	Failed in Phase I

Table 1.3 Advantages and limitations of DDS investigated for ovarian cancer therapy. Reprinted with permission [51].

System	Advantages	Limitations
Nano-sized systems	Passive targeting due to size, Active targeting, Ease of administration.	Small size may lead to rapid clearance and limited half-life, Frequent dosing required, May not be applicable for residual disease following cytoreductive surgery
Microspheres	Prolonged release profile, Several formulations have reached the market for other cancers	Peritoneal adhesions, Limited tumor penetration
Implants and injectable depots	Localized delivery, Sustained drug release, Lower systemic toxicity, Facilitates delivery of drugs with short half-life, Increased bioavailability by decreasing first-pass hepatic metabolism, Enhanced effect for cell cycle-specific drugs, Reduced dose dumping	Invasive, Surgical expertise needed for implantation and removal, Limited tumor penetration, Viscosity issues if injectable

1.3.1 Multidrug Resistance (MDR)

MDR refers to a phenomenon by which the cancer cells achieve the survival ability even if structurally and functionally different anticancer drugs are given[52]. The development of MDR can result in the chemotherapy failure in ovarian cancer. The appearance of MDR may relate to the following reasons: i) cancer cell genetics and phenotype; ii) tumor microenvironment and iii) inadequate drug exposure[51]. As mentioned above, The MDR issue may be circumvented by means of DDS strategy.

1.3.2 Nano-sized DDS: Nanoparticles, Block Copolymer Micelles, Liposomes and Drug Conjugates

Considerable nano-sized DDS such as nanoparticles[53-61], block copolymer micelles[62-69], liposomes[70-73] and drugs conjugates to peptides[74, 75], small molecules[76] or polymers[77-85] have been designed and studied for the purpose of ovarian cancer treatment. In fact, they can be perceived as a nano-scale (at least one dimension less than 100 nm) platform for drug loading. At such nano scale, they will possess new features in chemical, physical and biological aspects. After systemic administration, nano-sized DDS can actively accumulate at tumor sites through passive targeting due to the enhanced permeation and retention (EPR) effect[86-88]. The circulation lifetime following intravenous administration can be significantly prolonged in contrast to free drugs. Thus, the EPR effect of DDS can lead to the enhancement of therapeutic efficacy. Nano-sized DDS enables the MDR vastly minimized by directing endocytosis-mediated cellular internalization of drugs and/or interacting directly with efflux pumps[89-91]. To further enhance the therapeutic efficacy of drug-loaded nano-sized DDS, moieties which can be recognized by cancer cells have also been introduced onto the surface of DDS, realizing active targeting effect. Active targeting is also conducive to bypassing MDR, leading to an increased accumulation of drugs[92]. However, nano-sized DDS cannot remarkably prolong the peritoneal residence time of the drugs. Nano-sized DDS quickly pass through the peritoneal cavity into the lymphatic drainage[93-95].

1.3.3 Microspheres

The size of microsphere DDS normally ranges from 1 to 1000 μm. Compared with nano-sized DDS, microspheres present a longer peritoneal retention time following intraperitoneal administration[95]. However, it is still faced with the challenge of biocompatibility. So far, there are only limited preclinical tests undertaken on microsphere formulations for intraperitoneal chemotherapy for ovarian cancer treatment[95-97].

1.3.4 Implants and Injectable Depots

For the sake of localized and persistent anticancer drug delivery, implants and injectable depots DDS may provide a promising alternative. Their advantages are expected to be accumulated drug concentration at the tumor site, sustained drug release benefiting for cell cycle-specific anticancer agents, and low systemic toxicity[51]. On the other hands, there are still some concerns and issues impeding their application clinically. One concern is associated with the realization of homogeneous distribution of drug in the peritoneal cavity after administration. Moreover, metastatic regions beyond the peritoneal cavity are likely to be scarcely benefited based on such localized approach.

1.3.5 Folate Receptor (FR) Targeted Ovarian Cancer Therapy

Folic acid (FA), a water-soluble B9 vitamin, plays an important role in various cell functions such as DNA synthesis, repair, and methylation. Three types of proteins involved in the FA transport have been described: folate receptor, proton-coupled folate transporter, and reduced folate carrier. FR is known to be overexpressed in ovarian cancers, while present limitedly in normal tissues, making it a promising anti-tumor target [98-100]. Several studies has approved the FA-conjugated drug or/and gene delivery achieved a desired anti-cancer effect in ovarian cancer [101-105].

1.4 Graphene Quantum Dots (GQDs)

1.4.1 Graphene and Its Derivatives

Graphene is a type of single layer two-dimensional nanomaterial featured with sp^2 hybridized carbon atoms arranged in a honeycomb lattice[106-110]. Graphene is becoming a increasing recognized by the scientific community owing to its considerable unique properties in physical and chemical aspects. Specifically, these unique properties include high surface area, strong mechanical strength, extremely low toxicity and ease of functionalization, just to name a few. The derivatives of graphene, e.g. graphene oxide (GO)[111-114] and GQDs [115-118] inherits the majority of the superior properties of graphene, and they have been broadly investigated for a diversity of applications. In particular, scientists and researchers are spending more and more efforts regarding their biological applications, including, for example, bioimaging[119-121], drug delivery[122-126], and photothermal therapy. It has been reported that GO is a promising platform for drug loading, as molecules can be attached to it through physical adsorption[114, 122] or chemical binding[127, 128]. For those molecules containing aromatic structures, they can readily attach to graphene and its derivatives via strong π-π stacking interaction[129]. On the other hand, with the presence of –COOH[123] and other functional groups on the surface GO and GQDs, numerous molecules can be linked to GO via chemical bonds. According to the literature, GO and GQDs show very high water-solubility[130, 131], which enables to deliver a number of water-insoluble drugs into cells. Moreover, in contrast to single-walled carbon nanotubes, which load drugs mainly through outer face and tips, GO and GQDs permit drugs to be loaded on both faces and edges. Thus, the loading ratio of GO and GQDs present remarkably high loading capacity, theoretically even up to 200%[132].

1.4.2 GQDs

Visualization of living cells, namely bioimaging technique, is of great importance for diagnostic purpose or understanding cellular uptake mechanisms. Consequently, DDS is expected to be visually tracked in order to achieve the goals mentioned above. Indeed, several types of luminescent materials have been under investigations in recent years, such as organic dyes[133-135], semiconductor quantum dots[136-138], and lanthanide-doped nanocrystals[139-141]. However, organic dyes suffer from unwanted photobleaching; semiconductor quantum dots are challenged with toxicity; and lanthanide-doped nanocrystals is confined with their high cost. In addition, it needs to be pointed out that the high loading capacity platform discussed above, i.e. graphene or GO, can lead to severe luminescence quenching when conjugating with most of the preceding luminescent materials[142-145]. Therefore, it is desirable to develop a DDS with intrinsic luminescent properties, which also possesses the merits of graphene or GO. Such DDS can undertake imaging and implement drug delivery tasks without the need for external organic dyes, or semiconductor quantum dots. Fortunately, GQDs not only inherit the merits from graphene and GO, but also possess intrinsic photoluminescence, and thus affording a possible and promising solution for the challenge we are faced with. In this dissertation, I employed functionalized GQDs as a novel nano-scale drug delivery vehicle with tunable luminescence for ovarian cancer treatment.

1.4.3 The Chemical Structure of GQDs

The chemical structure of GQDs resembles the crystalline structure of single or a few layered graphene, typically with oxygen-containing groups such as -COOH, -OH presenting on their surfaces or edges (Figure 1.1) [146]. Their lateral dimension is normally reported a few nanometers though there are reports on their size as large as 60 nm[117]. Their shape is mainly either circular or elliptical, but the findings of triangular, quadrate and hexagonal GQDs are also reported in several articles[147].

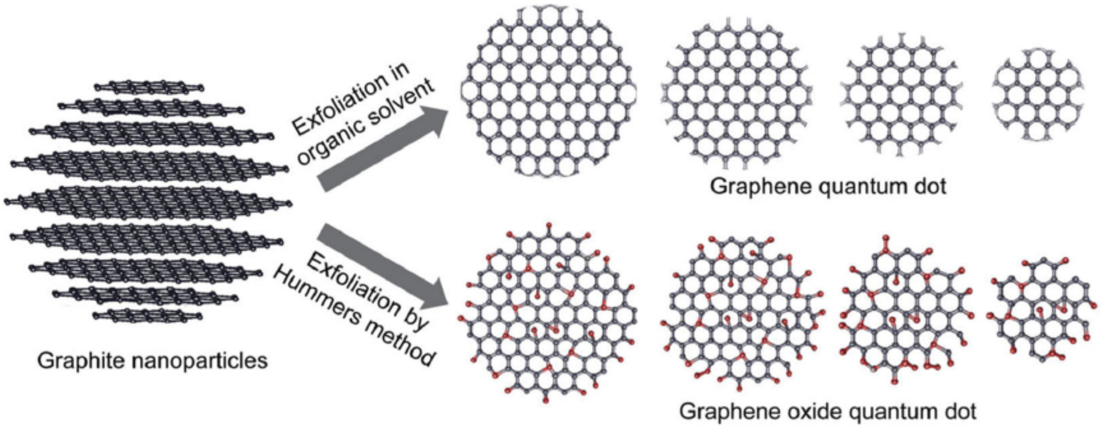

Figure 1.1 Schematic illustration of the structures of GQDs. Reproduced with permission[148].

According to results in the literature, the graphitic in-plane lattice spacing is usually 0.18~0.24 nm[149], while the graphitic inter-layer spacing is approximately 0.334 nm or even greater when considering the existence of functional groups[131, 150]. The physical and chemical properties of GQDs are highly associated with their structures, which will be introduced below.

1.4.4 Optical Properties

1.4.4.1 Absorbance

GQDs have a strong absorbance towards the short-wavelength region of the ultraviolet (UV)-visible spectrum owing to the π-π^* transition of C=C bonds. Typically, an obvious absorption band can be measured in the UV region (260-320 nm), with a tail covering the visible region[151, 152]. A shoulder peak located between 270 and 390 nm usually can be observed, which is ascribed to the n-π* transition of C=O bonds[153]. The absorption behavior can be affected by functional groups and surface passivation., which normally involves a creation of protective layer on the surface, making the base material less affected by surrounding environment [101].

1.4.4.2 Photoluminescence

The photoluminescence characteristics of GQDs are fascinating, as their emission colors are tunable by altering their particle sizes and functional groups, or using different excitation wavelengths, and they also exhibit upconversion photoluminescence. The upconversion refers to a nonlinear process in which the successive absorption of two or more photons with low energy followed the emission of a photon with high energy [102]. Compared with commonly used organic dyes, the strength of GQDs includes excellent non-photobleaching performance. In contrast to semiconductor quantum dots, the advantage of GQDs lies in non-photobleaching .

GQDs with different emission colors ranging from UV to red, and most commonly blue and green, have been successfully fabricated in the laboratory. Thus, GQDs are also good candidate for multi-color imaging.

Similar to semiconductor quantum dots, the luminescence of GQDs also show size-dependent characteristics[154]. The presented GQDs emit luminescence from far-UV to near-infrared (NIR) with their size varying from 0.5 nm to 2.4 nm. Basically, the smallest GQD emits at 235.2 nm, while the largest GQD emits at 999.5 nm. The size-dependent relationship is why the emission wavelength of GQDs covers the entire visible spectrum (400-780nm) as the size changes from 0.9 nm to 1.8 nm. It should be noted that as the particle size increases, the observed red-shift of the emission wavelength is attributed to the decline in band gap resulting from p-electron delocalization[154].

The existence of oxygen-containing functional groups also has impact on the luminescence properties of GQDs[154]. The oxidation of GQDs by –OH or –COOH results in red-shift phenomenon presumably due to the band gap reduction in a coverage dependent manner. Increasing –OH to their edge (from 0 to 100% coverage) alters GQDs from green (572nm) to red (732nm). The case of red-shift manner of edged –COOH groups exhibits the similar trend as that of –OH. In contrast to the edged situation, -OH groups attached on the basal plane render a more drastic red-shift probably due to the disruption of the graphitic carbon lattice. GQDs from the top-down strategy more often bear defects. The relevant calculations depict that the appearance of single or double vacancy defects also remarkably affected the emission wavelength. So the results indicate that the impact of vacancy defects cannot be neglected.

Interestingly, the photoluminescence of GQDs also present an excitation-dependent phenomenon[121, 155]. The emission peaks redshift with longer excitation wavelengths, while the emission intensity decreases, with the strongest excitation peak at the absorption band.

Upconversion refers to a nonlinear optical process, in which the energy of the emission photon is higher than that of excitation photons (namely the emission wavelength is shorter than the excitation wavelength), because of two or more consecutive photons at one time[156]. It has been reported that GQDs also exhibit comparatively higher upconversion efficiency compared to the traditional phosphors. Upconversion is desirable for *in vivo* imaging in that a longer excitation wavelength permits a deeper tissue penetration[157]. From the work by Chen *et al.*(Chen, Shen et al. 2012, we can observe that GQDs emit upconverted luminescence centered roughly at 450~475 nm with the excitation wavelength varying from 600 to 800 nm [157]. The upconverted ability of GQDs makes them more attractive for bioimaging, especially for deep tissue imaging.

1.4.4.3 Photoluminescence Mechanisms

To date, the luminescence mechanisms of GQDs are still not completely understood. The widely accepted luminescence mechanism at present is described as a transition from the lowest unoccupied molecular orbital (LUMO) to the highest occupied molecular orbital (HOMO) [147, 158, 159], as illustrated in Figure 1.2. The energy gap relies on the GQDs, which is determined by several parameters and the key factor is particle size. Generally, the energy decreases gradually as the size of GQDs expand. Figure 1.2(a) (I) & (ii) reveals the LUMO state and HOMO state of a GQD ($C_{96}H_{58}$) from ground state, while Figure 1.2 (c) further depicts the GQD ($C_{96}H_{58}$) consisting of 4 sp^2 domains (pyrene) separated by a sp^3 carbon network. To understand the upconversion mechanism of GQDs, the classic energy level structural model is employed and proposed (Figure 1.2 (a) (iii) & (iv)). In brief, a photon with low energy excites π-electrons (at intermediate energy level) to LUMO, followed by a relaxation into σ orbital (HOMO) emitting a higher energy photon[147].

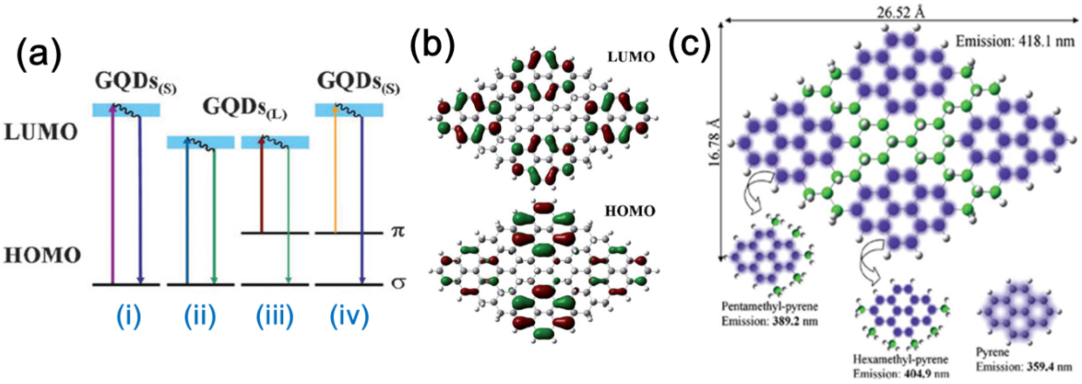

Figure 1.2. luminescence mechanisms of GQDs. (a) A schematic illustration of various typical electronic transitions processes of GQDs. Normal photoluminescence mechanisms in GQDs for small size (i) and large size (ii); Upconverted PL mechanisms in GQDs for large size (iii) and small size (iv). (b) Molecular orbitals for LUMO and HOMO from ground state. (c) GQD composed of four pyrene domains separated by sp3 carbons (green spheres). Reproduced with permission[160, 161] .

1.4.5 Cytotoxicity

Due to the potential applications of GQDs in biology, evaluation of their toxicity has been given lot of attention. A number of research groups have performed cytotoxicity tests, which confirm their low toxicity in the majority cell types.[162-164] For example, Zhu *et al*. [121] measured cell viability of human osteosarcoma MG-63 cells using methylthiazolyldiphenyl-tetrazolium bromide (MTT) assay. According to their results, the cell viability remained above 80% when 400 μg of GQDs were added to 150 mL culture medium (10^4 cells), indicating the minimum cytotoxicity of GQDs and the feasibility for biological applications. Zhang *et al*. [131] have conducted MTT assays on three kinds of stem cells:

Neurospheres cells, cardiac progenitor cells, and pancreas progenitor cells. Average cell viability for those cells were over 80% after 3 days culturing with GQDs at the concentration of 100 mg/mL. Furthermore, other types of cells have been evaluated, including mouse osteoblast precursor MC3T3 cells[165], human cervical cancer HeLa cells[166], and human breast cancer cells MCF-7 cells[166], MDA-MB-231[167], and T47D[168]. As expected, all of the results show that GQDs pose low toxic effects and are suitable for a diversity of biological applications.

1.4.6 Biological Applications

As introduced above, GQDs have considerable advantages over the conventional organic dyes and semiconductors, making them more desirable for cell or tissue imaging. For instance, Zhu *et al.*[121], have applied the green fluorescent GQDs for cell imaging in MG-63 cells for bioimaging application, respectively. In addition, upconversion cell imaging of GQDs have been investigated as upconversion luminescence usually requires NIR excitation, which allows deeper penetration and is less harmful compared with UV excitation [147]. Green and blue upconversion luminescence can be clearly observed inside of MC3T3 cells upon excitation at 808 nm, suggesting the availability of GQDs for upconversion luminescence cell imaging[169].

GQDs have also been developed as a drug delivery tool. Wang *et al.*[166] exploited folic acid-conjugated GQDs to load doxorubicin (DOX), a FDA approved anticancer drug. This nano-system can be internalized by target cells rapidly via receptor-mediated endocytosis and prolong the DOX release and accumulation in those cells. At the same time, the photoluminescence of GQDs permits the real-time monitoring of the cellular uptake of this nano-system. Based on their results, this nano-system can target and kill HeLa cells efficiently, while possesses significant low cytotoxicity to non-targeted cells.

Most recently, researchers have studied GQDs for their antibacterial ability, indicating their promising application for disinfection[170, 171]. The work by Gao *et al.*[170]demonstrated that GQDs are featured with peroxidase-like activity, enabling the generation of $^{\bullet}OH$ from H_2O_2. Based on the fact that $^{\bullet}OH$ possesses a higher antibacterial performance than that of H_2O_2, GQDs are likely to afford a more efficient antibacterial system when combined with a low dose of H_2O_2. This will circumvent the toxic concern of H_2O_2 at high concentration. Besides *in vitro* experiments, the systems even exhibit a superior antibacterial performance *in vivo.* The data strongly support that GQDs have the potential to serve as antibacterial agents for disinfection.

1.5 Hypothesis and Objectives

The goal of this study is to develop a novel and effective targeted drug delivery platform for the treatment of ovarian cancer. I hypothesize that a novel GQDs-based drug delivery system is a promising theranostic strategy for ovarian cancer. The GQDs-based drug delivery system is expected to enable the simultaneous monitoring, specific targeting to tumor, and minimizing toxicity to normal cells. To achieve the aforementioned goals, I proposed and worked on the following specific objectives: 1) to establish GQDs-based drug delivery system with the conjugation of folic acid as targeting ligand and Doxorubicin as anticancer drugs, 2) to validate the therapeutic efficacy of such theranostic platform towards ovarian cancer, and 3) to investigate the toxicity of the current GQDs-based drug delivery system to immune system.

1.6 Significance

Despite the remarkable understanding and prodigious development of research in aspects of cancers, ovarian cancer still remains one of the most devastating diseases worldwide. The major limitations of the mainstay therapy, chemotherapy, are the lack of response and distinct side effects due to the lack of selectivity of the chemo-drugs. Therefore, it would be desirable to develop innovative DDS for targeted therapy of ovarian cancer. The contribution of this work is significant for the reason that the GQDs-based drug delivery system is designed as a targeting and effective chemotherapy for ovarian cancer. Moreover, the knowledge gained from these studies will also advance our understanding of cellular uptake and immunotoxicity regarding graphene quantum dots, and meanwhile benefits the further discovery of GQDs-based nanomedicines.

1.7 Overview of Dissertation Chapters

Chapter 1 reviews the theoretical basis of ovarian cancer and current therapeutic strategies, including surgery, chemotherapy, and nanoparticle based theranostics. It also briefly introduces the motive, significance, novelty, rationale, and objectives of this project.

Chapter 2 introduces a one-step method to directly synthesize GQDs and their conjugation with targeting ligand and anti-cancer drug, and followed by the characterization of current material and the drug loading/releasing profiles of the GQDs-based nano-DDS.

Chapter 3 provides validation of the anti-cancer effects of this novel nano-DDS in folate receptor-overexpressing ovarian cancer cells and its low toxicity in normal ovarian epithelial cells.

Chapter 4 elucidates the biological interactions of GQDs with immune system and the underlying mechanisms.

Chapter 5 provides discussion and perspectives of directions for future research.

CHAPTER 2: SYNTHESIS OF GQDs AND GQDs-DDS

Abstract

Graphene quantum dots (GQDs) are a promising alternative fluorescent probe to traditional fluorophore probes. However, it is still a big challenge to fabricate GQDs in a rapid and cost-effective way, which limits their potential application. To address this problem, we developed a fast and facile preparation route of GQDs directly from graphite by a one-step hydrothermal reaction. Low cytotoxicity, highly green fluorescent GQDs with an average size of 3 nm and quantum yield of 13.1% had been synthesized. Raman spectroscopy and Flourier transform infrared spectroscopy indicated the successful preparation. This chapter thereafter introduced the method to conjugate GQDs with folic acid (FA) and doxorubicin (DOX). The successful conjugation of GQDs-FA-DOX has been confirmed using UV, FTIR, and fluorescent spectroscopy. Drug loading and releasing profiles of GQDs-FA-DOX have been examined.

2.1 Introduction

As mentioned in the first chapter, graphene and its derivatives have exhibited great potential in optical, electrochemical, and biomedical applications[120, 144]. Among them, the biomedical application of GQDs is relatively new, but fast-growing in areas, such as bioimaging[121, 126, 131, 152], biosensor[172], anti-bacterial[173, 174], and drug delivery[175, 176]. Combining the advantages of graphene and quantum dots，GQDs are expected to serve as an excellent theranostics.

Although progress has been made in synthesis of GQDs, there are still many shortcomings in those methods. For example, even though some groups have already succeeded using carbon fibers[177]or even coal[178] as the starting materials to synthesize GQDs, most methods are still based on GO[179].The past methods require to synthesize GO from graphite in the first step, and then to obtain GQD from GO, implying multiple and time-consuming steps. Therefore, the first objective of this chapter was to establish a fast and facile method to synthesize GQDs.

The second objective of this chapter was to construct the targeted GQDs drug nano-conjugation. The targeting ligand specifically guided this nano-conjugation to the targeted delivery site, while the drug was used for chemotherapy to kill the carcinomatous cells. In this study, FA was chosen as the targeting ligands and DOX, a type of FDA approved drug, was selected as the chemo-drug.

Folate receptors (FR) are high-affinity folate-binding proteins with an apparent molecular mass of 38kDa. The folate receptor exists in three major forms: FR-α, FR-β and FR-γ. Among them, FR-α is known to be overexpressed in ovarian cancers and is widely used as a molecular target for tumor-selective therapies[180]. According to previous studies[100, 181-184], FR-α overexpression occurs in more than 70% of primary and 80% of recurrent ovarian tumors. Therefore, the water-soluble B9 vitamin, FA, is widely adopted as a targeting ligand to folate receptor[105, 185, 186].

Doxorubicin, a topoisomerase inhibitor, is a second-line drug in metastatic ovarian cancer. It has been confirmed to significantly improve the ovarian cancer patients' survival[187, 188]. However, its usage is limited in clinical due to its severe cardiac toxicity[189-191]. The major side effect of DOX is the cause of chronic cardiomyopathy, and the mechanism is still not fully understood. The current proposed mechanism of DOX-induced cardiac toxicity includes generation of iron complexes, perturbation of calcium homeostasis, dysfunction of mitochondrial, and production of radical oxygen species (ROS)[192-194]. Using proper targeting delivery vehicles is considered to be a solution to reduce the cardiac toxicity of DOX.

2.2 Materials and Methods

2.2.1 Chemicals and Raw Materials

Graphite, potassium permanganate ($KMnO_4$), sodium carbonate (Na_2CO_3), ammonium hydroxide solution (NH_4OH),hydrogen peroxide (H_2O_2), sulfuric acid (H_2SO_4), nitric acid (HNO_3), dimethyl sulfoxide (DMSO), N-hydroxysuccinimide (NHS), 1-(3-dimethylaminopropyl)-3-ethylcarbodiimide hydrochloride (EDC), folic acid (FA), and Doxorubicin (DOX)were purchased from Sigma-Aldrich Inc. (St. Louis, MO, USA).

2.2.2 Synthesis of GQDs

GQDs nanoparticles were prepared from graphite in the one-step hydrothermal reaction (Figure 2.1). Briefly, 60 mg graphite and 180 mg $KMnO_4$ were weighted and added into 18 ml mixed acid (ratio of H_2SO_4 to HNO_3 is 5:1). The mixed solution was heated at 160 °C in a polytetrafluoroethylene-lined (also known as Teflon) autoclave reactor (20 ml) for 90 min. After the reaction, unreacted $KMnO_4$ and acids were removed by adding H_2O_2 solution and saturated by Na_2CO_3 solution, followed by a 24-h dialysis (dialysis membrane with a cut-off of 1,000 Da).

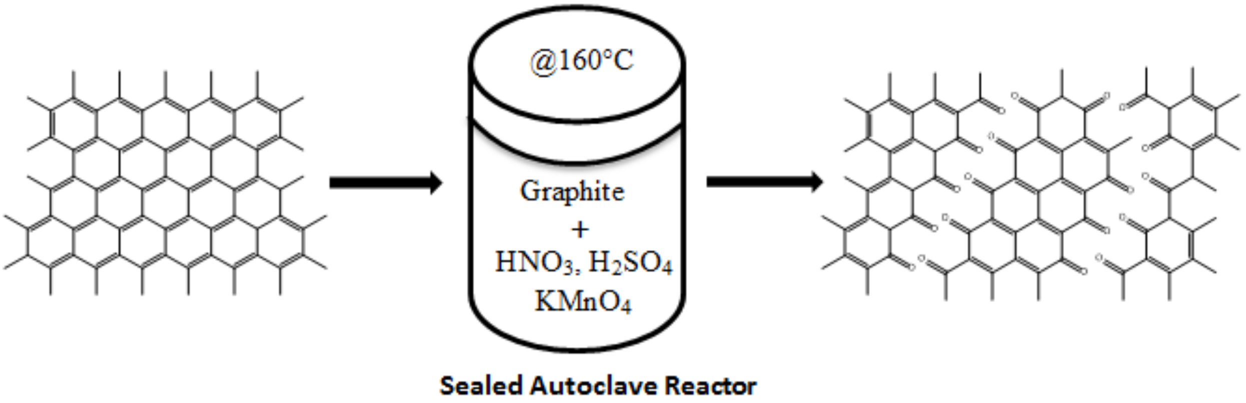

Figure 2.1 Scheme of the synthesis of GQDs from graphite via the one-step hydrothermal method.

2.2.3 Synthesis of the GQDs-FA-DOX Conjugates

The conjugation of GQDs with FA and DOX was modified and performed by following the previously described method [166]. In brief, synthesized GQDs were reacted with NHS and EDC in DMSO buffer for 30 min with sonication, followed by adding FA with stirring overnight. The solution was repeatedly dialyzed against distilled water using dialysis membrane tubing (cut-off 1,000 Da) for 28 h. DOX (200 μl of different concentration DOX solutions ranging from 100, 200, 300, 400 to 500 μg/ml) was loaded on GQDs (1ml of 1mg/ml) (via π-π stacking) in DMSO solution with stirring for 4 h. Then the mixture was centrifuge at 12,000 rpm for 30 min. The pellet was kept as the product of GQDs-FA-DOX. Free DOX remained in the supernatant, and the absorption at 480 nm was measured to calculate the free drug content. The drug loading efficiency was calculated based on the following equation: drug loading (%) = ((weight of drug added − weight of free drug in the bath solution)/weight of carriers) × 100. The release of DOX from GQD–FA was monitored in PBS buffer at 24h and 48h, respectively. Absorption at 480 nm was measured to calculate the free drug content in the PBS buffer for DOX releasing profile based on the following equation: drug releasing (%) = (weight of free drug in the supernatant / weight of drug loaded) × 100. The absorption of DOX at 480 nm was measured using the Synergy H4 hybrid multi-mode microplate reader (BioTek).

2.2.4 Characterization Techniques

2.2.4.1 Transmission Electron Microscopy (TEM)

The size and morphology of the samples were obtained using a JEOL-1400 transmission electron microscope operating at 100 kV. The size distribution was counted by ImageJ (NIH).

2.2.4.2 High-resolution Transmission Electron Microscopy (HRTEM)

The high-resolution images regarding the crystal lattice, including the selected area electron diffraction (SAED) patterns, were collected using a JEOL-2010 high-resolution transmission electron microscope operating at 200kV.

2.2.4.3 Atomic Force Microscopy (AFM)

The AFM measurements were acquired with digital instrument Dimension 3100 atomic force microscope in the semi-contact mode using a nano-sized tip.

2.2.4.4 Raman Microscopy

The morphology of GQD was examined using Raman microscopy (Olympus, IX71).

2.2.4.5 Fourier Transform Infrared (FTIR) Spectroscopy

The FTIR spectra were obtained using the Perkin Elmer Spectrum100 series instrument by collecting 64 scans with a resolution of 4 cm^{-1} at the mid-infrared region (400 – 4000 cm^{-1}).

2.2.5 Quantum Yield (QY) Measurement

Quinine sulfate in 0.1 M H_2SO_4 (QY=0.543) was chosen as the standard. The quantum yields of GQDs (in water) were calculated according to:

$$\phi_x = \phi_{st}\left(\frac{I_x}{I_{st}}\right)\left(\frac{\eta_x^2}{\eta_{st}^2}\right)\left(\frac{A_{st}}{A_x}\right)$$

Where ϕ is the quantum yield, I is the measured integrated emission intensity, η is the refractive index of the solvent, and A is the absorbance. The subscript "st" refers to standard with known quantum yield and "x" for the sample.

2.3 Results and Discussion

2.3.1 Characterization of GQDs

2.3.1.1 Morphology of GQDs

First, we synthesized GQDs using a novel one-step hydrothermal approach. The synthesized GQDs had a relatively narrow size distribution by TEM as shown in Figure 2.2 (A). The quantitative size distribution graph in Figure 2.2 (B) shows that the sizes of GQDs vary from 1.5 to 5.5 nm with an average diameter of 3.03 nm counted by the ImageJ. Figure 2.2 (C) shows the morphology of the GQDs with a lattice parameter of 0.24 nm, and Figure 2.2 (D) illustrates the selected area diffraction (SAD) pattern of GQDs.

The properties of the GQDs were further characterized by Raman spectroscopy. As shown in Figure 2.3(B), the Raman spectrum of GQDs was resolved into two distinctive D and G bands at ~1340 and ~1580 cm^{-1}, while those of graphite were at ~1328 and ~1572 cm^{-1}, respectively. In terms of the nano-crystalline graphite, the intensity ratio (I_D/I_G) is known to be inversely proportional to the crystalline grains [148]. The I_D/I_G of GQDs in Raman spectra was 1.005, while the I_D/I_G of graphite was 0.823. This suggests that GQDs are more defective than graphite sheets, possibly due to the dominant contributions from the edge states at the periphery of GQDs.

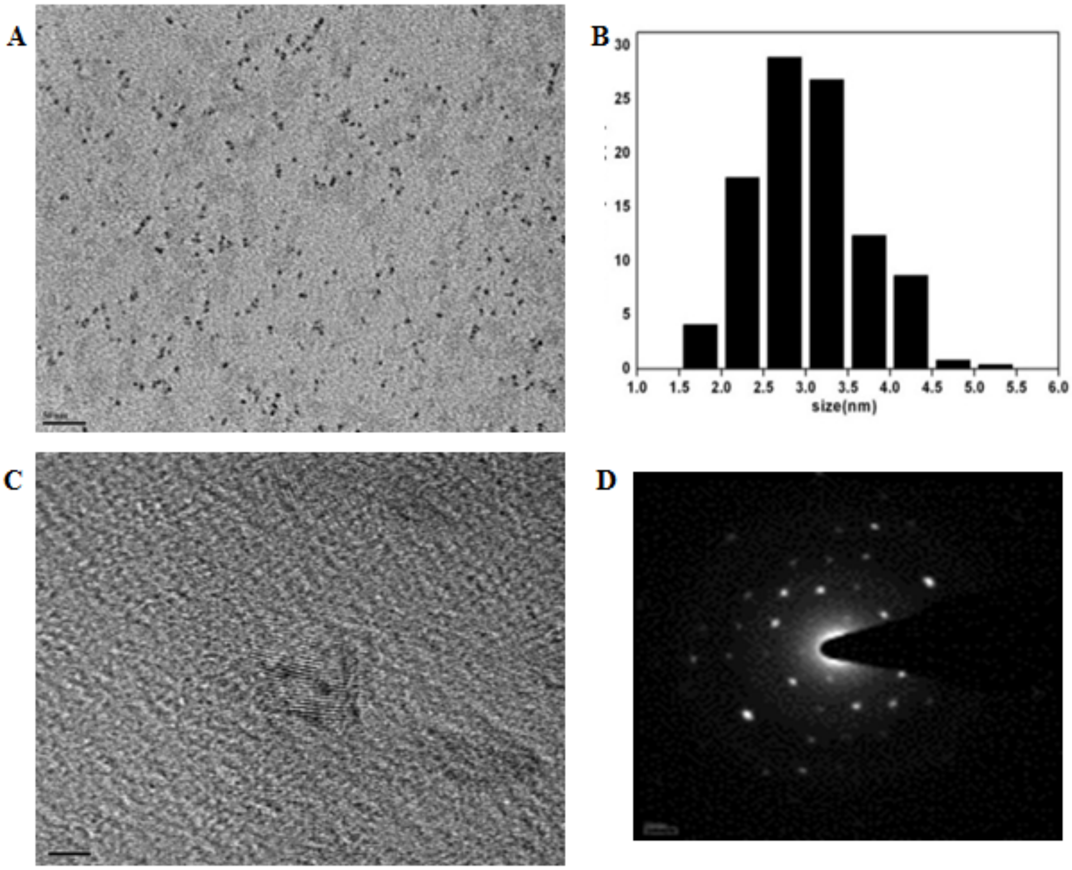

Figure 2.2 Morphology characterization of GQDs. (A) TEM image of GQDs. (B) Size distribution showing that the particle size range is within 1.5–5.5 nm, with an average size of 3.03 nm (scale bar = 50 nm). (C) HRTEM image showing the lattices structure of GQDs (scale bar = 2 nm). (D) Corresponding SAD pattern.

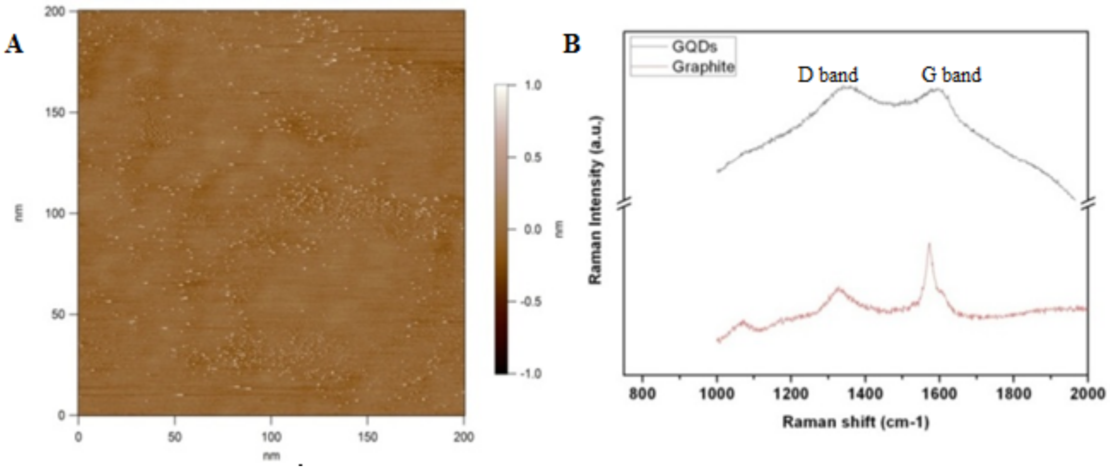

Figure 2.3 (A) AFM image indicating the single or bi-layer of GQDs. (B) Raman spectra showing the D and G bands at ~1340 and ~1580 cm^{-1} (I_D/I_G of 1.01).

2.3.1.2 Functional Groups of GQDs

In order to further examine the functional groups at the edges of GQDs, the FTIR spectrum was measured. The result in Figure 2.4 shows that a number of chemical groups, including C-O and C=O, were introduced to the edges of GQDs during the oxidative cutting process. Consequently, the resultant GQDs possessed an improved water-solubility. Moreover, these functional groups on the basal plane or edge enable GQDs to be further modified, as well as conjugated with target ligands and chemotherapeutic ligands to form a multifunctional theranostic system.

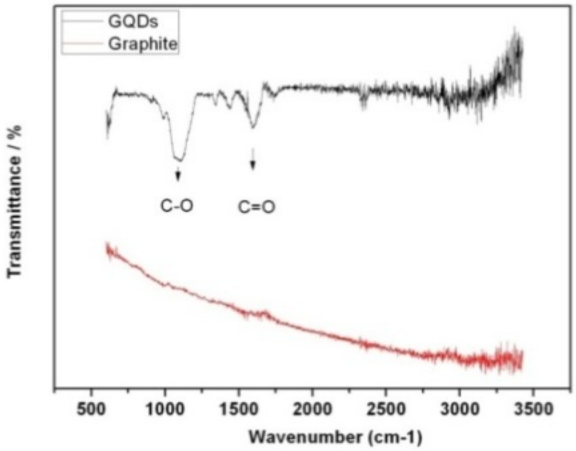

Figure 2.4 FTIR spectra of GQDs (black line) and graphite (red line).

2.3.1.3 Photoluminescence of GQDs

The photoluminescence of GQDs was then measured. Figure 2.5 (A) displays the photoluminescence spectrum of GQDs aqueous solution upon excitation at 440-nm wavelength. The inset in Figure 2.5 (A) is the photograph of GQDs in aqueous solution collected upon 365-nm UV light excitation in which green fluorescence could be observed with the naked eye. Like most luminescent carbon nanoparticles, the GQDs also exhibit an excitation-dependent PL behavior. To explore the optical properties of the GQDs, I undertook a detailed PL study using different excitation wavelengths. The emission peaks of GQDs shifted by varying excitation wavelengths, exhibiting excitation wavelength-dependent PL behavior as shown in Figure 2.5(B).

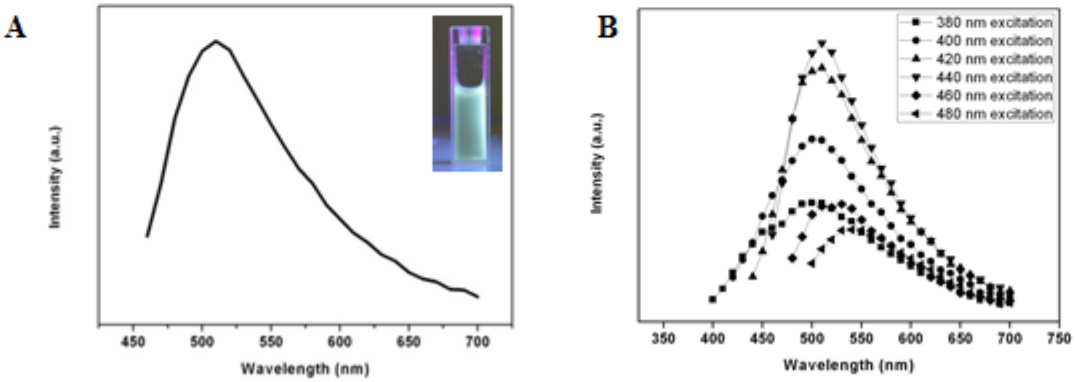

Figure 2.5 Photoluminescence emission spectra of GQDs. (A) with excitation at 440 nm wavelength (inset: visible green fluorescence of GQDs aqueous solution under 365 nm UV light, as observed with the naked eye) and (B) with different excitation wavelengths from 380 to 480 nm.

2.3.1.4 Modified Synthesis of GQDs

In order to optimize the synthesis approach, a series of reactions were performed at different temperatures or in the absence of oxidants. For safety concerns, the reaction temperatures were confined below 160 ºC, roughly varying from 100 ºC to 160 ºC. The reaction without $KMnO_4$ (at 160 ºC) was also carried out to determine the necessity of $KMnO_4$. Since graphite has a large size and is insoluble in water, graphite and its oxidant mixture has a black color, while the GQDs aqueous is clear yellow color under the natural light. Figure 2.6 (A) shows the color of the products at different reaction conditions. It can be seen that without $KMnO_4$ or under 100 ºC, the reaction barely happens and most of the products are expected to be graphite pieces instead of GQDs. Figure 2.6 (B) also shows the luminescent intensity of the resulting products tended to significantly attenuate, when reaction temperature was below 100 ºC or in the absence of $KMnO_4$. The results indicate the synergistic interaction of heat and oxidants in this hydrothermal reaction.

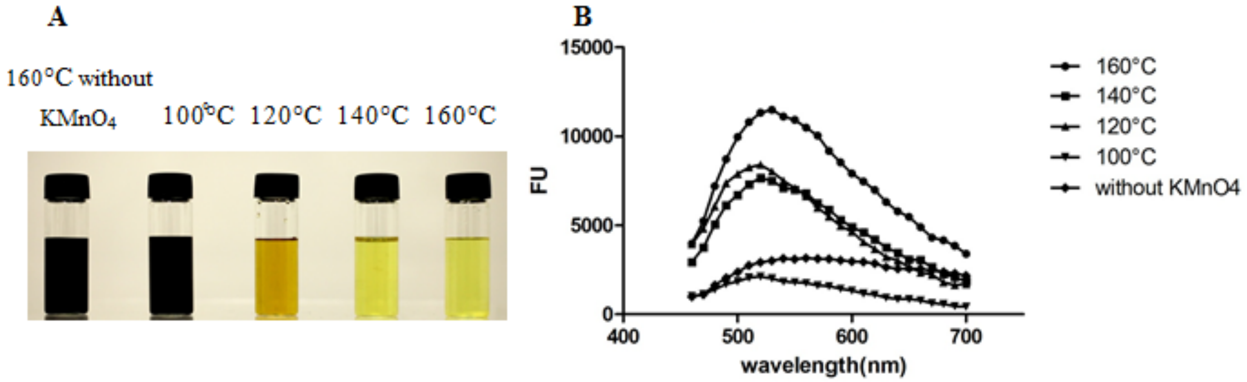

Figure 2.6 Photoluminescence behavior of the GQDs aqueous solution for temperature-dependent reactions. (A) The color of resulting products and (B) Photoluminescence emission spectra of GQDs aqueous solution at different synthesis temperatures.

2.3.1.5 Quantum Yield of GQDs

Table 2.1 shows the results obtained using the method and equation described in 2.2.3 to calculate the quantum yield. The photoluminescence quantum yield is determined to be 13.1% using quinine sulfate of 54% as the reference.

Table 2.1 Quantum yield of GQDs using quinine sulfate as a reference.

Sample	Integrated emission intensity(I)	Absorbance(A)	Refractive index of the solvent(η)	Quantum yield(ϕ)
Quinine sulfate	3432500	0.067	1.33	0.543
GQDs	1207000	0.097	1.33	0.131

2.3.2 Characterization of GQDs-FA-DOX

2.3.2.1 Morphology and Functional Groups of GQDs-FA-DOX

Upon preparation of GQDs from graphite following the one-step hydrothermal synthesis method, GQDs were then conjugated with FA following a modified previous report[166]. The synthesized GQDs-FA-DOX had a relatively narrow size distribution. TEM image shows that the sizes of GQDs-FA-DOX were between 9 - 12 nm as shown in Figure 2.7(A) and Figure 2.7(B) shows its size distribution counted by ImageJ. The conjugation of the FA and the loading capacity of DOX was confirmed by FTIR and UV absorbance spectra. Although the drug loading capacity of DOX was able to quantitatively measured and shown in later results, the stoichiometry of FA per GQD was unable to define in current experiment condition.

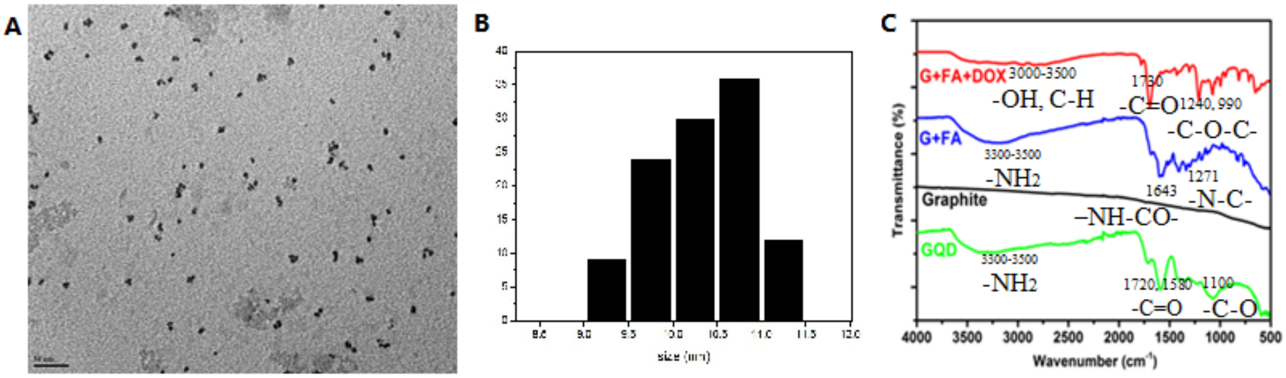

Figure 2.7 Morphology and functional groups of GQDs-FA-DOX. (A) TEM image and (B) size distribution of GQDs-FA-DOX. (C) FTIR spectra of graphite (black), GQDs (green), GQDs-FA (blue) and GQDs-FA-DOX (red).

The FTIR spectra results of GQDs, GQDs-FA, and GQDs-FA-DOX are shown in Figure 2.7(B). Graphite is only composed with C-C, which does not give any peaks in FTIR. Compared with GQDs, the appearance of new peaks at 1271 and 1560cm^{-1} suggests the conjugation with FA, which are assigned to C-N and N-H stretching, respectively. The new broad peak in the 3300–3500 cm^{-1} region corresponds to the N-H vibration. In addition, characteristic amide–carbonyl (-NH-CO-) stretching vibration is observed at 1643 cm^{-1}, which implies the formation of amide groups in GQDs–FA. For GQD–FA-DOX, the new peaks at 1730 cm^{-1} suggests the conjugation with DOX, which is assigned to the stretching vibration of ketone carbonyl (C=O) groups. The peaks at 1240 and 990 cm^{-1} are assigned to alkoxy (-C-O) groups. Those new groups suggested the successful loading of DOX.

2.3.2.2 UV Spectra of GQDs-FA-DOX

The UV-visible absorption spectrum is shown in Figure 2.8(A). At 230 nm, there is a strong absorption peak, indicating $\pi \rightarrow \pi^*$ transition of aromatic sp^2 domains of GQDs. After conjugated with FA, GQDs-FA presents a new peak at 280nm, which is in accordance with the previous study by Wang *et al*[166]. The doxorubicin has a strong absorbance at around 480nm, which can be observed in GQDs-FA-DOX.

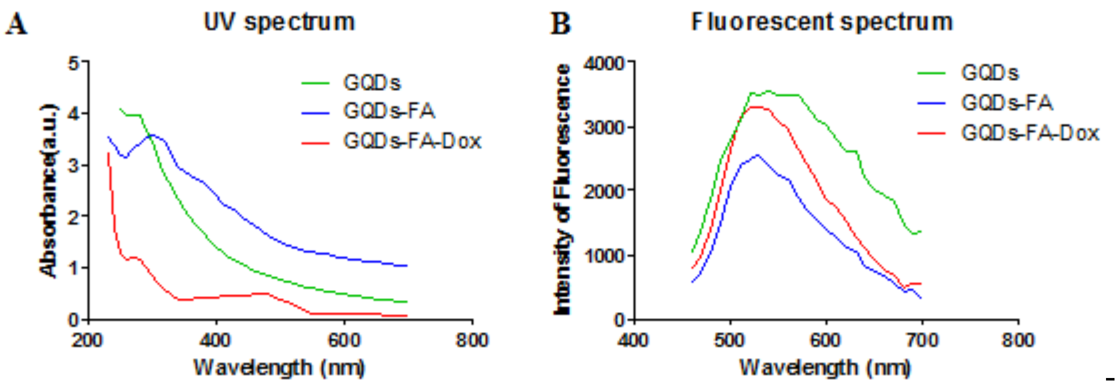

Figure 2.8 (A) UV spectra and (B) fluorescent emission spectra of GQDs (green), GQDs-FA (blue), and GQDs-FA-DOX (red).

2.3.2.3 Fluorescent Emission Spectra of GQDs-FA-DOX

In addition, the photoluminescence behavior of GQDs, GQDs-FA, and GQDs-FA-DOX were examined and shown in Figure 2.8(B). When excited at 480 nm, GQDs, GQDs-FA, and GQDs-FA-DOX show an emission peak at 540nm. The fluorescence of GQD is slightly reduced after the conjugation with FA presumably due to the changes of the chemical groups. Interestingly, DOX is supposed to show a strong red fluorescent emission at 560-590 nm upon excitation at 480 nm. However, the red emission of DOX was not observed after loading to GQDs-FA.

2.3.3 Drug Reloading and Releasing Profile

The absorbance at 480 nm versus the different concentrations of DOX was normalized by linear regression. The standard curve for the drug loading followed a good linear correlation (

Figure 2.9). The typical equation of the standard curve was described: Y=6.466*X-0.6904.The R2 of the standard curve is 0.9720, which indicates a good fit of the linear regression model.

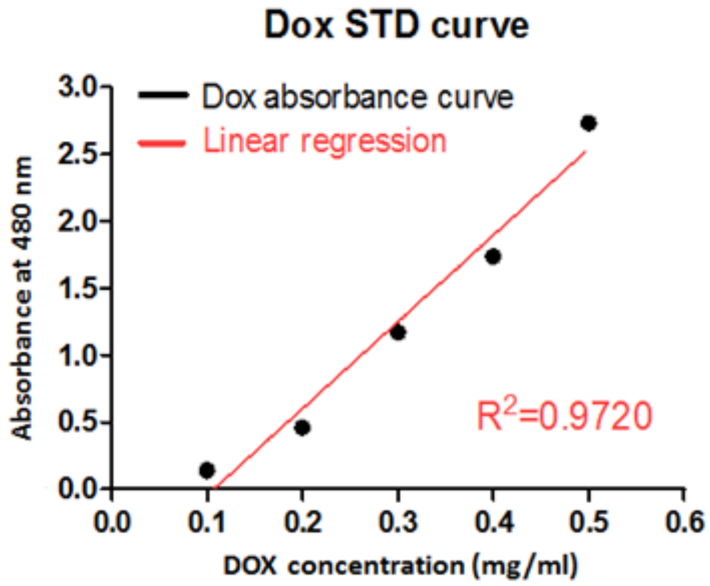

Figure 2.9 DOX-absorbance standard curve

Since the products of GQDs-FA-DOX remain in the pellet, the drug loading and releasing are based on the free DOX in the supernatant. The absorption of DOX at 480 nm was measured to calculate the free drug content. The DOX loading efficiency was calculated based on the following equation: drug loading (%) = ((weight of drug added − weight of free drug in the bath solution)/weight of carriers) × 100. The DOX releasing profile based on the following equation: drug releasing (%) = (weight of free drug in the supernatant / weight of drug loaded) × 100. As shown in Figure 2.10(A), the maximum loading efficiency capacity of DOX in GQDs-FA was achieved at 64% when the loading ratio of DOX to GQDs-FA was 1:2. The release of DOX from GQD–FA was monitored in cell culture medium at 24 h and 48 h, respectively. The drug releasing of GQD-FA-DOX turned out to be in a time-dependent manner. The release of DOX could reach as high as 50% within 48 h, as seen in Figure 2.10(B).

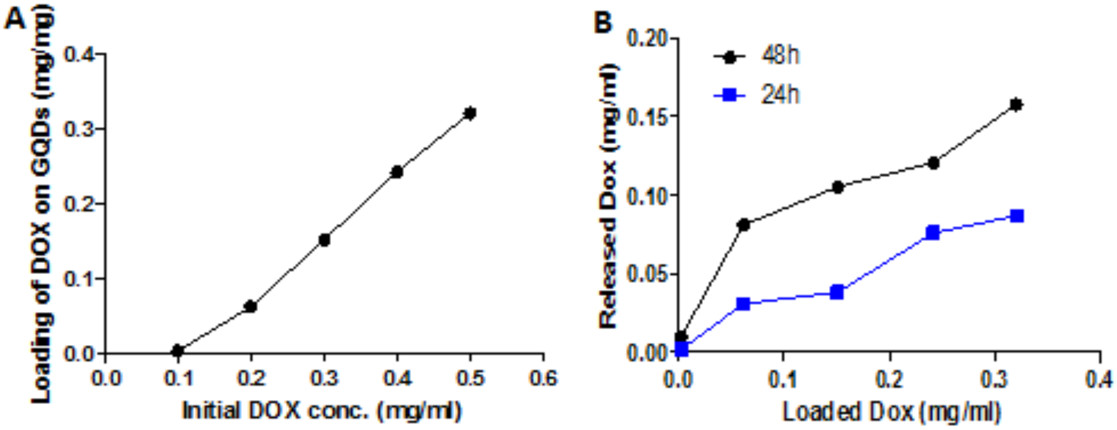

Figure 2.10 Drug Loading (A) and releasing (B) profile of GQDs-FA-DOX in aqueous solution

2.4 Conclusions

In my approach, GQDs with green fluorescence were synthesized directly from graphite powders using a one-step chemical oxidation reaction. This method required less reaction time, as fast as 90 min, and offered a high product yield of up to 30% with the photoluminescence quantum yield of 13.1% (quinine sulfate of 54% as the reference). GQDs exhibited bright fluorescence and excellent solubility in aqueous solution, thus enabling potential biomedical applications. The GQDs-FA-DOX DDS was successfully synthesized with a maximum loading efficiency capacity of 64% in terms of DOX.

CHAPTER 3: VALIDATION OF THE ANTI-CANCER EEFECTOF GQDs-DDS

Abstract

A new type of graphene quantum dots (GQDs)-based nano-sized drug delivery systems (DDS) was introduced for ovarian cancer treatment. My results demonstrate that doxorubicin (DOX) was successfully loaded onto the folic acid (FA)-conjugated GQDs, and satisfactory therapeutic efficacy was reached. Moreover, the real-time monitoring of cellular uptake has also been achieved utilizing the luminescent property of GQDs. Such superb drug loading capability and the luminescent property herald GQDs as a desirable theranostic tool for cancer therapy, and also hold the promise of acting as a multifunctional platform for other disease treatment. In this chapter, the results show that the GQDs-FA-DOX nano-conjugates can be an excellent targeted drug delivery nano-platform for folic receptor-overexpressed ovarian cancer.

3.1 Introduction

Ovarian cancer, one of the most dreadful malignancies of the female reproductive system, poses a lethal threat to women worldwide. It has been reported as the leading cause of cancer mortality among gynecological malignancies in the United States[1, 2]. The current frontline strategy for ovarian cancer treatment is cytoreductive surgery followed by chemotherapy with carboplatin and paclitaxel[10, 12-16]. Less often, treatment may include radiotherapy. Primary surgery ensures the removal of large tumor masses and is indeed a critical first step to improve patient survival[15, 16]. Even though most of the cancer may have been removed during surgery, there may still be some residual tumors present. For this reason, chemotherapy is typically required for the purpose of attacking cancer cells and slowing or stopping their growth. Although promising clinical outcomes have been witnessed through current treatment strategy, chemotherapy will inevitably jeopardize normal healthy cells while killing cancer cells. In addition, another concern is associated with the multidrug resistance (MDR)[52, 75]. To overcome such unwanted side effects caused by chemotherapy, drug delivery systems (DDS) have been perceived as a significant approach for cancer therapy, and increasing attention has been focused on their design and development. In particular, when their sizes are reduced to nanoscale, the nano-sized DDS present more distinguished merits including: (i) enhanced permeation and retention (EPR) effect, (ii) further improving drug accumulation at tumor sites owing to the presence of targeting moieties (i.e. active targeting), (iii) eschewing MDR mechanisms, and (iv) increasing solubility of poorly soluble drugs. Consequently, NDDS are expected to bring about new breakthroughs for the development of cancer treatment by researchers.

More recently, graphene quantum dots (GQDs), a novel type of carbon nanomaterials with combined properties of graphene and quantum dots (QDs), are highly likely to be exploited as an ideal NDDS for cancer therapy. First of all, like other members in carbon materials, GQDs have been proved to have relatively low cytotoxicity as per the previous reports[195-197]. More importantly, GQDs exhibit an excellent loading capability since a diversity of chemical groups can be easily functionalized on their surface, enabling the successful conjugation with targeting moieties[166, 198, 199]. On the other hand, the aromatic structure of GQDs permits the absorption of drugs through π-π stacking interactions. Furthermore, GQDs possess inherent luminescent properties, which, while similar to other QDs, are less toxic and more chemically stable[195, 200, 201].There are even reports on their upconverted luminescence upon near-infrared light excitation[202, 203]. Such properties make it possible for GQDs to be employed as luminescent probes, and thus the delivery efficacy can be tracked by detecting their luminescent signal. Based on the above advantages, GQDs are considered as versatile DDS for anti-cancer drug delivery and some preliminary research results of GQDs indicate the feasibility and reliability of the current DDS[166, 175].

However, the majority of previous investigations, to the best of our knowledge, principally concentrated on the synthesis and characterization of GQDs. Research on the practical cancer treatment using GQDs as DDS is still insufficient and unsystematic, especially for ovarian cancer treatment. Herein, I have systematically investigated folic acid (FA)-conjugated GQDs as a vehicle of the anti-cancer drug doxorubicin (DOX) for ovarian cancer treatment. The results imply that our designed DDS could significantly minimize the adverse effect of DOX on normal ovarian epithelial cells, the anti-cancer drug distribution could be monitored via the luminescence produced from GQDs, and good ovarian cancer treatment efficacy has been realized. Taken together, our studies not only have demonstrated that GQDs is a promising multifunctional platform for multidrug loading, but can also be a useful reference to the investigations of other DDS and disease.

3.2 Materials and Methods

3.2.1 Chemicals and Raw Materials

Ribonuclease, propidium iodide (PI), DMSO, MTT, crystal violet, folic acid, and Doxorubicin were purchased from Sigma-Aldrich Inc. (St. Louis, MO, USA). McCoy's 5a Medium, 5-(and 6)-chloromethyl-2',7'-dichlorodihy-drofluorescein diacetate (CM-H_2DCFDA), fetal bovine serum (FBS), penicillin and streptomycin, and phosphate buffered saline (PBS) were obtained from Invitrogen Inc. (Carlsbad, CA, USA). Hoechst 33342, a nucleus staining dye, was purchased from Enzo life sciences (Farmingdale, NY, USA). Membrane Protein Extraction Kit was purchased from Thermofisher (Waltham, MA, USA). The polyvinylidene difluoride (PVDF) membrane was purchased from Millipore Inc. (Bedford, MA, USA). Primary monoclonal antibodies against human folate receptor were purchased from Cell Signaling Technology Inc. (Beverly, MA, USA). The antibody against human β-actin was purchased from Santa Cruz Biotechnology Inc. (Santa Cruz, CA, USA). Visualization was performed using the BioRad system (Hercules, CA, USA) with the electro-chemiluminescence substrate purchased from Pierce (Hudson, NH, USA).

3.2.2 Cell Culture

The normal ovarian epithelial cell line T80 and ovarian carcinoma cell line OVCAR3 were obtained from American Type Culture Collection (Manassas, VA, USA). Cells was cultured in McCoy's 5a Medium containing 10% non-heated-inactivated FBS and 0.5% penicillin and streptomycin in a humidified incubator of 5% CO_2/95% air at 37 ℃.

3.2.3 Cell Viability Assay

Cells were treated with various concentrations of GQDs-FA-DOX (0, 0.25, 0.5, 1, 2, and 4 μM equivalent to DOX) for 24 h and 48 h, respectively. Cell viability was determined by the MTT assay. In brief, the cells were treated with GQDs-FA-DOX conjugates, 10 μL MTT (5 mg/ml) was added into each well and incubated for 4 h, culture medium was removed and 100 μL DMSO was added to dissolve formazan crystals. Absorbance was read at 560 nm for formazan and 670 nm for background using the Synergy H4 hybrid multi-mode microplate reader (BioTek). The results were given as relative value to the control in percent.

3.2.4 Colony Formation Assay

Colony formation assay can determine the effectiveness of the nano-drug delivery system based on the ability of a single cell to grow into a colony. First, two hundred cells were seeded into six-well plates. After treatment with various agents, including GQDs, GQD-FA-DOX, GQD-DOX, and DOX, cells remained in the cell culture medium for 14 days. Colonies were fixed with 4% paraformaldehyde solution and then stained with 0.5% crystal violet.

3.2.5 ROS Generation Assay

Intracellular ROS level was determined using a fluorescent dye (CM-H_2DCFDA). Briefly, T80 and OVCAR3 cells were seeded in 96-well plates for 2 days. After treatment with various agents, including GQDs, GQD-FA-DOX, GQD-DOX, and DOX, for 24 hours, 5 μMCM-H_2DCFDA dye was added, and the cells were incubated for 15 min at 37 °C. Then the mean intensity of fluorescence of 2',7'-dichlorofluorescein (DCF) was determined using a Synergy H4 hybrid microplate reader upon 485 nm excitation and detection at 525 nm. The fluorescence was measured every 5 min for 45 min. The results were given as the relative value to the control in percentage. Cell-free test has been done without any interference due to different excitation/emission between GQDs and DCF. LPS was used as the positive control in parallel experiments. Each experiment was performed three different times (i.e. on three different days) and each time it was run in triplicates.

3.2.6 Quantification of Apoptosis

Apoptotic cells were detected using the FITC Annexin V apoptosis kit (eBiosciences, San Diego, CA, USA) according to the manufacturer’s instruction. In brief, macrophages were incubated with different concentrations of GQDs and at different time points. Cells were washed with PBS, centrifuged and re-suspended in 100 μL binding buffer containing 5 μL of Annexin V-FITC and 5 μL of PI. After 15 min incubation at 37 ºC in the dark, cells were analyzed using flow cytometry.

3.2.7 Determination of Cellular Localization and Uptake

For the localization assay by confocal laser microscopy, the cells were seeded to eight-chamber slides. The cells were cultured for 24 h, washed thrice with PBS, and then incubated with GQD–FA-DOX (1µM) for 1h. After washing thrice with cold PBS, cells were incubated with Hoechst 33342 for nuclear staining. After 10 min, the cells were washed again with PBS buffer. Fluorescence of cells was observed using a confocal microscope (Olympus, Japan). Hoechst 33342 was excited with 405 nm laser, and the signal was collected from 425 nm to 475nm. GQDs and DOX were excited with a 488nm laser, and their signals were collected from 500 nm to 530 nm and 552 nm to 617 nm, respectively.

For the drug uptake quantification assay by flow cytometry, the cells were seeded to six-well plates. The cells were cultured for 24 h, washed thrice with PBS, and then incubated with GQD–FA-DOX and GQD-DOX (1µM) for 1h. Cells were then detached by 5% trypsin and washed with cold PBS. Cells were incubated with Hoechst 33342 for nuclear staining. After 10 min, the cells were washed again with PBS buffer and observed by flow cytometry (Olympus, Japan).

3.2.8 Western Blotting Assay

The membrane proteins of OVCAR3 and T80 cells were extracted using the Mem-PER Plus Membrane Protein Extraction kit following the manufacturer's protocol and previous published method [204]. The concentration of the proteins was quantified by BCA assay. Proteins were diluted in 4 × SDS-PAGE sample loading buffer (Bioworld, Atlanta, GA, USA) and denatured at

95 ºC for 10 min. An aliquot of total protein (20 μg) was added to the gel, and the proteins were electrophoresed on 12% SDS-PAGE mini gels and transferred onto PVDF membranes. Membranes were blocked at room temperature with 5% bovine serum albumin (BSA) in Tris-buffered saline Tween-20 (TBST) buffer and probed with targeted primary antibodies overnight in the cold room; then they were blotted with the respective secondary antibody. Visualization was performed using the BioRad system (Hercules, CA, USA) with an electro-chemiluminescence substrate. Protein level was normalized to the matching densitometric value of an internal control.

3.2.9 Statistical Analysis

Statistical analysis was performed using the Prism GraphPad software (Chicago, IL, USA). All experiments were performed at least three independent times in triplicate. All mean values are presented with the standard deviation. Treatment effects were analyzed using one-way analysis of variance (ANOVA). The differences between groups were tested by Tukey's multiple range tests with $p < 0.05$ considered as statistically significant.

3.3 Results and Discussions

3.3.1 FR Expression by OVCAR3 Ovarian Cancer &T80 Normal Epithelial Cells

FR is a glycosyl-phosphatidylinositol-anchored protein on the membrane[205]. The localization of FR usually on the cell membrane, but some studies also indicated FR can translocate to the nucleus[206]. In this dissertation, FR was used as the receptor for GQDs-FA-DOX to specifically target the tumor cells. Therefore, the relative expression levels of FR on cell membrane were important to define the cell models. Thus, the whole membrane proteins of OVCAR3 and T80 cells were extracted and the FR expression level was determined by western blotting assay. Figure 3.1 is the representative western blotting imaging and the quantitative bar graph of the FR expression in OVCAR3 cells and T80 cells. The FR expression in OVCAR3 cells was 13.3-folder higher than that of T80 cells. Therefore, OVCAR3 cells were used as FR-positive cell model in this dissertation, while T80 cells were used as the FR-negative model.

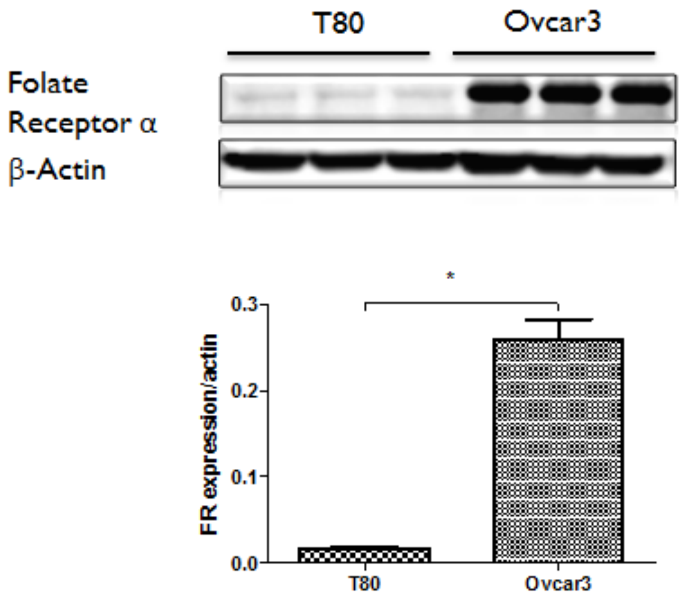

Figure 3.1 Western blotting imaging and the quantitative bar graph of the FR expression in T80 and OVCAR3 cells. Data are presented as the mean ± SD from three independent experiments. * $p < 0.05$; by one-way ANOVA.

3.3.2 Uptake of GQDs-FA-DOX by Ovarian Cancer and Normal Epithelial Cells

The uptake of GQDs-FA-DOX by ovarian cancer & normal epithelial cells were examined using confocal laser microscopy. Figure 3.2 illustrates the images obtained from confocal laser microscope. Figure 3.2(A) illustrates the GQDs-FA-DOX uptake by OVCAR3 cells, Figure 3.2(B) is the OVCAR3 cells without GQDs-FA-DOX. Figure 3.2(C) illustrates the GQDs-FA-DOX uptake by T80 cells. Figure 3.2(D) illustrates the T80 cells without GQDs-FA-DOX. For each row, the first column was the green fluorescence from the GQDs, which indicates the localization of GQDs-FA-DOX in the cytosol. The second column illustrates the Hoechst 33342 staining of the nucleus of cells. The third column illustrates the images of cells under differential interference contrast (DIC). The fourth column illustrates the merged image of GQDs staining, Hoechst, and DIC illumination. DOX staining is not shown here since the fluorescent was quenched and no obvious signal could be obtained using the confocal microscopy. Compared the results of Figure 3.2 (A) with that of Figure 3.2 (B), it is obvious that the GQDs-FA-DOX can enter into the FR overexpressed OVCAR3 cells based on the strong bright green fluorescent signalin Figure 3.2 (A). In the current experiment condition, the ratio of the DDS uptake and binding surface was unable to quantitate. However, the relative ratio of the uptake in OVCAR3 cells and T80 cells were determined using flow cytometry in later results. In Figure 3.2 (D), T80 cells has some auto-fluorescent signal even without the GQDs-FA-DOX. The results of incubation of GQDs-FA-DOX with FR negative expressed cells are shown in Figure 3.2 (D), and no significant change in the fluorescent intensity is observed. This may be due to no uptake of GQDs-FA-DOX by T80 cells. Therefore, GQDs-FA-DOX can specifically target FR-overexpressed ovarian cancers without entering the ovarian normal cells, which is a favorable property for the nano drug delivery system.

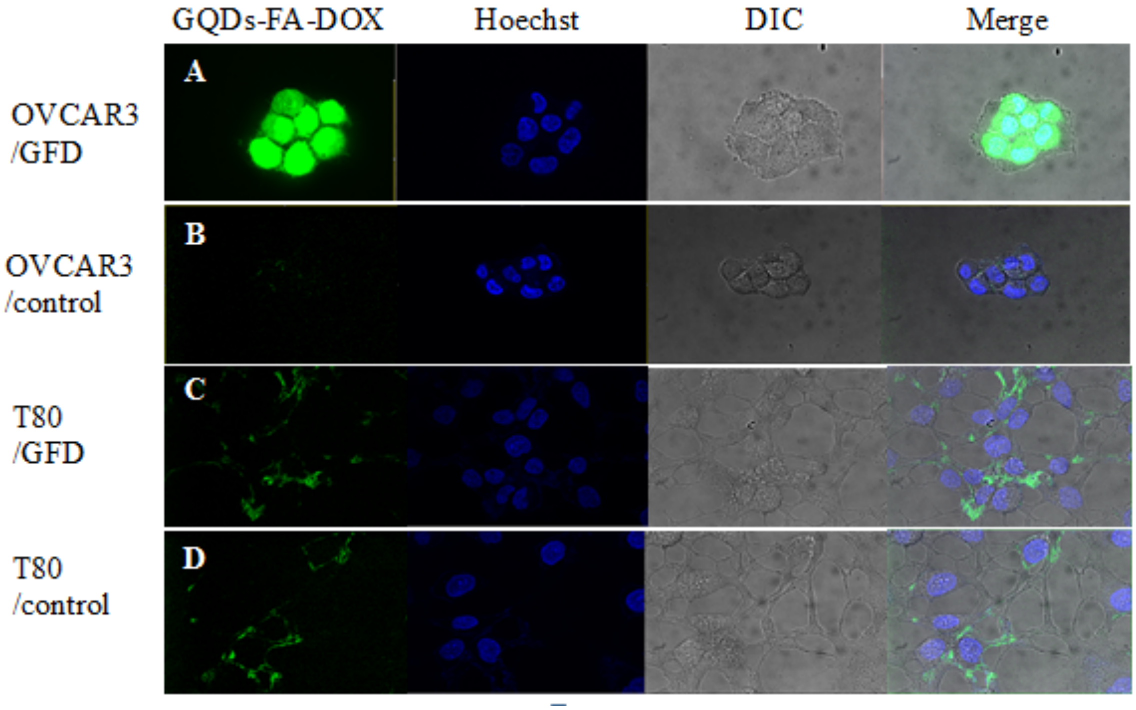

Figure 3.2 Confocal microscopy imaging for GFD or GD treatment to OVCAR3 cells or T80 cells for 30 minutes

The quantitative measurement of GQDs-FA-DOX uptake by ovarian cancer and normal epithelial cells were examined using flow cytometry. Figure 3.3(A) and (C) represent histograms of T80 cells and OVCAR3 cells without any treatment as controls while (B) and (D) were histograms of T80 cells and OVCAR3 cells treated with GQDs-FA-DOX for 30 min. Figure 3.3(E) is the quantitative bar graph of the fluorescent intensity of GQDs-FA-DOX. It is obvious that for OVCAR3 cells, untreated cells barely had a fluorescent signal, while GQDs-FA-DOX treated cells presented a significant increase in green fluorescence. However, there was no significant change between treated T80 cells and untreated T80 cells. The treated OVCAR3 cells had a significant 20 folder higher fluorescent intensity than the treated T80 cells. Figure 3.3 (F) shows the percentage of cells that uptake GQDs-FA-DOX. Define the gate to set both control group as zero percent, and the 25% of T80 cells may uptake GQDs-FA-DOX, while 100% of OVCAR3 cells uptake GQDs-FA-DOX. Those results confirmed that GQDs-FA-DOX specifically entered into FR overexpressed ovarian cancers without entering the ovarian normal cells, indicating a desired targeting effect for the nano drug delivery system.

To determine whether the targeting effect was based on FR or not, folic acid was used to competitively inhibit the binding of GQDs-FA-DOX (GFD) to the FR. After 30 min incubation with free FA, GQDs-FA-DOX was added into the OVCAR3 cells and the cellular fluorescent intensity of GQDs-FA-DOX was examined by flow cytometry. Figure 3.4 (A), (B), and (C) are histograms of untreated, GQDs-FA-DOX treated, and FA+ GQDs-FA-DOX treated OVCAR3 cells, respectively. The FA significantly decreased the cellular fluorescent intensity of GQDs-FA-DOX by 70% percent as shown in Figure 3.4 (D). Figure 3.4(E) showed a one-quarter decrease of the uptake cell percentage. The extend of decreasing in uptake cell percentage was less than the decreasing of the fluorescent intensity, which may be due to the fact that the FA binding to FR is a dynamic process and FA is a competitive inhibitor, which would not completely inhibit the binding between GQDs-FA-DOX and FR.

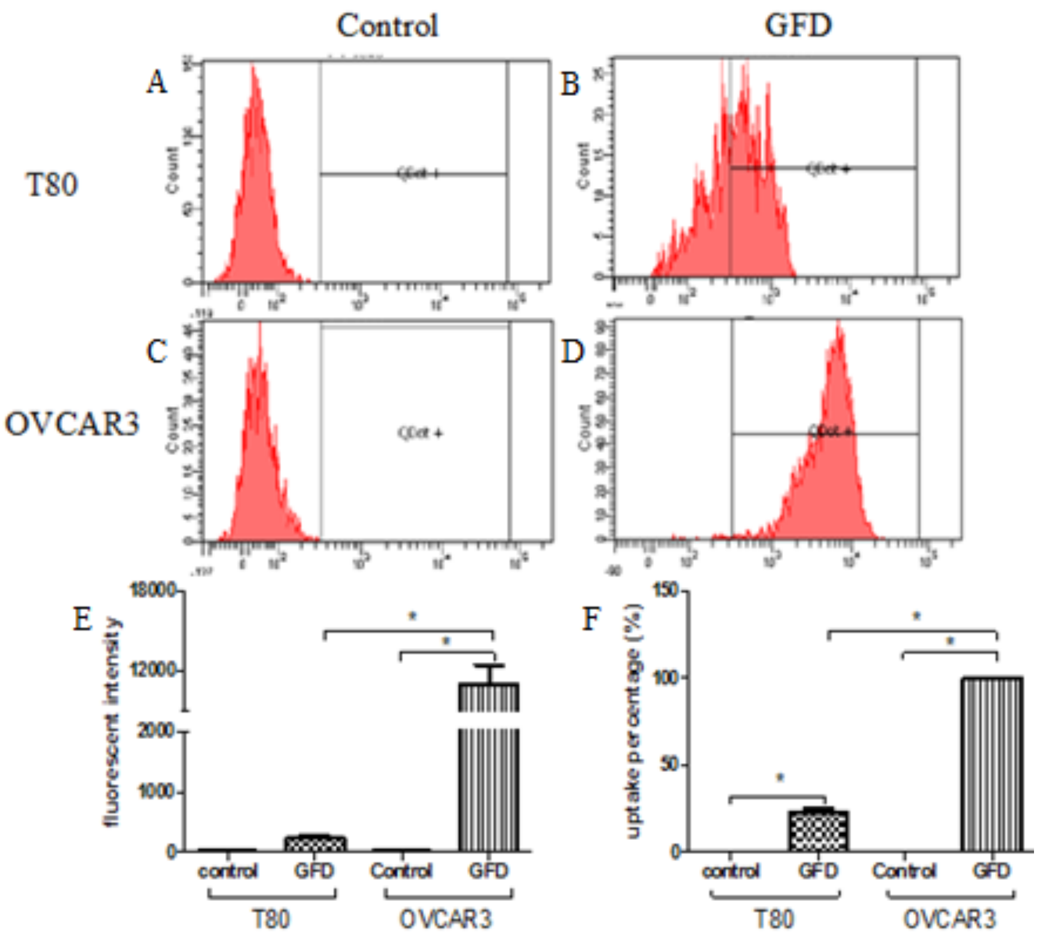

Figure 3.3 Quantitative measurement of uptake GFD by T80 and OVCAR3 cells using flow cytometry. Data are presented as the mean ± SD from three independent experiments. * $p < 0.05$; by one-way ANOVA.

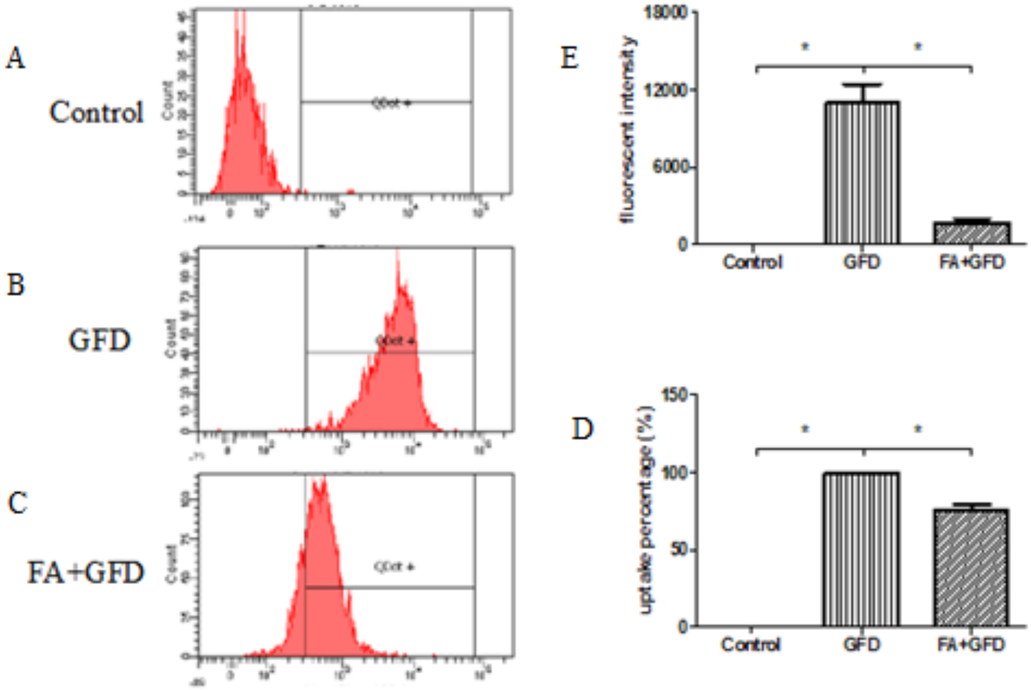

Figure 3.4 Quantitative measurement of uptake GFD inhibited by folic acid treatment 30 minutes before treated with GFD by OVCAR3 cells using flow cytometry. Data are presented as the mean ± SD from three independent experiments. * $p < 0.05$; by one-way ANOVA.

3.3.3 Effect of GQDs-FA-DOX on Cellular Viability

To determine the effective dosage of GQDs-FA-DOX on ovarian cancer cells and normal cells, a dose-course MTT assay was undertaken on both T80 and OVCAR3 cells. The cells were treated with 0.25, 0.50, 1, 2, and 4 μM (equivalent to DOX concentration) GQDs-FA-DOX, GQDs-DOX, or DOX for 24 h. The corresponding IC_{50} for GQDs-FA-DOX, GQDs-DOX, or DOX in T80 cells was 5.05, 6.95, and 0.86 μM as shown in Figure 3.5(A). The corresponding IC_{50} for GQDs-FA-DOX, GQDs-DOX, or DOX in OVCAR3 cells was 1.70, 9.71, and 0.93 μM as shown in Figure 3.5(B). Therefore, the 1μM (equivalent to DOX concentration) of

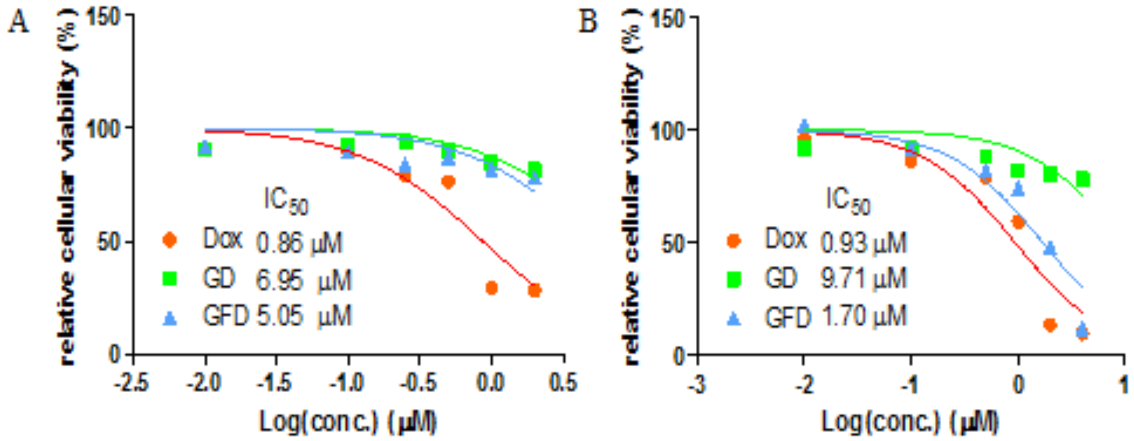

Figure 3.5 The IC50 of DOX, GQDs-DOX (GD) and GQD-FA-DOX (GFD) on (A) T80 and (B) OVCAR-3 for 24 hour treatment. Data are presented as the mean ± SD from three independent experiments.

GQDs-FA-DOX and GQDs-DOX were chosen as the working concentration in the following studies.

3.3.4 Effect of GQDs-FA-DOX on Colony Formation Ability

To determine the effectiveness of the GQDs based nano-drug delivery system, colony formation assay was used. The colony formation examines the ability of a single cell to grow into a colony. Figure 3.6 (A) exhibits the OVCAR3 cells and (B) T80 cells grown for 14 days after being treated for 24 hours naturally, GQDs, GQD-DOX, GQD-FA-DOX, FA+GQD-FA-DOX, and DOX, from left to right. For OVCAR3 cells, colony numbers and sizes of GQDs, GQDs-DOX, and FA pre-treated 30 min then treated with GQDs-FA-DOX had no significant difference. However, GQDs-FA-DOX and DOX treated OVCAR3 had a significant decrease in OVCAR3 colony numbers and sizes comparing to the untreated control group. For T80 cells,

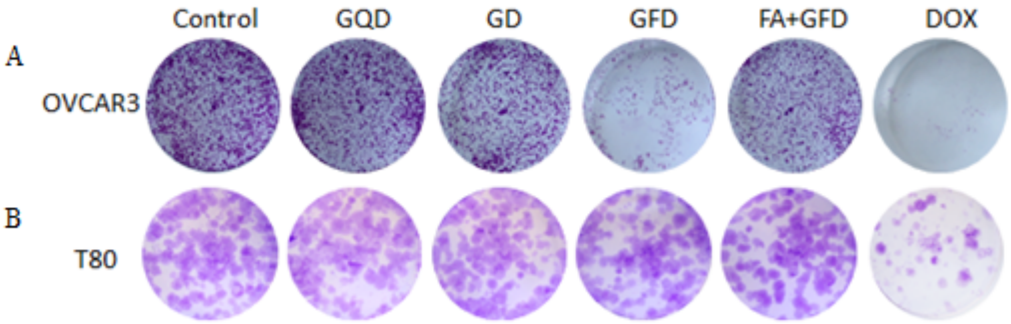

Figure 3.6 colony formation assay of (A) OVCAR3 and (B) T80 cells.

there was no difference for GQDs, GQD-DOX, GQD-FA-DOX, and FA+GQD-FA-DOX in colony numbers and sizes comparing to the control group. Only the DOX treated groups had a significant decrease. Therefore, GQD-FA-DOX selectively inhibited the colony growth in OVCAR3 cells, suggesting a desired targeting and therapeutic effect to FR overexpressed ovarian cancer cells.

3.3.5 Effect of GQDs-FA-DOX on ROS Generation

The ROS-induced injury is known as an important mechanism of DOX's antitumor activity. Therefore, ROS generation of OVCAR3 and T80 cells was examined. As shown in Figure 3.7(A), after 24 h of treatment, GQDs-FA-DOX significantly increased ROS in OVCAR3 cells by 2.2 folds, while GQDs-DOX and GQDs did not significantly increase ROS.. FA treatment for 30 min before the GQDs-FA-DOX treatment for 24 hours also significantly decrease the ROS generation comparing to those treated with GQDs-FA-DOX but without FA. Figure 3.7 (B) shows ROS generation for the same treatment with the T80 cells. Only the positive controls

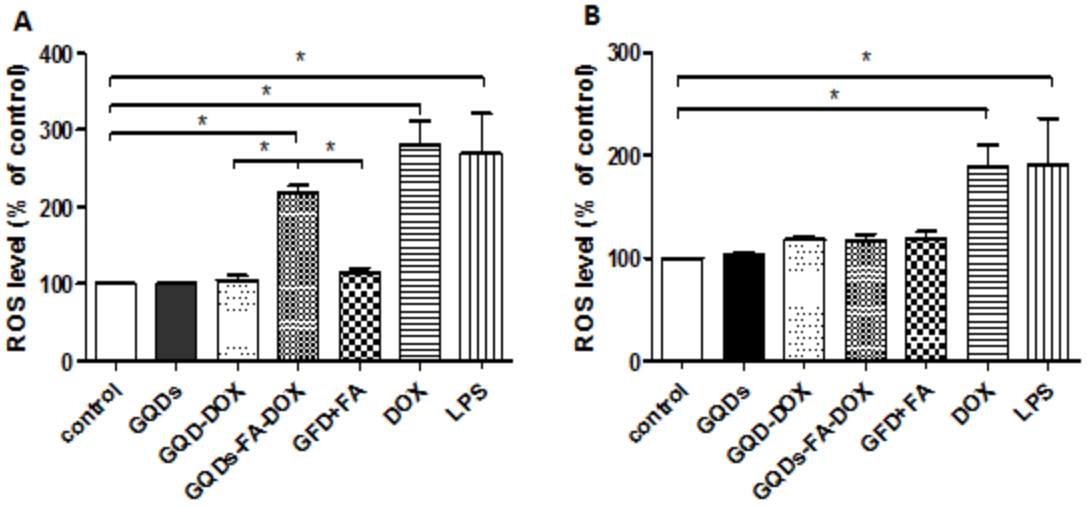

Figure 3.7 The ROS generation of GQDs, GQDs-DOX (GD) and GQD-FA-DOX (GFD), FA+GQDs-FA-DOX, DOX, and LPS on (A) T80 and (B) OVCAR-3 for 24 hour treatment. Data are presented as the mean ± SD from three independent experiments. * $p < 0.05$; by one-way ANOVA.

DOX and LPS significantly increased the ROS generation, but GQDs-FA-DOX has no significant effect on ROS generation in T80 cells. Therefore, GQDs-FA-DOX would selectively target the OVCAR3 cells and increased its ROS generation, and FA inhibited this process.

3.3.6 Apoptosis Effect of GQDs-FA-DOX on Ovarian Cancer and Normal Epithelial Cells

To further examine the anti-cancer effect of GQDs-FA-DOX on ovarian cancer cells, the effect of various nano-systems on cellular apoptosis was quantified by flow cytometry using Annexin-V-FITC and PI staining. The T80 cells and OVCAR3 cells were treated with GQDs, GQDs-DOX (GD) and GQD-FA-DOX (GFD), and DOX, respectively, for 24 hours. The number of apoptotic cells without any treatment for both cell lines were 3-5.0% (early + late apoptosis). As shown in Figure 3.8 (A), DOX alone caused significant apoptosis in T80 cells, while GQDs-FA-DOX had no effect on T80 cells. However, for OVCAR3 cells, GQDs-FA-DOX

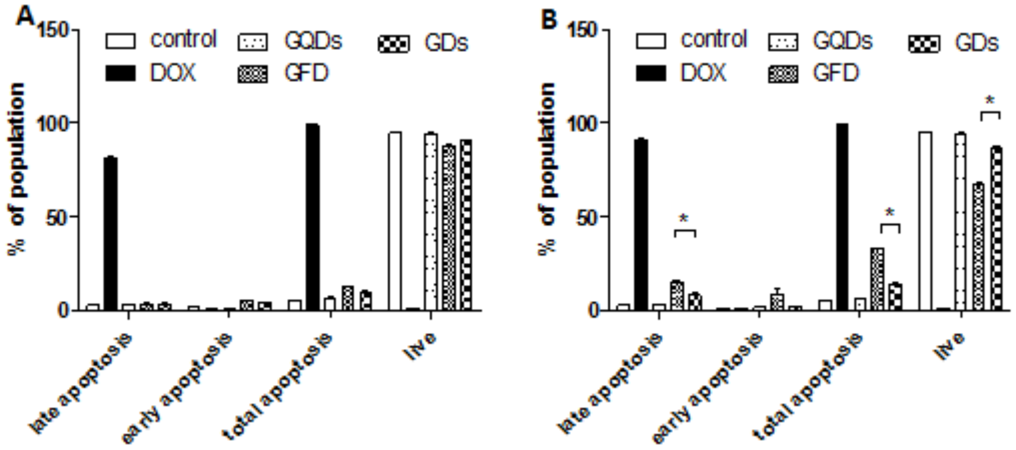

Figure 3.8 The apoptosis effect of DOX, GQDs, GQDs-DOX, and GQD-FA-DOX on (A) T80 and (B) OVCAR-3 for 24 hour treatment. Data are presented as the mean ± SD from three independent experiments. * $p < 0.05$; by one-way ANOVA.

caused significant apoptosis (i.e., 42%) comparing to the untreated group or the GQDs-DOX group. Therefore, it was apparent that GQDs-FA-DOX could selectively lead to the apoptosis of ovarian cancer cells, but had a very limited effect on the apoptosis of normal ovarian epithelial cells.

3.4 Conclusion

In this chapter, the anti-cancer effect of the novel GQDs-based NDDS, GQDs-FA-DOX, was validated. Luminescent GQDs enabled the real-time tracking of the cell uptake and drug distribution. The targeted ligand FA for such GQDs-based NDDS effectively and selectively targeted the FR ovarian cancer cells. Overall, GQDs-FA-DOX presented a desired therapeutic effect to ovarian cancer cells with no side effects on ovarian normal cells, indicating a potential tumor-targeted drug to the ovarian cancer treatment. My current studies on GQDs based NDDS will not only benefit ovarian cancer therapy, but also could be extended to the therapy of other cancers by loading appropriate targeting ligand and therapeutic compounds.

CHAPTER 4: ELUCIDATION OF GQDs IMMUNOTOXICITY[1]

Abstract

The biomedical application of graphene quantum dots (GQDs) is a new emerging area. However, data addressing their safety is scarce. Particularly, the effect of GQDs on the immune system remains unknown. This chapter describes studies addressing the interaction of GQDs with macrophages and the underlying mechanisms. We show that GQDs slightly reduce macrophage cell viability and membrane integrity, and correspondingly increase reactive oxygen species (ROS) generation and apoptotic and autophagic cell death. Treatment with GQDs increase in the expression level of Bax, Bad, caspase 3, caspase 9, beclin 1, and LC3-I/II, and a decrease in Bcl-2. Furthermore, low concentrations of GQDs significantly increased the expression of tumor necrosis factor-α (TNF-α), interleukin-1β (IL-1β), IL-8, whereas high concentrations of GQDs elicited opposite effects on the production of cytokines. SB202190, a selective inhibitor of p38 mitogen-activated protein kinase (MAPK), abolished the cytokine-inducing effect of GQDs in macrophages. Moreover, GQDs significantly increased the phosphorylation of p38 MAPK and p65, and promoted the nuclear translocation of nuclear

---

[1] This chapter has been reprinted from Toxicology, 327, Qin, Y., et. al., *Graphene quantum dots induce apoptosis, autophagy, and inflammatory response via p38 mitogen-activated protein kinase and nuclear factor-kappaB mediated signaling pathways in activated THP-1 macrophages*, p. 62-76, 2015, with permission from Elsevier. Permission documentation may be found in the Appendix.

factor-κB (NF-κB). Taken together, these results show that GQDs induce ROS generation, apoptosis, autophagy, and inflammatory response via p38MAPK and NF-κB mediated signaling pathways in THP-1 activated macrophages.

4.1 Introduction

The increasing interest in the biomedical application of GQDs, it raises a concern on the potential organ toxicities of GQDs. Currently, the most widely used QDs are made from cadmium and selenium which possess remarkable cytotoxic effects[207]. Due to the distinct physico-chemical features between GQDs and QDs, it has been suggested that GQDs could be a new type of nanomaterial with improved compatibility with the biological system and its cytotoxic effect has been examined in a number of cancer cell models[195, 201, 208, 209]. For example, Zhang's group compared the GQDs' cytotoxicity with micrometer-sized GO and the results suggested that small-sized GQDs exhibited a low cytotoxicity in gastric and breast cancer cells[195]. Moreover, the cytotoxic effect of structurally modified GQDs was also examined. Yuan et al. reported a low cytotoxic effect of GQDs with several modifications on functional groups, including -NH2, COOH and CO-N(CH3)2 in lung cancer cell model[208]. Furthermore, the distribution and toxicology of GQDs have been examined in vivo, and it showed no obvious toxicity in mice[201]. Above all, there is the lack of information on the modulatory effect of GQDs on the immune system. Human immune system is the first and foremost safeguard of the body against infection, malignancy, and xenobiotic exposure. The immune system also interacts with almost all other organ systems.

Due to the key role of the immune system as the primary defense mechanisms against infectious agents and xenobiotic exposure, undesired suppression or stimulation of immune system is harmful to the body. Thus, the unfavorable effect of GQDs on immune system will compromise the biomedical application of GQDs. However, the interaction of GQDs with the immune system is unknown, and the related mechanism is unclear. In this regard, we attempted to evaluate the immunotoxicity and the underlying mechanism of newly synthesized GQDs in macrophages.

4.2 Materials and Methods

4.2.1 Chemical and Reagents

Phorbol myristate acetate (PMA), PI, DMSO, MTT, *N*-acetyl-L-cysteine (NAC, a ROS scavenger), apocynin (APO), diphenyleneiodonium (DPI), Nω-nitro-L-arginine methyl ester hydrochloride (L-NAME), lipopolysaccharide (LPS), DOX, and sodium azide (NaN_3) were purchased from Sigma-Aldrich Inc. (St. Louis, MO, USA). SB202190 [4-(4-fluorophenyl)-2-(4-hydroxyphenyl)-5-(4-pyridyl)1*H*-imidazole (SB), a selective inhibitor of p38 mitogen-activated protein kinase (MAPK) used as an autophagy inducer], CM-H_2DCFDA, RPMI 1640 medium, fetal bovine serum (FBS), penicillin and streptomycin, and PBS were obtained from Invitrogen Inc. (Carlsbad, CA, USA). Rapamycin (RAP), an autophagy inducer, and Hoechst 33342, a nucleus staining dye, were purchased from Enzo Life Sciences Inc. (Farmingdale, NY, USA). The polyvinylidene difluoride (PVDF) membrane was purchased from Millipore Inc. (Bedford, MA, USA). Primary monoclonal antibodies against human Bcl 2, Bax, Bad, caspase 9, cleaved caspase 3, microtubule-associated protein 1A/1B-light chain 3 (LC3)-I/II, beclin 1, nuclear factor-κB (NF-κB) p65, E-cadherin, zinc finger E-box binding homeobox (TCF-8/ZEB1), vimentin, β-catenin, snail, and phosphorylated (p-) NF-κB at Ser536, p38 MAPK and p-p38 MAPK at Thr180/Tyr182 were purchased from Cell Signaling Technology Inc. (Beverly, MA, USA). The antibodies against human β-actin and histone 3 and NF-κB Inhibitor CAS 213546-53-3 (CAS) were purchased from Santa Cruz Biotechnology Inc. (Santa Cruz, CA, USA). Visualization was performed using BioRad system (Hercules, CA, USA) with electro-chemiluminescence substrate (Hudson, NH, USA).

4.2.2 Cell Culture

THP-1 derived macrophage cells were widely used to examine the immunotoxicity of nanoparticles[210, 211]. The THP-1 monocyte cell line obtained from American Type Culture Collection (Manassas, VA, USA) was cultured in RPMI1640 medium containing 10% non-heated-inactivated FBS and 0.5% penicillin and streptomycin in a humidified incubator of 5% CO_2/95% air at 37 ℃. Cells were suspended in the culture medium. Upon reaching confluence, differentiation into macrophage-like cells was performed by adding 12.4 ng/ml PMA and then cells were incubated for 48 h before the further experiment.

4.2.3 Cell Viability and Membrane Integrity Assay

PMA-induced macrophages from THP-1 cells were treated with various concentrations of GQDs (5, 10, 50, 100, and 500 μg/ml) for 24 h. Cell viability was determined by the MTT assay. In brief, the cells were treated with GQDs, 10 μL MTT (5 mg/ml) was added to each well and the cell were incubated for 4 h, then the culture medium was removed and 100 μL DMSO was added to dissolve formazan crystals. Absorbance was recorded at 560 nm for formazan and 670 nm for background using the Synergy H4 hybrid multi-mode microplate reader (BioTek). The results were given as relative value to the control in percent. The membrane integrity was evaluated by testing the level of lactate dehydrogenase (LDH) using the CytoTox-ONE kit (Promega, Madison, WI, USA). PMA-activated macrophages were treated with different concentrations of GQDs over 48 h. The culture medium was collected and released LDH was measured by converting resazurin into fluorescent resorufin. Each experiment was performed three different times (i.e. on three different days) and each time it was run in triplicates.

4.2.4 Measurement of Intracellular ROS Levels

Intracellular ROS level was determined using a fluorescent dye (CM-H_2DCFDA). Briefly, macrophages in 96-well plates were treated with GQDs at different concentrations over 72 h. The mean intensity of fluorescence of 2',7'-dichlorofluorescein (DCF) was determined using a Synergy H4 hybrid microplate reader upon 485 nm excitation and 525 nm for detection. The fluorescence was measured every 5 min for 45 min. The results were given as the relative value to the control in percentage. Cell-free test has been done without any interference due to different excitation/emission between GQDs and DCF. LPS was used as the positive control in parallel experiments. Each experiment was performed three different times (i.e. on three different days) and each time it was run in triplicates.

4.2.5 Determination of the Effect of GQDs on Cell Cycle Distribution

The effect of GQDs on cell cycle distribution of activated macrophages was evaluated using PI as the DNA stain by flow cytometry as described previously[208].Briefly, macrophages were treated with GQDs at concentrations of 10, 50, 100, and 200μg/ml for 24 h. In separate experiments, THP-1 cells were treated with 100 μg/ml GQDs for 4, 8, 24, 48, and 72 h, respectively. Cells were trypsinized and then fixed with 70% ethanol at 4°C overnight. The cells were incubated with 50 μg/ml PI and ribonuclease at 37ºC in the dark for 30 min. A total number of 1×10^4 cells were subject to cell cycle analysis using a flow cytometer. Each experiment was performed three different times (i.e. on three different days) and each time it was run in triplicates.

4.2.6 Quantification of Cellular Apoptosis and Autophagy by Flow Cytometry

Apoptotic cells were detected by FITC Annexin V apoptosis kit (eBiosciences, San Diego, CA, USA) according to the manufacturer's instruction. In brief, macrophages were incubated with different concentrations of GQDs and different time points. Cells were washed with PBS, centrifuged and re-suspended in 100 μL binding buffer containing 5 μL of Annexin V-FITC and

5 μL of PI. After 15 min incubation at 37 ºC in the dark, cells were analyzed using a flow cytometer. Autophagy was quantified by measuring the dye-stained autolysosomes in the cells using Cyto-ID autophagy detection kit (Enzo Life Sciences Inc., Farmingdale, NY, USA). After treatment with GQDs for different times, the THP-1 derived macrophages were washed with PBS and re-suspended in 100 μL assay buffer containing 5 μL green detection reagent. After incubation for 10 min at 37 °C, cells were washed with assay buffer and analyzed using flow cytometry. DOX was used as the positive control for induction of apoptosis in parallel experiments. In addition, Rap was used as the positive control for autophagy induction in parallel experiments. Each experiment was performed three different times (i.e. on three different days) and each time it was run in triplicates.

4.2.7 Western Blotting Assay

Cells were harvested and lysed with radioimmunoprecipitation assay (RIPA) lysis buffer (Pierce, Rockford, IL, USA) with protease inhibitor cocktail and centrifuged at 3,000 *g* for 10 min at 4 °C. Proteins were resuspended in 4 × sodium dodecyl sulfate polyacrylamide gel electrophoresis (SDS-PAGE) sample loading buffer (Bioworld, Atlanta, GA, USA) and denatured at 95 ºC for 10 min. An aliquot of total protein (20 μg) was electrophoresed on 12% SDS-PAGE mini gels and transferred onto PVDF membranes. Membranes were blocked at room temperature with 5% bovine serum albumin in Tris-buffered saline Tween-20 (TBST) buffer and probed with targeted primary antibodies overnight at cold room and then blotted with the respective secondary antibody. Visualization was performed using BioRad system (Hercules, CA, USA) with the electro-chemiluminescence substrate. Protein level was normalized to the matching densitometric value of internal control. Each experiment was performed three different times (i.e. on three different days) and each time it was run in triplicates.

4.2.8 Total RNA Isolation and Quantitation by Real-Time Polymerase Chain Reaction (PCR)

THP-1 derived macrophages were treated with GQDs for 6 h before RNA harvesting, Trizol reagent (Invitrogen, Carlsbad, CA, USA) was used to extracting total RNA. Reverse transcription of total RNA to single-stranded cDNA was performed using the iScript reverse transcriptase supplied with the iScript cDNA Synthesis Kit (Bio-Rad Laboratories, Hercules, CA, USA). Reverse transcription amplification was performed using a LightCycler thermal cycler system and quantitative real-time PCR with the use of FastStart Universal Probe Master (Roche Diagnostics Co., Indianapolis, IN, USA). Pro-inflammation probe sets for human tumor necrosis factor-α (TNF-α), interleukin (IL)-1β, IL-8, and glyceraldehyde-3-phosphate dehydrogenase (GAPDH) genes were purchased from Integrated DNA Technologies Inc. (Coralville, IA, USA). The relative amount of target mRNA was calculated by the comparative cycle threshold method with *GAPDH* as the internal reference and expressed as the percentage change relative to untreated controls. Quantification data were corrected for reaction efficiencies. LPS was used as the positive control. Each experiment was performed three different times (i.e. on three different days) and each time it was run in triplicates.

4.2.9 Enzyme-linked Immunosorbent Assay (ELISA)

The media levels of IL-8, and TNF-α after macrophage exposure to GQDs were determined by commercial ELISA Ready-SET-Go kits (eBioscience, San Diego, CA, USA) according to the manufacturer's instruction. In brief, the 96-well ELISA plate was incubated with 100 μL/well of coating buffer with capture antibody overnight at 4°C. Then the plate was washed 3 times with washing buffer (PBS with 0.05% Tween-20) and blocked by the assay diluent for 1 h at room temperature. After washing three times, 100 μL of detectionELISA antibody was added to each well and incubated for 1 h at room temperature followed by 3 times of wash. The plates were then incubated for 15 min at room temperature with 100 μL/well substrate solution and stopped by adding 50 μL of stop solution (1 M H_3PO_4) to each well. The absorbance at 450 nm was obtained using a H4 hybrid microplate reader for the IL-8 and TNF-α expression level analysis. Cell-free test has been done without any interference due to different absorbance of GQDs and detection wavelength of the ELISA reactions. LPS was used as the positive control in parallel experiments. Each experiment was performed three different times (i.e. on three different days) and each time it was run in triplicates.

4.2.10 Statistical Analysis

Statistical analysis was performed by Prism GraphPad software 6.0 (Chicago, IL, USA). All mean values are presented with the standard deviation. Treatment effects were analyzed using one-way analysis of variance (ANOVA). The differences between groups were tested by Tukey's multiple range tests with $p < 0.05$ considered as statistically significant.

4.3 Results and Discussion

4.3.1 Uptake of GQDs by THP-1-derived macrophages

The first question for the immunotoxicity of GQDs was whether the GQDs entered the macrophages or not. So the uptake of GQDs by macrophages was first examined by confocal microscopy. ThP-1 induced macrophages was incubated in the 8-well chamber and treated with GQDs for 1 hour. Bright field image of THP-1-derived macrophages was shown in

Figure 4.1 (A), Hoechst 33342 staining of the nucleus and localization of GQDs in the cytosol of THP-1-derived macrophages are shown in (B) and (C). The strong green fluorescent signal of GQDs was obtained in cytosol after 50 μg/mL GQD treatment for 1h.

Figure 4.1 (D) shows the merged image of nuclear staining and GQDs staining, which clearly showed that GQDs entered into the macrophages and located in the cytosol.

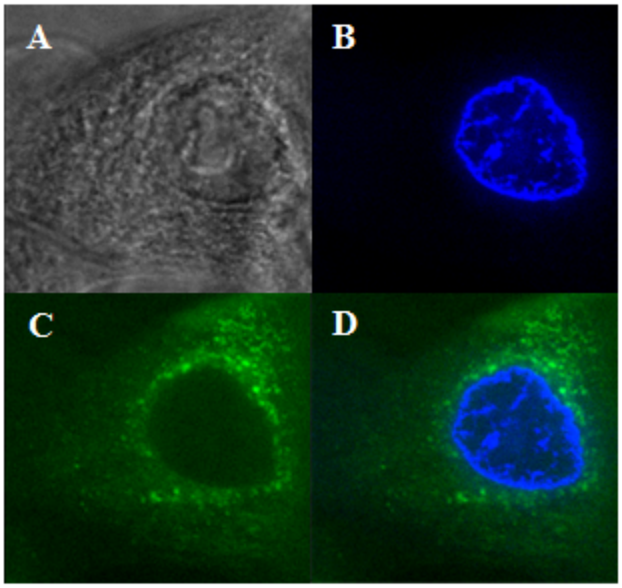

Figure 4.1 Uptake of GQDs (50 µg/ml, 1h) by THP-1-derived macrophages by confocal microscopy at a magnificationof 60 X. (A: Bright field image of THP-1-derived macrophages, B: Hoechst 33342 staining for nucleus, C: Localization of GQDs in cytosol of THP-1-derived macrophages, D: Merge of B and C).

4.3.2 Effect of GQDs on Cellular Viability and Membrane Integrity

Since GQDs definitely entered into the macrophages, the effect of GQDs on macrophages cellular viability was then examined using the MTT assay. THP-1 cells were treated with 12.4 ng/mL PMA and differentiated into macrophages. Subsequently, the macrophages were incubated with GQDs at concentrations of 1, 5, 10, 50, 100, and 200 µg/mL for 24 h, and the cell viability was found to be 103.6%, 106.8%, 98.3%, 95.8%, 93.8%, and 82.4%, respectively (Figure 4.2A). These GQDs concentrations were chosen on the basis of previous studies related to their cytotoxicity and bioactivity[195, 196, 201, 208]. Incubation of macrophages with GQDs for 48 h led to a lower cell viability than that of 24 h treatment. The cell viability was 95.6%, 92.7%, 92.2%, 87.3%, 76.1%, and 62.2%, respectively (Figure 4.2A). The IC_{50} value for GQDs was greater than 2000 and 400 μg/ml for 24 and 48 h, respectively.

To further evaluate the cytotoxic effect of GQDs on macrophages, the plasma membrane integrity was examined by measuring the extracellular level of LDH. Macrophages were treated with various concentrations of GQDs ranging from 1 to 200 μg/ml for 6 and 24 h. In comparison to the control group, there was no significant alteration in the extracellular LDH level (Figure 4.2B), whereas incubation of macrophages with lysis buffer, as a positive control, resulted in a 2.0-fold increase in the extracellular LDH level. These data demonstrated that GQDs had a low to moderate cytotoxicity towards THP-1-derived macrophages in a concentration-dependent manner.

Apart from the observations of favorable physicochemical properties of the as-synthesized GQDs, their immunotoxicity was evaluated in the present study as well. There was only a slight cytotoxicity of GQDs observed at low concentrations in macrophages with IC_{50} value greater than 2000 and 400 μg/ml for 24 and 48 h based on the MTT results. Moreover, GQDs did not damage the plasma membrane as shown in the LDH leakage assay. These results presented a favorable biological feature of GQDs with low cytotoxicity.

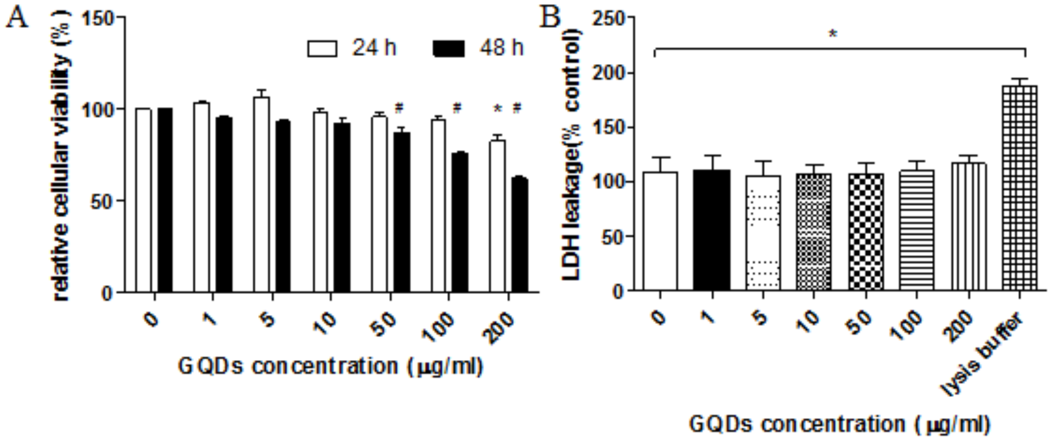

Figure 4.2 (A) Cell viability of THP-1-derived macrophages determined by the MTT assay in THP-1-derived macrophages. (B) Effects of GQDs on the plasma membrane integrity in THP-1-derived macrophages determined by LDH leakage. Data are presented as the mean ± SD from three independent experiments. *, # $p < 0.05$; by one-way ANOVA.

4.3.3 Effect of GQDs on Cell Cycle Distribution of Human Macrophages

In order to further determine the effect of GQDs on cell growth, the cell cycle distribution of macrophages was tested. The cells were treated with 100 µg/mL GQDs over 72 h. An increasing percentage of G1-delayed cells was found. A significant G1 phase arrest was observed at 72 h as shown in Figure 4.3(A). In separate experiments, incubation of cells with GQDs at concentrations of 10, 50, 100, and 200 µg/mL for 24 h caused a slight alteration in the percentage of cells in G1, G2/M, and S phases as shown in Figure 4.3(B). Only 200 µg/mL GQD treatment showed a statistical significance in G1 phase delay. Such results suggested that long time (72 h) or high concentration (200 µg/mL) GQD treatment had a significant effect on macrophage cell cycle distribution.

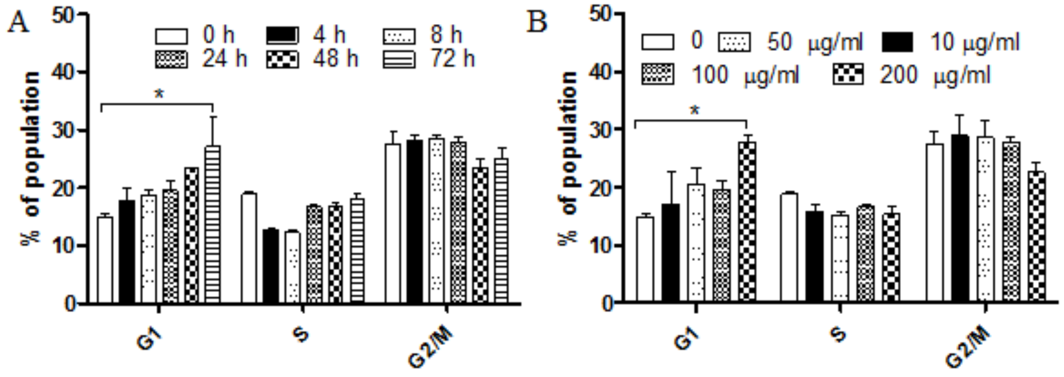

Figure 4.3 (A) Time-course and (B) dose–response effects of GQDs on the cell cycle in THP-1-derived macrophages determined by flow cytometry. Bar graphs showed the effects of GQDs on the cell cycle distribution of THP-1-derived macrophages. Data are presented as the mean ± SD from three independent experiments. * $p < 0.05$; by one-way ANOVA.

4.3.4 Effect of GQDs-induced Apoptosis In Macrophages

To further explore the mechanism of cytotoxic effect of GQDs on macrophages, the effect of GQDs on cellular apoptosis was quantified by flow cytometry analysis. The number of apoptotic cells without GQD treatment was 3-5.0% (early + late apoptosis) (Figure 4.4A-B). Macrophages exposed to GQDs at 10, 50, 100, and 200 μg/mL for 24 h caused slightly dose-dependent increase in the proportion of total apoptosis by 6.6%, 7.0%, 9.3%, and 14.4%, respectively (Figure 4.4A). Treatment of the cells with 200 μg/mL GQDs significantly increased the total apoptosis 2.9-fold and DOX (as a positive control) increased total apoptosis 7.9-fold. When the cells were treated with 100 μg/mL GQDs for 2, 4, or 8 h, there was no significant change in the apoptosis of the macrophages. When the incubation time was increased to 24 or 48 h, a significant increase in apoptosis was observed. Notably, the 48-h treatment increased the apoptosis 4.3-fold in macrophages (Figure 4.4B).

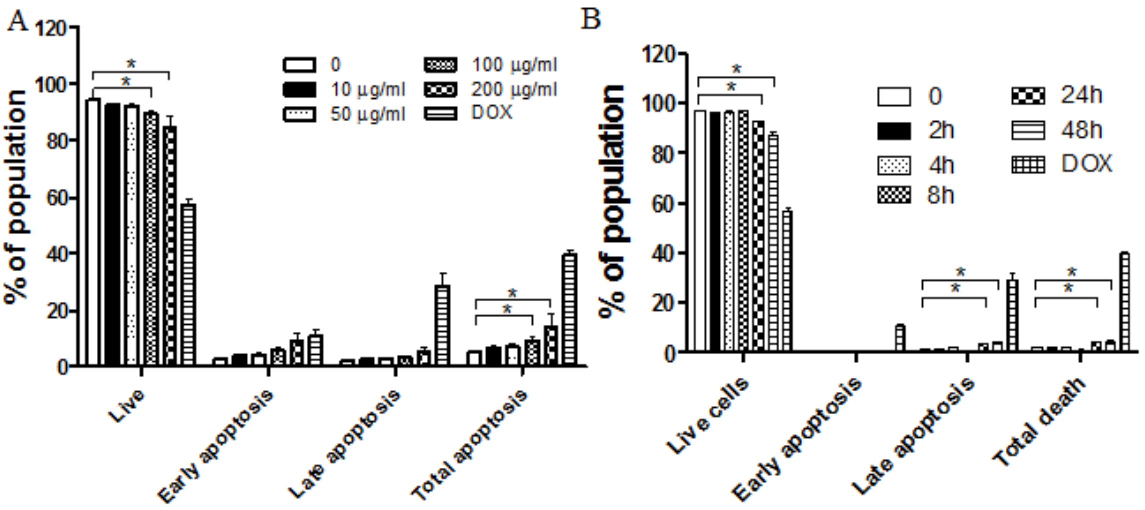

Figure 4.4 Effects of GQDs on the apoptosis of THP-1-derived macrophages determined by flow cytometry. (A) Dose–response and (B) time-course effect of GQDs on apoptosis in THP-1-derived macrophages by flow cytometry. *, # $p < 0.05$; by one-way ANOVA.

To further elucidate the underlying mechanism for the apoptosis-inducing effect of GQDs in macrophages, we investigated the effect of GQDs on mitochondria-related cell death pathway with a focus on Bcl-2, Bax, Bad, caspase 9, and caspase 3. As shown in Figure 4.5, treatment of the cells with GQDs at 50, 100, and 200 µg/mL decreased the expression of anti-apoptosis protein Bcl-2 by 4%, 23%, and 54%, respectively, while GQDs increased the expression levels of Bax and Bad. The expression level of Bad was increased 1.1- and 1.5-fold with the treatment of GQDs at concentrations of 100, and 200 µg/mL, respectively, and 1.8-, 2.2-, 2.9-, and 1.9-fold increase in Bax level with GQDs at concentrations of 10, 50, 100, and 200 µg/mL, respectively. Importantly, the ratio of Bcl-2 over Bax was significantly decreased by the exposure of GQDs at concentrations of 10, 50, 100, and 200 µg/mL. Furthermore, GQDs increased the levels of cleaved caspase 3 and cleaved caspase 9 in macrophages, while total caspase 9 expression level was decreased. Taken together, GQDs induced cell apoptosis via the mitochondria-related pathway involving the activation of caspase families.

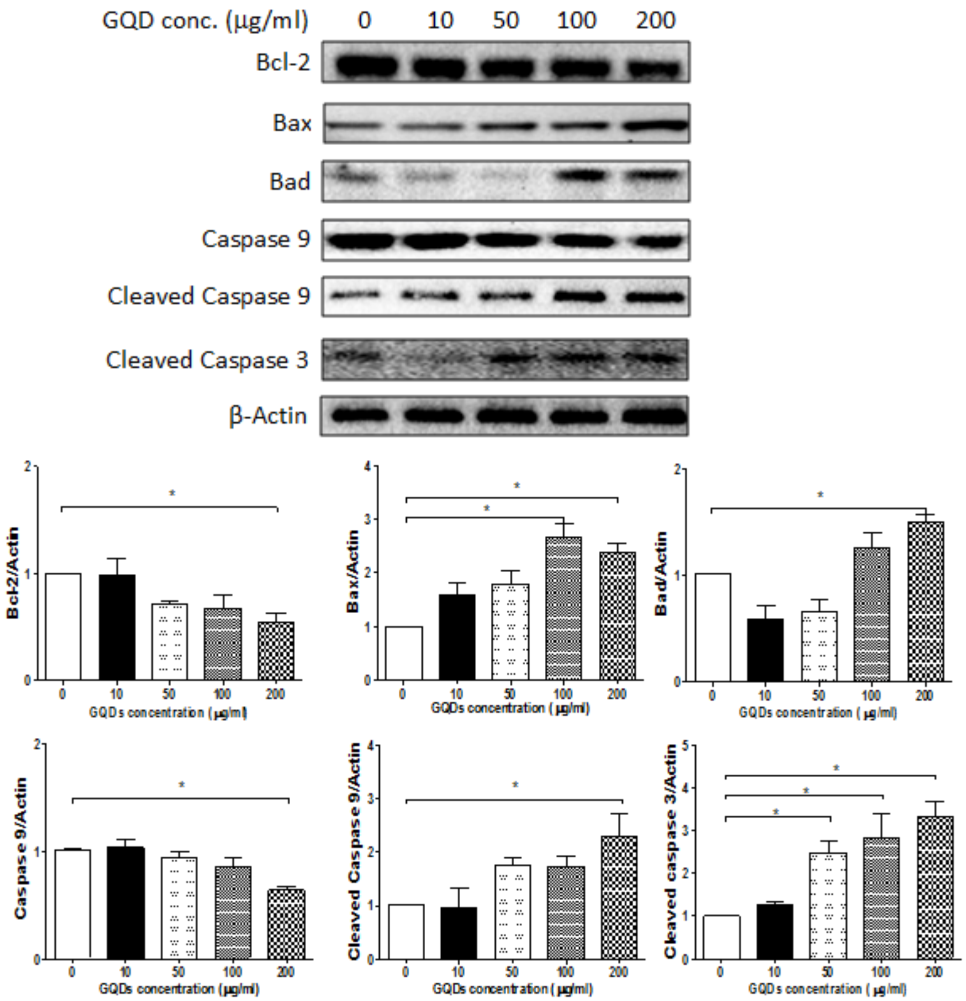

Figure 4.5 Representative Western blots of apoptosis-associated proteins including Bcl-2, Bax, Bad, caspase 9, cleaved caspase 9 and cleaved caspase 3. The bar graphs show the blot intensity mean ± SD. Data are presented as the mean ± SD. *$p < 0.05$; by one-way ANOVA.

4.3.5 GQDs induce autophagy in macrophages

Since we have observed the apoptotic effect of GQDs on macrophages, the autophagic effect of GQDs on macrophages was tested. As shown in Figure 4.6, there was a significant increase in autophagy in concentration- and time-dependent manners. The flow cytometry analysis suggested that GQDs increased the autophagy 2.0-, 4.2-, 4.6-, and 5.1-fold at 10, 50, 100, and 200 µg/mL, respectively (Figure 4.6A). When macrophages were exposed to 100 µg/mL GQDs for 8, 1,2, 24 and 48 h, the number of autophagic cells were increased 2.7-, 4.3-, 5.1-, 5.8-, and 6.4-fold ($p< 0.05$), respectively, compared to the control (Figure 4.6B).

I further examined the effect of GQDs on the expression of LC3-I/II and beclin 1 in macrophages. Incubation of cells with 10, 50, 100, and 200 µg/mL GQDs for 24 h resulted in 1.5-, 1.8-, 2.2-, and 2.3-fold increase in the expression of beclin 1, respectively. For LC3-I and II, GQDs increased the expression level for both LC3 forms ($p> 0.05$), however, the ratio of LC3-II over LC3-I was significantly increased 5.8- and 5.4-fold at 100 and 200 µg/mL GQD, respectively (Figure 4.7).

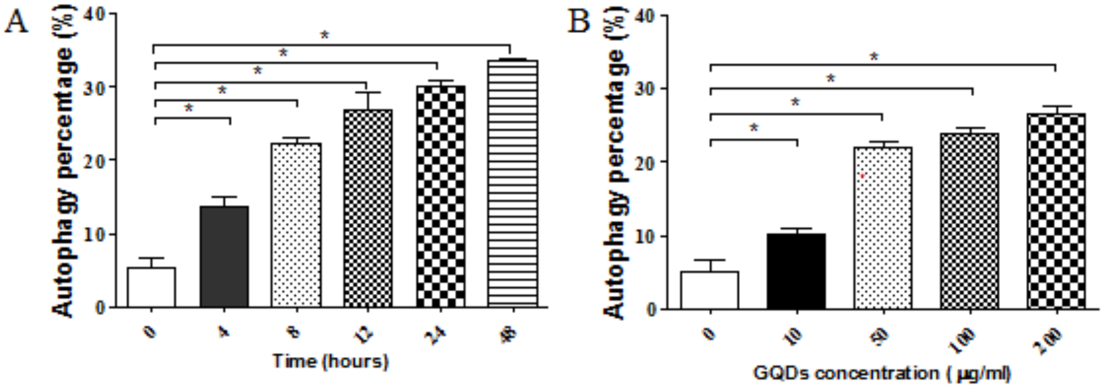

Figure 4.6 Effects of GQDs on the autophagy of THP-1-derived macrophages determined by flow cytometry and the underlying mechanisms. (A) Confocal microscopic images of autophagy in THP-1-derived macrophages treated with GQDs for 24 h. (B) Time-course and dose–response effect of GQDs on autophagy.Data are presented as the mean ± SD. $p < 0.05$; by one-way ANOVA.

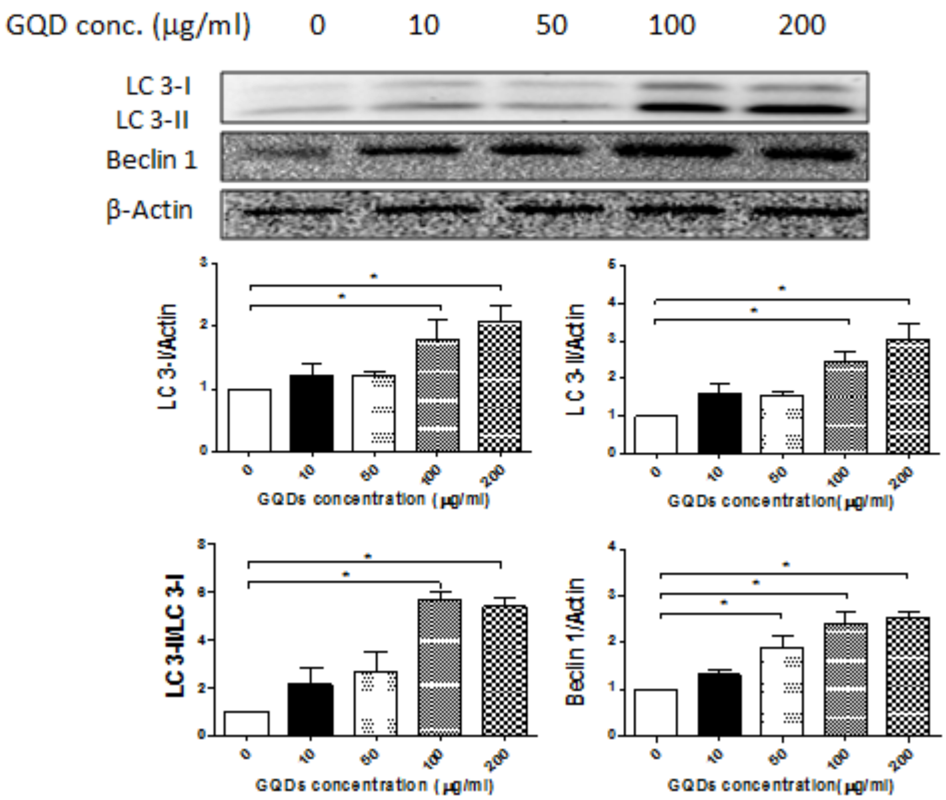

Figure 4.7 Representative Western blots of autophagy-associated proteins including LC3-I, LC3-II, and beclin 1. Bar graphs of the Western blot results. Data are presented as the mean ± SD. $p < 0.05$; by one-way ANOVA.

4.3.6 GQDs Increase Intracellular ROS Generation In Macrophages

ROS plays an important role in the inflammatory response and many other important biological processes and has been proposed as a main contributing factor to nano-toxicity in preclinical experimental models[212-214]. To further evaluate the immunotoxic effect of GQDs in macrophages, the effect of GQDs on ROS generation was examined. Macrophages were treated with GQDs at concentrations of 10, 50, 100, and 200 μg/mL for 24 h. There was a significant increase in the intracellular level of ROS. As shown Figure 4. 8, GQDs concentration-dependently enhanced the ROS generation, with a 1.4-, 1.6-, and 1.6-fold rise in the level of ROS at 50, 100, and 200 µg/mL GQDs, respectively (*p*< 0.05). In addition, LPS was used at the positive control to induce ROS generation in macrophages. The exposure of macrophages to 30 ng/mL LPS led to a 3.2-fold increase in the ROS level (Figure 4. 8A). In separate experiments, macrophages were treated with GQDs at 50 µg/mL for 1, 2, 4, 6, 8, 12, 24, 48, or 72 h. There was a significant elevation in ROS generation when cells were treated for 1 to 48 h (Figure 4. 8B). However, there was no significant effect of GQDs on ROS generation after cells were treated for 72 h (Figure 4. 8B).

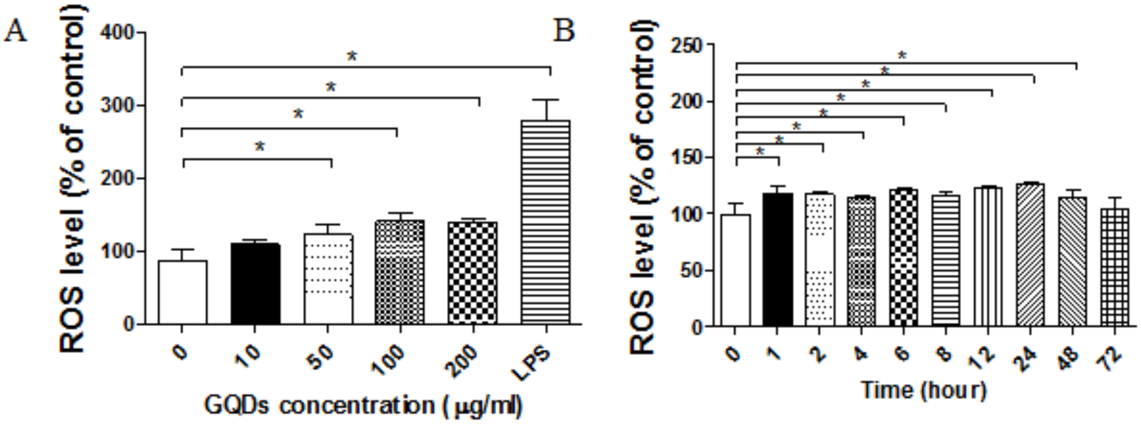

Figure 4. 8 Effects of GQDs on the ROS generation in THP-1-derived macrophages. (A) Effect on ROS production in THP-derived macrophages treated with GQDs at different concentrations for 24 h. (B) Effect on ROS production in THP-derived macrophages treated with 50 µg/mL GQDs for different exposure times. (C) Determination of the source of GQDs-induced ROS generation in THP-1-derived macrophages. Data are presented as the mean ± SD from three independent experiments. *p < 0.05; by one-way ANOVA.

Moreover, a number of intracellular sources contribute to ROS generation, including NADPH oxidase, nitric oxide (NO) synthase, xanthine oxidase[215]. Thus, several pharmacological agents were used in order to elicit the source of GQD-induced ROS generation. APO (an inhibitor of phagocytic NADPH oxidase), DPI (an inhibitor of flavoprotein-dependent oxidase), L-NAME (an inhibitor of NO synthase), or NAC (an antioxidant and a ROS scavenger) was separately added 30 minutes before the exposure to 50 µg/mL GQDs. APO at 100 µM, 5 µM DPI, 500 µM L-NAME, and 100 µM NAC decreased 40%, 47%, 21%, and 35% of the ROS production in macrophages incubated with 50 µg/mL GQDs (Figure 4.9), respectively. These data suggested that GQD-induced ROS production was mainly mediated by NADPH oxidase and with a lesser contribution by NO synthase. These findings indicated that GQDs induced ROS production in concentration- and time-dependent manners. GQD-induced ROS generation was associated with several oxidases, including NADPH oxidase and NO synthase.

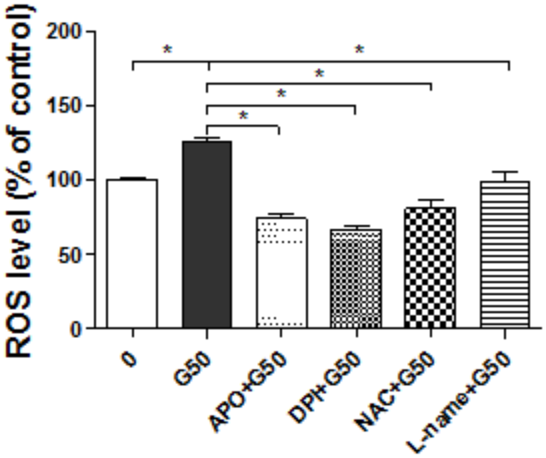

Figure 4.9 Determination of the source of GQDs-induced ROS generation in THP-1-derived macrophages. Data are presented as the mean ± SD from three independent experiments. $^*p < 0.05$; by one-way ANOVA.

4.3.7 GQDs Trigger Cytokine Production in Activated Macrophages

The effect of GQDs on the production of pro-inflammatory cytokines is one of the major possible perturbations of the immune response. The expression of cytokines was measured at transcriptional and posttranscriptional levels by RT-PCR and ELISA, respectively. As seen in Figure 4.10A, there was a similar gene expression profile of *TNF-α*, *IL-1β*, and *IL-8* after macrophages were treated with GQDs for 6 and 24 h. Exposure of cells to 10 and 50 µg/mL GQDs for 6 h increased 1.6- and1.3-fold in the expression of *IL-1β*, and 1.4-, and 1.7-fold in the expression of *IL-8*, respectively ($p < 0.05$). When the incubation time was increased to 24 h, there was a 1.6- and 1.3-fold increase in the expression of *IL-1β*, and 1.4-, and 1.7-fold in the expression of *IL-8* after cells were treated with 10 and 50 µg/mL GQDs, respectively ($p < 0.05$). There was only a slight increase in the expression of *TNF-α* with the treatment of 10 and 50 µg/mL GQDs for 6 and 24 h. However, incubation of cells with 100 and 200 µg/mL GQDs significantly decreased the expression of *TNF-α*, *IL-1β*, and *IL-8*.

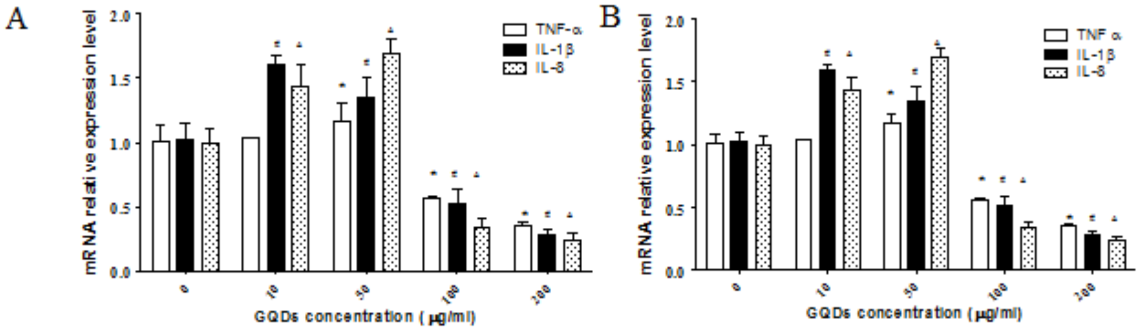

Figure 4.10 Effects of GQDs on the mRNA levels of TNF-α, IL-1β, and IL-8 in THP-1-derived macrophages for (A) 6 h and (B) 24 h. Data are presented as the mean ± SD from three independent experiments. *, #, Δ $p < 0.05$; by one-way ANOVA.

The effect of GODs on the protein level of TNF-α and IL-8 was examined as well. The results showed that GQDs increased 7.5- and 7.3-fold in TNF-α and 2.2- and 2.2-fold in IL-8 at concentrations of 10 and 50 µg/mL, respectively (Figure 4.11$p < 0.05$). In separate experiments, macrophages were treated with 50 µg/mL GQDs over 48 h. There was a 1.6-, 1.6-, and 1.5-fold increase in the expression level of IL-8 after cells were treated with GQDs for 12, 24, and 48 h, respectively ($p < 0.05$). Similarly, treating cells with GQDs for 12, 24, and 48 h resulted in a 2.5-, 2.5-, and 2.7-fold increase in the expression of TNF-α, respectively ($p < 0.05$). LPS at 30 ng/mL was used as the positive control of cytokine production, which increased the IL-8 and TNF-α level by 3.1- and 11.3-fold, respectively. In addition, SB202190, a p38 MAPK selective chemical inhibitor, abolished the inducing effect of GQDS on cytokine expression in macrophages. These results indicated that GQDs increased the generation of cytokines involving p38 MAPK-mediated signaling pathway.

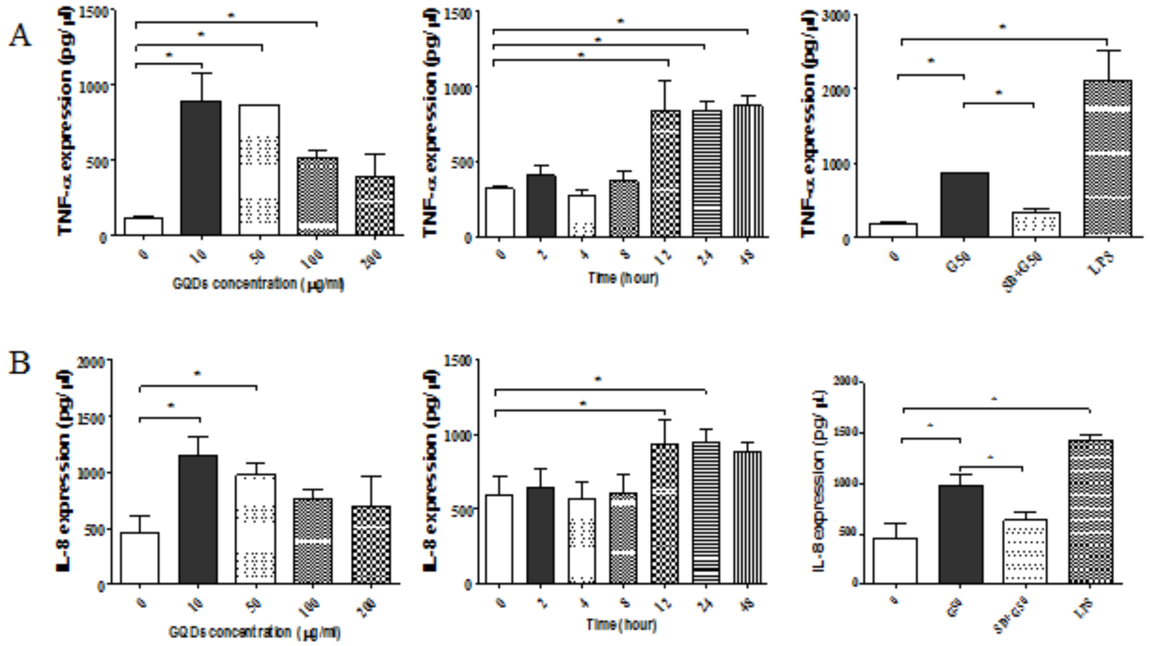

Figure 4.11 Dose, time and p38 MAPK inhibitor effects of GQDs exposure on the excretion of (A) TNF (B) IL-8 in THP-1-derived macrophages at protein levels. Data are presented as the mean ± SD from three independent experiments. *, #, Δ $p < 0.05$; by one-way ANOVA.

4.3.8 Effect of GQDs on Epithelial-mesenchymal Transition (EMT) of Macrophages

To further understand the mechanisms for the immune-modulating effects of GQDs, we studied the effect of GQDs on the expression levels of several key EMT markers in human macrophages. When the cells were treated with GQDs at 10, 50, 100, and 200 μg/mL, the expression of E-cadherin was only slightly reduced while the expression of β-catenin was slightly increased (Figure 4.12). Although the expression of snail and TCF-8 was reduced by 67% and 46% when the cells were treated with 200 μg/mL, respectively, the differences did not achieve statistical significance.

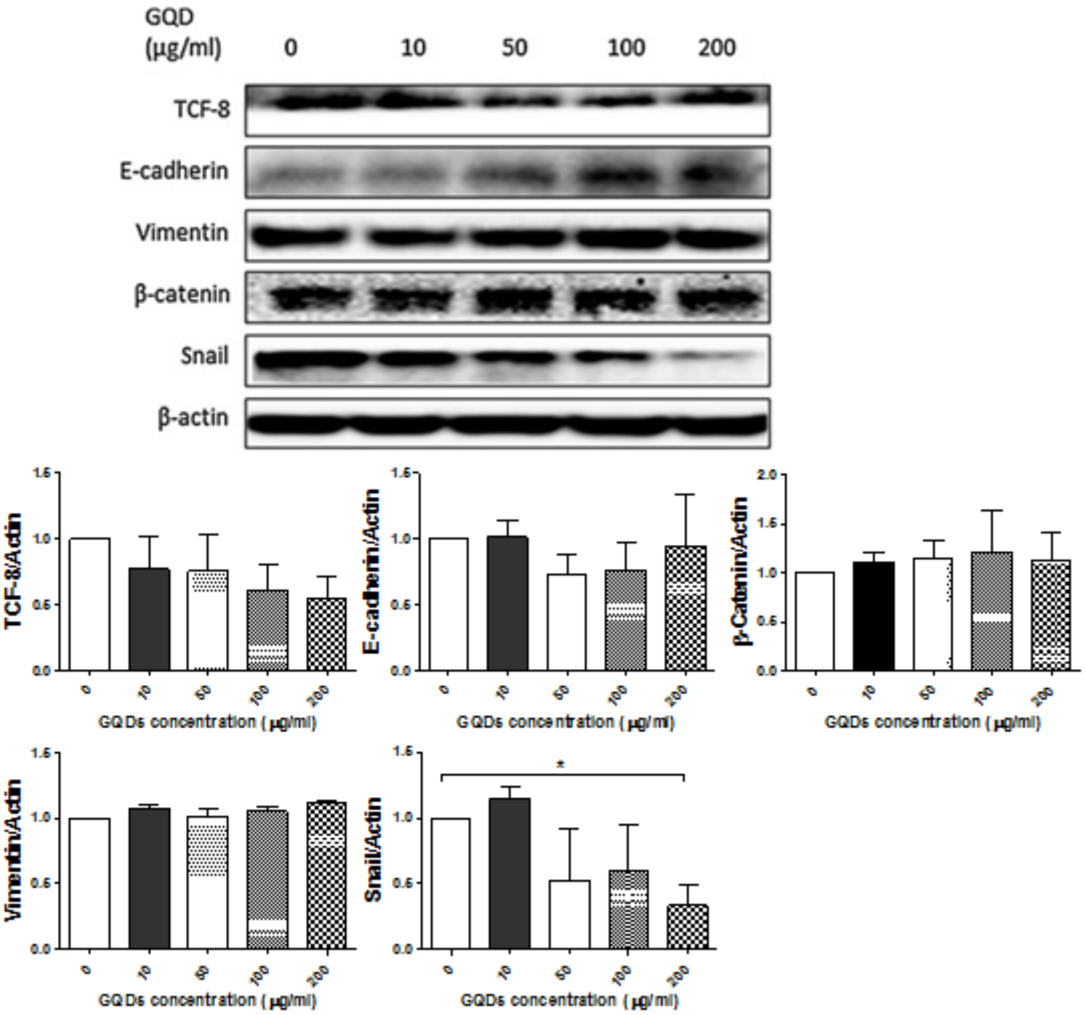

Figure 4.12 Effects of GQDs on the expression levels of selected markers of EMT in THP-1 derived macrophages. Cells were treated with GQDs at 10, 50, 100, and 200 μg/mL for 24 h and the cellular protein levels of E-cadherin, vimentin, β-catenin, TCF-8, and snail were determined using Western blotting analysis. Representative blots of the EMT markers and bar graphs showing the effect of GQDs on the expression of EMT markers. No statistical significance was observed. Data are presented as the mean ± SD from three independent experiments. * $p < 0.05$; by one-way ANOVA.

4.3.9 GQDs Upregulate p38 MAPK and NF-κB Signaling Pathways in Macrophages

In order to further examine the regulatory effect of GQDs on inflammatory response, the expression and phosphorylation level of p38 MAPK and NF-κB were determined. p38 MAPK regulates cellular responses to cytokines and stress and thus controls cell differentiation, cell death, cell migration, and invasion[216]. In contrast to the control group, there were 4.6- and 3.3-fold increases in the phosphorylation level of p38 MAPK with the treatment of GQDs at 100 and 200 μg/mL, respectively ($p < 0.05$), and there was no significant alteration in the expression level of total p38 MAPK (Figure 4. 13).

To confirm the effect of GQDs on macrophages via upregulating p38 MAPK and NF-κB expression, the inhibitors of these two proteins were utilized. The p38 MAPK selective chemical inhibitor SB202190 (SB, 20 μM) or NF-κB inhibitor CAS 213546-53-3 (CAS, 10 μg/mL) was incubated with THP-1-derived macrophages for 30 min before 100 μg/mL GQDs was added to trigger the apoptosis and autophagy. The results showed that CAS significantly decreased the total death of THP-1-derived macrophages induced by GQDs, while SB did not significantly affect it (Figure 4. 14A-B). This implied that GQD-induced apoptosis was regulated via the activation of NF-κB signal pathway.

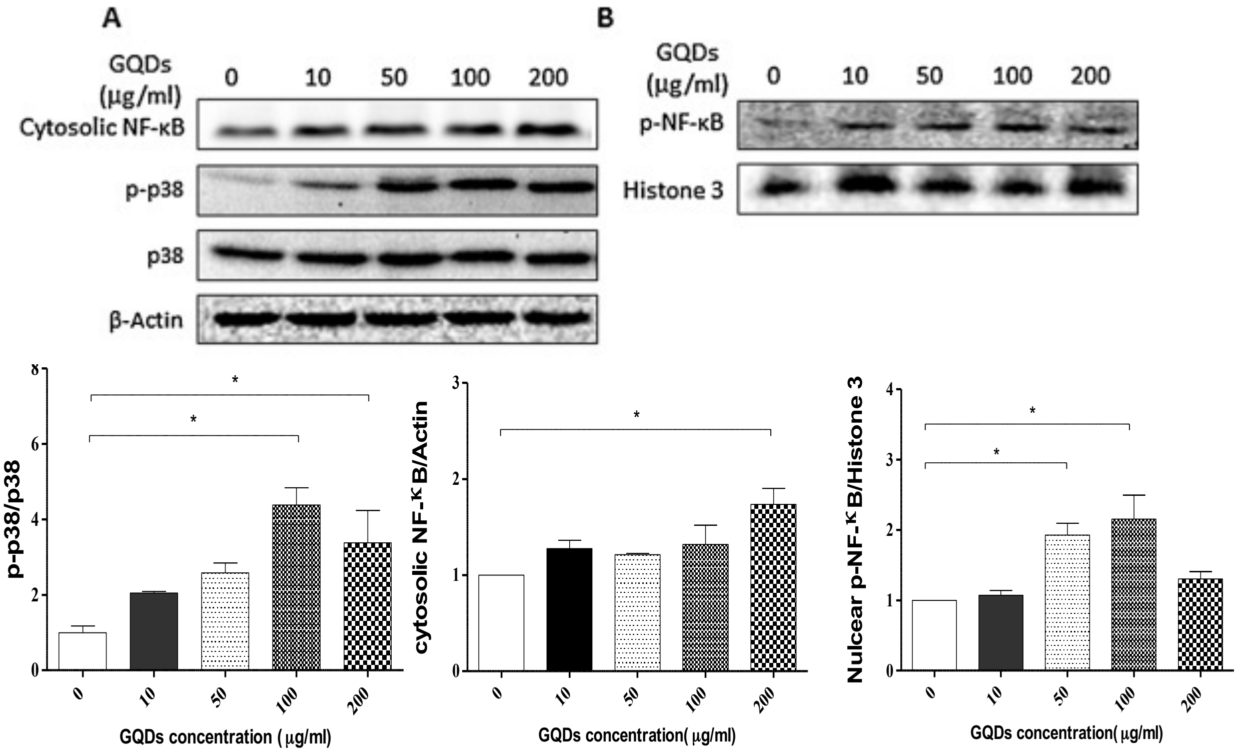

Figure 4. 13 Effects of GQDs on the expression of nuclear phosphorylated p65 and cytosolic p65 and key proteins regulated by NF-κB in THP-1-derived macrophages. (A) Effects of GQDs on the expression of phosphorylated p38MAPK, cytosolic NF-κB (p65) in THP-1-derived macrophages. (B) Effects of GQDs on the expression of nuclear phosphorylated NF-κB p65 in THP-1-derived macrophages. The bar graphs show the above blot intensity mean ± SD. $*p < 0.05$; by one-way ANOVA.

NaN_3 at 10 mM was used to deplete ATP, thus blocking the endocytosis and phagocytosis[217, 218]. GQD-induced autophagic effect on THP-1-derived macrophages was measured after p38 MAPK, NF-κB, and phagocytosis were inhibited. Rap, an mTOR inhibitor, was used as a known inducer of autophagy. 100 nM Rap increased the autophagy of THP-1-derived macrophages 7.14-fold compared to the untreated group. SB, CAS, and NaN_3 significantly decreased GQD-induced autophagy by34%, 54%, and 57%, respectively, compared to the group treated with 100 µg/ml GQDs only (Figure 4. 14C). This indicated that the

GQD-induced autophagy of THP-1-derived macrophages was significantly via the activation of p38MAPK, NF-κB pathway, and phagocytosis process.

NaN_3, the inhibitor of the endocytosis and phagocytosis, significantly decreased the ROS generation. This suggested that GQDs were internalized into macrophages in the first step, and then triggered the ROS production. Furthermore, both SB and CAS did not significantly affect the ROS production in THP-1-derived macrophages exposed to 50 μg/ml GQDs for 24 h. No significant decrease of intracellular ROS generation was found after p38 MAPK and NF-κB were inhibited. This result showed that ROS generation induced by GQDs did not require the activation of p38 MAPK and NF-κB (Figure 4. 14 D). Combined with findings from published studies, we concluded that ROS production did not locate downstream of the p38 MAPK and NF-κB signal pathways[219, 220].

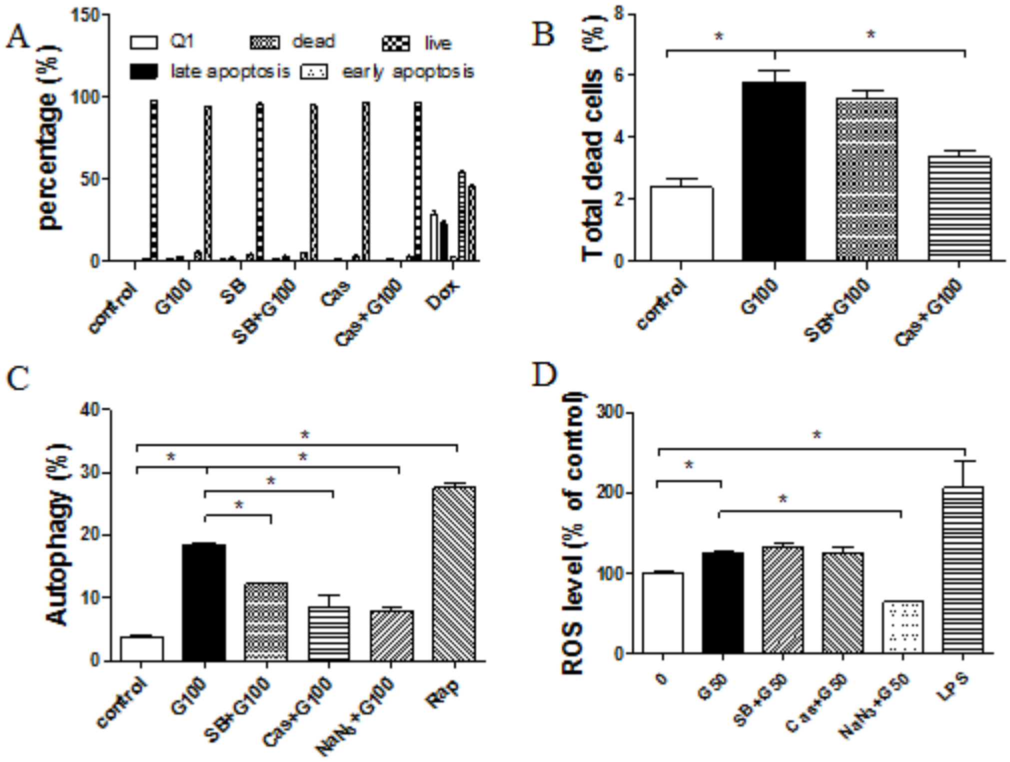

Figure 4. 14 Effect of p38 MAPK inhibitor (SB: SB202190) or NF-κB (CAS: CAS 213546-53-3) inhibitor on GQDs-induced (A) apoptosis, (B) total cell death, (C) autophagy, and (D) ROS generation. The bar graphs show the above blot intensity mean ± SD. $*p < 0.05$; by one-way ANOVA.

Through comprehensive analysis, all the results above suggested that GQDs triggered the inflammatory response, apoptosis, and autophagy via the regulation of p38 MAPK and NF-κB signaling pathway.

4.4 Conclusion

In summary, I successfully evaluated immunotoxicity of GQDs in human macrophages. I have also demonstrated that GQDs could induce the inflammatory response, apoptosis, and autophagy in human macrophages via p38 MAPK and NF-κB signaling pathways. This study has provided new insights into how GQDs interact with the biological systems which must be taken into account when GQDs are used as novel theranostics. Further studies are needed to elucidate the underlying mechanisms for the size- and surface area- effects of GQDs on the immune system and the safety implications.

CHAPTER 5: DISCUSSION[2]

In recent decades, nanomedicine has been perceived as a promising field for disease therapy, diagnosis, and control of the biological system, so it has attracted increasing attention[221, 222]. GQDs, one of the most promising alternative biomaterials for nanomedicine, are widely studied and applied due to their unique properties. In this dissertation, I described the design and investigation of a novel GQDs DDS for ovarian cancer therapy. The translation of basic science to clinical application is an emerging area, which aims to translate the nanomedicine from bench to bedside. This dissertation has laid the foundation to develop a novel GQDs based DDS to enhance the targeted therapeutic activity for ovarian cancer.

First, to establish a facile method to the synthesize the GQDs is a big challenge, as well as a prerequisite. From this point of view, a novel one-step synthesis method of GQDs was established and introduced in chapter 2. The study results demonstrate that GQDs with strong florescent illumination and excellent water solubility were directly fabricated from graphite by a hydrothermal reaction. In comparison to previous studies, the basic analyses including TEM, HRTEM, AFM, XRD, FTIR, Raman spectrum, depicted the structure of the GQDs. The sizes of the synthesized GQDs were in a narrow range from 1.5 nm to 4 nm with a single- or bi-layer.

---

[2] Part of this section is published as reference 197. Ibid.

Functional groups, such C-O and C=O, were introduced to the edge of the GQDs, enabling the conjugation with targeting ligands or therapeutic components for further biomedical applications. The one-step GQDs synthesis approach used in this study was superior to conventional ones. Moreover, the fluorescent spectra of GQDs exhibited excitation-dependent emission behavior. GQDs in aqueous solution could produce bright green fluorescence upon excitation at 365 nm, which could be applied for bioimaging application. Their morphologic and optical properties are consistent with previous studies[223, 224].

Moreover, the conjugation of GQDs with targeting ligand and chemotherapeutic drug is the foundation of the dissertation. FA is a specified targeting ligand to ovarian cancer overexpressed receptor, FR-α. The conjugation of FA and GQDs is based on the EDC-NHS crosslinking reaction (Figure 5.1**)**. The successful conjugation of FA to GQDs was confirmed by FTIR and UV absorption spectroscopies. The properties of the GQDs-FA were in agreement with previous studies[117, 176, 225, 226]. DOX, a FDA approved second-line drug for metastatic ovarian cancer, was attached on the GQDs sheet via π-π stacking. DOX has an UV absorbance maximum at 480 nm and a strong red emission at 560-590 nm with the 480 nm excitation. The successful loading of DOX on GQDs-FA was in agreement with the work of other groups [175, 176, 199, 224]. The UV-Vis absorption spectrum showed an obvious peak at 480 nm. However, the red emission of DOX was quenched after loading to GQDs-FA. Both fluorescent spectroscopy and confocal microscopy could detect the strong signal of GQDs with the absence of fluorescent signal from DOX. Several possible explanations of the fluorescence quenching involve static quenching, exciplex, Dexter electron transfer, and Förster resonance energy transfer[227-229]. There are few studies on the DOX fluorescent quenching effect, but some groups assumed that fluorescence of DOX may be self-quenched at high concentrations or in collision with water molecules[230]. Although the underlying mechanism of DOX quenching in this study is unclear at the present, it is an interesting topic and hopefully can be solved by optical physicists.

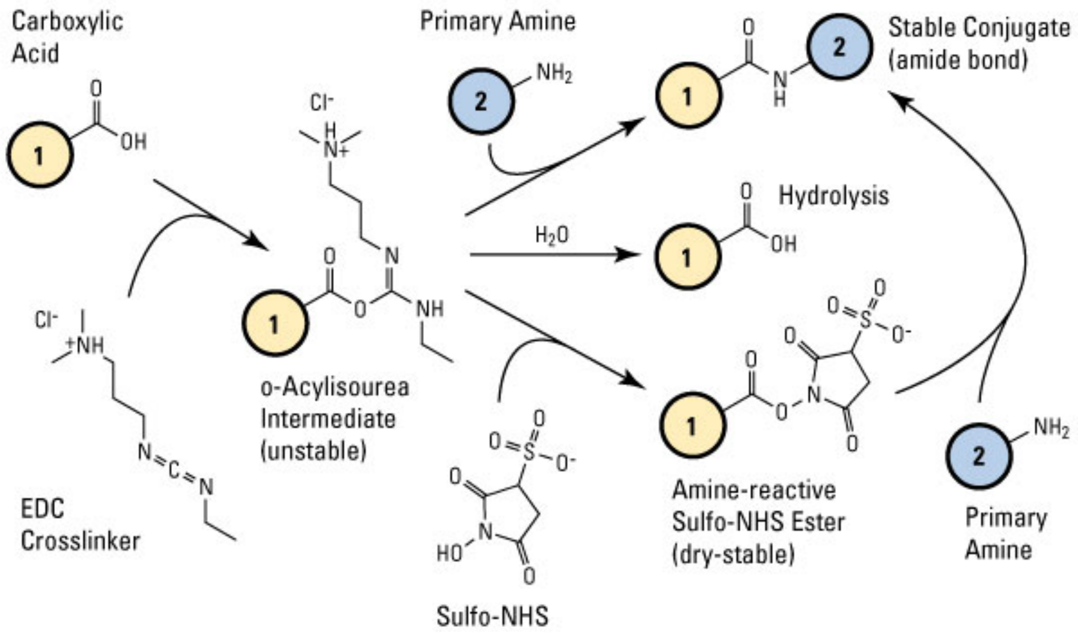

Figure 5.1 NHS plus EDC (carbodiimide) crosslinking reaction scheme for GQDs-FA conjugation. Reprint with permission from manufacturer (Thermo Fisher Scientific).

Although DOX has been proved to have strong antitumor activity in a wide variety of malignancies, including ovaries, its usage is limited in clinical cases due to its severe cardiac toxicity[189, 231]. The major concern of using DOX is its side effect of causing chronic cardiomyopathy. Using DDS to deliver DOX is an alternative choice, but current commercial product DOXIL still has some problems including acute hypersensitivity reaction and non-specificity[232-234]. Therefore, GQDs-FA-DOX in this dissertation research was a potent DDS for FR overexpressed ovarian cancer. The anti-cancer effect of the GQDs-FA-DOX DDS was validated in chapter 3. The results presented in this chapter are very encouraging. Not only the targeted DDS specifically delivers DOX into the tumor site, which enhances the ovarian cancer cells uptake, promotes ROS generation, and induces apoptosis, but also the DDS has limited toxicity to normal ovarian epithelial cells. The targeting feature of the GQDs-FA-DOX is determined by FA, which actively binds to the FR. Both confocal microscopy (Figure 3.2) and flow cytometry results (Figure 3.3) indicate that GQDs-FA-DOX was efficiently targeted to the FR overexpressed ovarian tumor cells OVCAR3. Moreover, the competitive experiment of FA confirms the FR-mediated uptake mechanism of the GQDs-FA-DOX (Figure 3.4). The fluorescent intensity of the cells pre-treated with FA decrease by 70% indicating that fewer GQDs-FA-DOX entered per cell. However, 72% of the cells still uptake GQDs-FA-DOX if they pre-treated with FA. The possible explanation of this phenomenon may be due to that the binding of the FA to FR is a dynamic process. Therefore, pre-treatment with FA to FR overexpressed cells could not fully inhibit the FR. The colony assay and apoptosis assay demonstrate the anti-tumor effect of the GQDs-FA-DOX to FR overexpressed ovarian tumor cells. The potential effect of the drug delivery vehicle itself is excluded since GQDs cause no significant effect on colony formation and cell apoptosis. The inhibition effect of FA to GQDs-FA-DOX in FR overexpressed is obvious that no significant change in the size and numbers of the formed-colonies. ROS generation is one of the well-known mechanisms of DOX's therapeutic effect. Intracellular ROS interacts with macromolecules, such as including DNA and functional proteins, leading to the cellular dysfunction and signal transductions disruption [193, 235]. Consistent with that idea, the findings in the ROS experiment shows that GQD-FA-DOX strongly induced ROS generation in FR overexpressed cells, while no significant effect in FR negative cells (Figure 3.7). Again, the vehicle itself, GQDs, results in no change in ROS generation. EMT is a key step of cancer invasion by losing their epithelial morphology and undergoing migratory behavior. Therefore, this DDS improves the therapeutic activity to the tumor site, while minimizes the toxic effect to normal ovarian epithelial cells.

Last but not least, with the growing investigation of GQDs for biomedical applications, their environmental and biologic toxic effects have become a major concern. Thus, it is important to decipher the toxicological profiles of GQDs. Although there were a few studies on their toxicity/biocompatibility[195, 196, 201], study on the effect of GQDs on the immune system was still lacking. The immune system protects the host by responding to the external and internal stimuli. The potential immunotoxicity of nanoparticles may disturb the immune system, resulting in undesirable suppression or overstimulation. The phagocytic cells (e.g., macrophages) of the immune system are the first safeguard to nanoparticles in most circumstance. The interactions between nanoparticles and these cells may promote inflammatory process or suppress the body immunity. Considering the important roles of on immune system, it is of great significance to investigate the possible inhibitory or enhancing response of the immune-related cells to the exposure of GQDs.

There was only a slight cytotoxicity of GQDs observed at low concentrations in macrophages with an IC_{50} value greater than 2000 and 400 μg/mL for 24 and 48 h based on the MTT results. Moreover, GQDs did not damage the plasma membrane as shown in the LDH leakage assay. These results presented a favorable biological feature of GQDs with low cytotoxicity. The results showed a significant decrease in mitochondrial dehydrogenase activity at high concentration of GQDs in macrophages. A possible explanation might be associated with ROS-induced cell death[236]. Intracellular ROS interact with macromolecules including DNA and functional proteins, rendering the disruption of signal transductions and cellular dysfunction. Consequently, enhanced ROS generation causes cell death. Indeed, my findings showed that GQDs significantly increased the intracellular ROS generation, apoptosis, and autophagy in macrophages. Apoptosis and autophagy are two dominant cell programmed cell death and interplay with each other[237]. Apoptosis is initiated by the release of cytochrome c resulting in the imbalance between pro-apoptotic and anti-apoptotic proteins and executed by caspase families through two main pathways, including the extrinsic death receptor pathway and the intrinsic mitochondrial/cytochrome c-mediated pathway[238, 239]. In this current study, GQDs decreased the expression level of Bcl-2 and increased the expression level of Bax and Bad, leading to a decline in the ratio of Bcl-2 over Bax. Moreover, my results showed that GQDs increased the expression level of cleaved caspase 3 and caspase 9 which eventually resulted in cell death. On the other hand, autophagy has multifaceted roles in the maintenance of cellular homeostatic function and it can counteract the apoptotic cell death[237]. In my study, GQDs showed a significant inducing effect on autophagy in macrophages while showing little apoptotic effect on macrophages, especially at low concentrations.

Therefore, it is highly likely that autophagy was an innate defending mechanism utilized by macrophages against GQDs. Beclin 1 and LC3 were two key proteins in the process of autophagy pathway and the conversion of cytosolic form LC3-I (18 kD) to membrane-bound lapidated form of LC3-II (16 kD) was a common indicator of autophagy[240]. Both beclin 1 expression and LC3-II/LC3-I conversion ratio were enhanced, confirming the accumulation of autophagosomes in macrophages exposed to GQDs. When phagocytosis and autophagy occur in macrophages, it requires the internalization of GQDs. As shown in Figure 4. 14, the inhibitory effect of NaN_3, which is a known inhibitor of endocytosis and phagocytosis, was observed. These results indicated that the inhibition of internalization of GQD particles reduced both autophagy and ROS production. This suggested that GQD-induced immunotoxicity involved internalizing GQD particles followed by ROS generation production and triggering programmed cell death.

The inflammatory response is critical for immune system responding to stimuli by producing a variety of pro-inflammatory cytokines, including TNF-α, IL-1, and IL-8. They have an important role in the regulation of various cellular functions including cell proliferation, apoptosis, and autophagy[241]. In the present study, we found an increasing effect of GQDs on the expression of TNF-α, IL-1, and IL-8 at low concentrations, whereas a high concentration of GQDs suppressed the expression of TNF-α, IL-1, and IL-8 in macrophages. Furthermore, we found that SB202190, a p38 MAPK selective chemical inhibitor, abolished the effect of GQDs on the generation of cytokines. This indicated that the regulatory effect of the inflammatory response may involve p38 MAPK-mediated signaling pathway. Indeed, our findings showed that GQDs significantly increased the phosphorylation of p38 MAPK. Moreover, we observed that GQDs promoted the nuclear translocation of NF-κB and increased the phosphorylation of p65. NF-κB is a critical transcription factor involved in various cellular responses to stimuli such as cytokines[242-245]. In particular, NF-κB has a pivotal role in the regulation of inflammatory and immune responses by interplaying with various signaling pathways, which regulate the intracellular and extracellular levels of pro-inflammatory cytokines, such as TNF-α, IL-1β, and IL-8. In addition to the immune response, NF-κB also plays an important role in a variety of physiological and pathological processes. The activation of NF-κB can either promote or inhibit the cell survival depending on the cell type and the stimuli[236-239]. In our case, NF-κB was possibly involved in GQD-induced apoptotic cell death. CAS 213546-53-3, a selective chemical inhibitor of NF-κB phosphorylation and translocation, significantly decreased the GQD-induced cell apoptosis. Moreover, both p38 MAPK and NF-κB pathways were involved in GQD-induced autophagy of macrophages, although they did not have any effect on ROS production induced by GQDs. Taken together, the effect of GQDs on inflammatory response, apoptosis, and autophagy might be ascribed to the modulation of p38 MAPK and NF-κB mediated signaling pathways.

In general, although GQDs exhibited favorable biocompatibility, they still moderately triggered immune responses and programmed cell death with the involvement of p38 MAPK and NF-κB signaling pathways (

Figure 5. **2**). Chemical modification or change of the synthesis approach of GQDs may help avoid the undesirable stimulation of the immune system. On the other hand, GQDs may be applied as an adjunct to develop new vaccines.

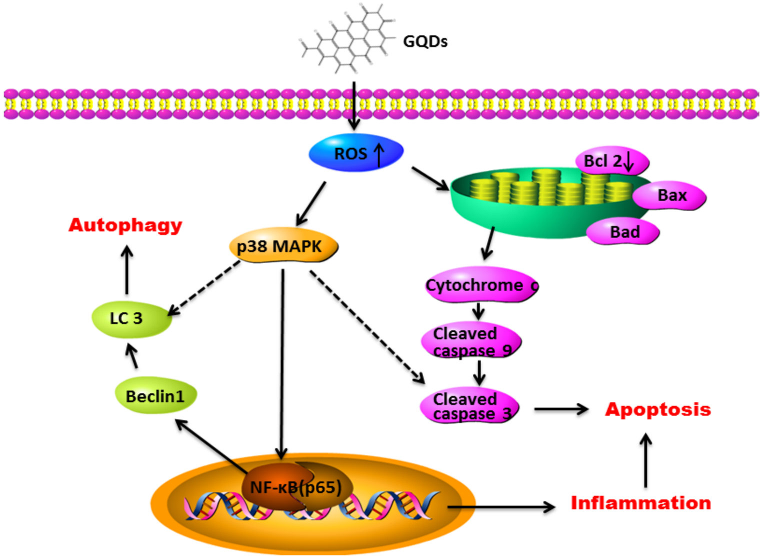

Figure 5. 2 Schematic diagram of signaling pathways involved in GQDs-induced immunotoxicity in human macrophages.

To further study and optimize the GQDs-based DDS, the following recommendations are proposed in attempt to, hopefully, improve the translational science of the nanomedicine to ovarian cancer. First of all, NIR-trigger controlled releasing and photothermal therapy of the GQDs-based DDS is an emerging topic. Previous studies demonstrated that GQDs possesses strong NIR absorbance and generates heat after triggered by laser. On one hand, the generated heat could disrupt the $\pi - \pi$ stacking between GQDs and drug, rendering to a controlled releasing of the drug. On the other hand, the generated heat can also provide a hyperthermia environment in cells, making cells more fragile to the drug and realize the combination of photothermal therapy and chemotherapy. Moreover, biodistribution, degradation, pharmacokinetics, and pharmacodynamics of nanomaterials the remains a major challenge in translational science. Luckily, GQDs presents strong fluorescence and enables real-time tracking *in vivo*. Therefore, it is possible to investigate pharmacology profile of this GQDs-based DDS, as well as its anti-cancer effect in animal studies. Finally, large-scale synthesis and quality control of the DDS are always a key point to translate the research findings from bench to bedside.

REFERENCES

1. Stewart, D.E., et al., *Information Needs and Decisional Preferences among Women with Ovarian Cancer.* Gynecologic Oncology, 2000. **77**(3): p. 357-361.
2. Panici, P.B., et al., *Systematic aortic and pelvic lymphadenectomy versus resection of bulky nodes only in optimally debulked advanced ovarian cancer: a randomized clinical trial.* Journal of the National Cancer Institute, 2005. **97**(8): p. 560-566.
3. Creasman, W.T. and P.J. DiSaia, *Screening in ovarian cancer.* American journal of obstetrics and gynecology, 1991. **165**(1): p. 7-10.
4. Zhang, D., et al., *Retinoids and ovarian cancer.* Journal of cellular physiology, 2000. **185**(1): p. 1-20.
5. Reles, A., et al., *Correlation of p53 mutations with resistance to platinum-based chemotherapy and shortened survival in ovarian cancer.* Clinical Cancer Research, 2001. **7**(10): p. 2984-2997.
6. Goff, B.A., et al., *Development of an ovarian cancer symptom index: possibilities for earlier detection.* Cancer, 2007. **109**(2): p. 221-7.
7. Yancik, R., *Ovarian cancer. Age contrasts in incidence, histology, disease stage at diagnosis, and mortality.* Cancer, 1993. **71**(2 Suppl): p. 517-23.
8. Sundar, S., R.D. Neal, and S. Kehoe, *Diagnosis of ovarian cancer.* BMJ, 2015. **351**: p. h4443.
9. Vaughan, S., et al., *Rethinking ovarian cancer: recommendations for improving outcomes.* Nat Rev Cancer, 2011. **11**(10): p. 719-25.
10. Slotman, B. and B. Rao, *Ovarian cancer (review). Etiology, diagnosis, prognosis, surgery, radiotherapy, chemotherapy and endocrine therapy.* Anticancer research, 1987. **8**(3): p. 417-434.
11. Thomas, G.M. and A.J. Dembo, *Integrating radiation therapy into the management of ovarian cancer.* Cancer, 1993. **71**(S4): p. 1710-1718.
12. Christian, J. and H. Thomas, *Ovarian cancer chemotherapy.* Cancer treatment reviews, 2001. **27**(2): p. 99-109.
13. McGuire, W.r. and M. Markman, *Primary ovarian cancer chemotherapy: current standards of care.* British journal of cancer, 2003. **89**: p. S3-S8.
14. Markman, M. and J.L. Walker, *Intraperitoneal chemotherapy of ovarian cancer: a review, with a focus on practical aspects of treatment.* Journal of clinical oncology, 2006. **24**(6): p. 988-994.

15. Elit, L., et al., *Outcomes in surgery for ovarian cancer.* Gynecologic oncology, 2002. **87**(3): p. 260-267.
16. HACKER, N.F., et al., *Primary cytoreductive surgery for epithelial ovarian cancer.* Obstetrics & Gynecology, 1983. **61**(4): p. 413-420.
17. Yap, T.A., C.P. Carden, and S.B. Kaye, *Beyond chemotherapy: targeted therapies in ovarian cancer.* Nature Reviews Cancer, 2009. **9**(3): p. 167-181.
18. Nukolova, N.V., et al., *Folate-decorated nanogels for targeted therapy of ovarian cancer.* Biomaterials, 2011. **32**(23): p. 5417-5426.
19. Lord, C.J. and A. Ashworth, *Targeted therapy for cancer using PARP inhibitors.* Current opinion in pharmacology, 2008. **8**(4): p. 363-369.
20. Mørch, L.S., et al., *Hormone therapy and ovarian cancer.* Jama, 2009. **302**(3): p. 298-305.
21. Glud, E., et al., *Hormone therapy and the impact of estrogen intake on the risk of ovarian cancer.* Archives of internal medicine, 2004. **164**(20): p. 2253-2259.
22. Ozols, R.F., *Ovarian cancer*. Vol. 1. 2003: PMPH-USA.
23. Bookman, M.A. *Biological therapy of ovarian cancer: current directions*. in *Seminars in oncology*. 1998.
24. Papadia, A. and M. Morotti, *Diaphragmatic surgery during cytoreduction for primary or recurrent epithelial ovarian cancer: a review of the literature.* Arch Gynecol Obstet, 2013. **287**(4): p. 733-41.
25. Neijt, J., et al., *Randomised trial comparing two combination chemotherapy regimens (Hexa-CAF vs CHAP-5) in advanced ovarian carcinoma.* The Lancet, 1984. **324**(8403): p. 594-600.
26. Herzog, T.J., et al., *Ovarian cancer clinical trial endpoints: Society of Gynecologic Oncology white paper.* Gynecol Oncol, 2014. **132**(1): p. 8-17.
27. Swan, G.W., *Role of optimal control theory in cancer chemotherapy.* Mathematical biosciences, 1990. **101**(2): p. 237-284.
28. Coates, A., et al., *On the receiving end—patient perception of the side-effects of cancer chemotherapy.* European Journal of Cancer and Clinical Oncology, 1983. **19**(2): p. 203-208.
29. Partridge, A.H., H.J. Burstein, and E.P. Winer, *Side effects of chemotherapy and combined chemohormonal therapy in women with early-stage breast cancer.* Journal of the National Cancer Institute. Monographs, 2000(30): p. 135-142.
30. Conklin, K.A., *Dietary antioxidants during cancer chemotherapy: impact on chemotherapeutic effectiveness and development of side effects.* Nutrition and cancer, 2000. **37**(1): p. 1-18.
31. Galotto, M., et al., *Stromal damage as consequence of high-dose chemo/radiotherapy in bone marrow transplant recipients.* Experimental hematology, 1999. **27**(9): p. 1460-1466.

32. Saleh, S., et al., *Protective effects of the angiotensin II receptor blocker losartan on cisplatin-induced kidney injury.* Chemotherapy, 2009. **55**(6): p. 399-406.
33. Lau, W., et al., *Selective internal radiation therapy for nonresectable hepatocellular carcinoma with intraarterial infusion of 90 yttrium microspheres.* International Journal of Radiation Oncology* Biology* Physics, 1998. **40**(3): p. 583-592.
34. Perez, C.A., et al., *Localized carcinoma of the prostate (stages T1B, T1C, T2, and T3). Review of management with external beam radiation therapy.* Cancer, 1993. **72**(11): p. 3156-3173.
35. Reinhard, E.H. and C.V. Moore, *Radioactive phosphorus as a therapuetic agent; a review of the literature and analysis of the results of treatment of 155 patients with various blood dyscrasias, lymphomas, and other malignant neoplastic diseases.* The Journal of laboratory and clinical medicine, 1946. **31**: p. 107.
36. Teunen, D., *The European Directive on health protection of individuals against the dangers of ionising radiation in relation to medical exposures (97/43/EURATOM).* J Radiol Prot, 1998. **18**(2): p. 133-7.
37. Julian, C.G., C.H. Amarinalsingh, and L.S. Burnett, *Radioactive Phosphorus and External Radiation as an Adjuvant to Surgery for Ovarian Carcinoma.* Obstetrics and Gynecology, 1978. **52**(2): p. 155-160.
38. Meirow, D. and D. Nugent, *The effects of radiotherapy and chemotherapy on female reproduction.* Hum Reprod Update, 2001. **7**(6): p. 535-43.
39. Green, N., *The Avoidance of Small-Intestine Injury in Gynecologic Cancer.* International Journal of Radiation Oncology Biology Physics, 1983. **9**(9): p. 1385-1390.
40. O'Mahony, D. and M. Bishop, *Monoclonal antibody therapy.* Frontiers in bioscience: a journal and virtual library, 2005. **11**: p. 1620-1635.
41. Adams, G.P. and L.M. Weiner, *Monoclonal antibody therapy of cancer.* Nature Biotechnology, 2005. **23**(9): p. 1147-1157.
42. Perren, T.J., et al., *A phase 3 trial of bevacizumab in ovarian cancer.* New England Journal of Medicine, 2011. **365**(26): p. 2484-2496.
43. Ferrara, N., K.J. Hillan, and W. Novotny, *Bevacizumab (Avastin), a humanized anti-VEGF monoclonal antibody for cancer therapy.* Biochemical and biophysical research communications, 2005. **333**(2): p. 328-335.
44. Ledermann, J., et al., *Olaparib maintenance therapy in platinum-sensitive relapsed ovarian cancer.* New England Journal of Medicine, 2012. **366**(15): p. 1382-1392.
45. Weston, V.J., et al., *The PARP inhibitor olaparib induces significant killing of ATM-deficient lymphoid tumor cells in vitro and in vivo.* Blood, 2010. **116**(22): p. 4578-4587.
46. Legha, S.S., *Tamoxifen in the treatment of breast cancer.* Annals of internal medicine, 1988. **109**(3): p. 219-228.

47. Miller, W., et al., *Growth of human breast cancer cells inhibited by a luteinizing hormone-releasing hormone agonist.* 1985.
48. Wood, A.J., I.E. Smith, and M. Dowsett, *Aromatase inhibitors in breast cancer.* New England Journal of Medicine, 2003. **348**(24): p. 2431-2442.
49. Kershaw, M.H., et al., *A phase I study on adoptive immunotherapy using gene-modified T cells for ovarian cancer.* Clinical Cancer Research, 2006. **12**(20): p. 6106-6115.
50. Bookman, M.A., *Biological therapy of ovarian cancer: current directions.* Semin Oncol, 1998. **25**(3): p. 381-96.
51. Zahedi, P., et al., *Recent advances in drug delivery strategies for treatment of ovarian cancer.* Expert opinion on drug delivery, 2012. **9**(5): p. 567-583.
52. Liscovitch, M. and Y. Lavie, *Cancer multidrug resistance: a review of recent drug discovery research.* IDrugs, 2002. **5**(4): p. 349-355.
53. Lu, H., et al., *Paclitaxel nanoparticle inhibits growth of ovarian cancer xenografts and enhances lymphatic targeting.* Cancer chemotherapy and pharmacology, 2007. **59**(2): p. 175-181.
54. Feng, Z., et al., *Preclinical efficacy studies of a novel nanoparticle-based formulation of paclitaxel that out-performs Abraxane.* Cancer chemotherapy and pharmacology, 2010. **65**(5): p. 923-930.
55. Paraskar, A.S., et al., *Harnessing structure-activity relationship to engineer a cisplatin nanoparticle for enhanced antitumor efficacy.* Proceedings of the National Academy of Sciences, 2010. **107**(28): p. 12435-12440.
56. Dinulescu, D.M., et al., *Role of K-ras and Pten in the development of mouse models of endometriosis and endometrioid ovarian cancer.* Nature medicine, 2005. **11**(1): p. 63-70.
57. Devalapally, H., et al., *Poly (ethylene oxide)-modified poly (beta-amino ester) nanoparticles as a pH-sensitive system for tumor-targeted delivery of hydrophobic drugs: part 3. Therapeutic efficacy and safety studies in ovarian cancer xenograft model.* Cancer chemotherapy and pharmacology, 2007. **59**(4): p. 477-484.
58. Dong, X., et al., *Doxorubicin and paclitaxel-loaded lipid-based nanoparticles overcome multidrug resistance by inhibiting P-glycoprotein and depleting ATP.* Cancer research, 2009. **69**(9): p. 3918-3926.
59. Devalapally, H., et al., *Paclitaxel and ceramide co-administration in biodegradable polymeric nanoparticulate delivery system to overcome drug resistance in ovarian cancer.* International Journal of Cancer, 2007. **121**(8): p. 1830-1838.
60. van Vlerken, L.E., et al., *Augmentation of therapeutic efficacy in drug-resistant tumor models using ceramide coadministration in temporal-controlled polymer-blend nanoparticle delivery systems.* The AAPS journal, 2010. **12**(2): p. 171-180.
61. Devalapally, H., et al., *Modulation of drug resistance in ovarian adenocarcinoma by enhancing intracellular ceramide using tamoxifen-loaded biodegradable polymeric nanoparticles.* Clinical Cancer Research, 2008. **14**(10): p. 3193-3203.

62. Zheng, D., et al., *Enhanced antitumor efficiency of docetaxel-loaded nanoparticles in a human ovarian xenograft model with lower systemic toxicities by intratumoral delivery.* Oncology reports, 2010. **23**(3): p. 717-724.
63. Li, Y., et al., *Well-defined, reversible disulfide cross-linked micelles for on-demand paclitaxel delivery.* Biomaterials, 2011. **32**(27): p. 6633-6645.
64. Xiao, K., et al., *A self-assembling nanoparticle for paclitaxel delivery in ovarian cancer.* Biomaterials, 2009. **30**(30): p. 6006-6016.
65. Kim, D., et al., *In vivo evaluation of doxorubicin-loaded polymeric micelles targeting folate receptors and early endosomal pH in drug-resistant ovarian cancer.* Molecular pharmaceutics, 2009. **6**(5): p. 1353-1362.
66. Xu, P., et al., *Anticancer efficacies of cisplatin-releasing pH-responsive nanoparticles.* Biomacromolecules, 2006. **7**(3): p. 829-835.
67. Jin, W., et al., *Degradable cisplatin-releasing core-shell nanogels from zwitterionic poly (β-aminoester)-graft-PEG for cancer chemotherapy.* Drug delivery, 2007. **14**(5): p. 279-286.
68. Gao, Z.-G., H.D. Fain, and N. Rapoport, *Controlled and targeted tumor chemotherapy by micellar-encapsulated drug and ultrasound.* Journal of Controlled Release, 2005. **102**(1): p. 203-222.
69. Rapoport, N.Y., et al., *Controlled and targeted tumor chemotherapy by ultrasound-activated nanoemulsions/microbubbles.* Journal of Controlled Release, 2009. **138**(3): p. 268-276.
70. Liu, Y., et al., *Enhancement of therapeutic effectiveness by combining liposomal honokiol with cisplatin in ovarian carcinoma.* International Journal of Gynecological Cancer, 2008. **18**(4): p. 652-659.
71. Zhao, H., et al., *RGD-based strategies for improving antitumor activity of paclitaxel-loaded liposomes in nude mice xenografted with human ovarian cancer.* Journal of drug targeting, 2009. **17**(1): p. 10-18.
72. Pastorino, F., et al., *Enhanced antitumor efficacy of clinical-grade vasculature-targeted liposomal doxorubicin.* Clinical Cancer Research, 2008. **14**(22): p. 7320-7329.
73. Staffhorst, R.W., et al., *Antitumor activity and biodistribution of cisplatin nanocapsules in nude mice bearing human ovarian carcinoma xenografts.* Anti-cancer drugs, 2008. **19**(7): p. 721-727.
74. Dings, R.P., et al., *Inhibiting tumor growth by targeting tumor vasculature with galectin-1 antagonist anginex conjugated to the cytotoxic acylfulvene, 6-hydroxylpropylacylfulvene.* Bioconjugate chemistry, 2009. **21**(1): p. 20-27.
75. Dubikovskaya, E.A., et al., *Overcoming multidrug resistance of small-molecule therapeutics through conjugation with releasable octaarginine transporters.* Proceedings of the National Academy of Sciences, 2008. **105**(34): p. 12128-12133.

76. Somjen, D., et al., *A daidzein–daunomycin conjugate improves the therapeutic response in an animal model of ovarian carcinoma.* The Journal of steroid biochemistry and molecular biology, 2008. **110**(1): p. 144-149.
77. Li, C., et al., *Tumor irradiation enhances the tumor-specific distribution of poly (L-glutamic acid)-conjugated paclitaxel and its antitumor efficacy.* Clinical cancer research, 2000. **6**(7): p. 2829-2834.
78. Li, C., et al., *Potentiation of ovarian OCa-1 tumor radioresponse by poly (L-glutamic acid)-paclitaxel conjugate.* International Journal of Radiation Oncology* Biology* Physics, 2000. **48**(4): p. 1119-1126.
79. Li, C., et al., *Antitumor activity of poly (L-glutamic acid)-paclitaxel on syngeneic and xenografted tumors.* Clinical cancer research, 1999. **5**(4): p. 891-897.
80. Li, C., et al., *Complete regression of well-established tumors using a novel water-soluble poly (L-glutamic acid)-paclitaxel conjugate.* Cancer research, 1998. **58**(11): p. 2404-2409.
81. Milas, L., et al., *Poly (L-glutamic acid)-paclitaxel conjugate is a potent enhancer of tumor radiocurability.* International Journal of Radiation Oncology* Biology* Physics, 2003. **55**(3): p. 707-712.
82. Peterson, C.M., et al., *Combination chemotherapy and photodynamic therapy with N-(2-hydroxypropyl) methacrylamide copolymer-bound anticancer drugs inhibit human ovarian carcinoma heterotransplanted in nude mice.* Cancer research, 1996. **56**(17): p. 3980-3985.
83. Shiah, J.-G., et al., *Combination chemotherapy and photodynamic therapy of targetable N-(2-hydroxypropyl) methacrylamide copolymer–doxorubicin/mesochlorin e 6-OV-TL 16 antibody immunoconjugates.* Journal of controlled release, 2001. **74**(1): p. 249-253.
84. Tang, H., et al., *Curcumin polymers as anticancer conjugates.* Biomaterials, 2010. **31**(27): p. 7139-7149.
85. Zhu, S., et al., *PEGylated PAMAM dendrimer-doxorubicin conjugates: in vitro evaluation and in vivo tumor accumulation.* Pharmaceutical research, 2010. **27**(1): p. 161-174.
86. Hara, T., et al., *Mathematical description of drug movement into tumor with EPR effect and estimation of its configuration for DDS.* Colloids and Surfaces B: Biointerfaces, 2010. **75**(1): p. 42-46.
87. Allen, T.M. and P.R. Cullis, *Drug delivery systems: entering the mainstream.* Science, 2004. **303**(5665): p. 1818-1822.
88. Maeda, H., *Macromolecular therapeutics in cancer treatment: the EPR effect and beyond.* Journal of Controlled Release, 2012. **164**(2): p. 138-144.
89. Bansal, T., et al., *Novel formulation approaches for optimising delivery of anticancer drugs based on P-glycoprotein modulation.* Drug discovery today, 2009. **14**(21): p. 1067-1074.

90. Elamanchili, P., C. McEachern, and H. Burt, *Reversal of multidrug resistance by methoxypolyethylene glycol‐block‐polycaprolactone diblock copolymers through the inhibition of P‐glycoprotein function.* Journal of pharmaceutical sciences, 2009. **98**(3): p. 945-958.
91. Kabanov, A.V., E.V. Batrakova, and V.Y. Alakhov, *Pluronic® block copolymers for overcoming drug resistance in cancer.* Advanced drug delivery reviews, 2002. **54**(5): p. 759-779.
92. Jabr-Milane, L.S., et al., *Multi-functional nanocarriers to overcome tumor drug resistance.* Cancer treatment reviews, 2008. **34**(7): p. 592-602.
93. Hlrano, K. and C. Anthony Hunt, *Lymphatic transport of liposome‐encapsulated agents: Effects of liposome size following intraperitoneal administration.* Journal of pharmaceutical sciences, 1985. **74**(9): p. 915-921.
94. Kohane, D.S., et al., *Biodegradable polymeric microspheres and nanospheres for drug delivery in the peritoneum.* Journal of Biomedical Materials Research Part A, 2006. **77**(2): p. 351-361.
95. Tsai, M., et al., *Effects of carrier on disposition and antitumor activity of intraperitoneal paclitaxel.* Pharmaceutical research, 2007. **24**(9): p. 1691-1701.
96. Kang, B.K., et al., *Controlled release of paclitaxel from microemulsion containing PLGA and evaluation of anti-tumor activity in vitro and in vivo.* International journal of pharmaceutics, 2004. **286**(1): p. 147-156.
97. Lu, Z., et al., *Tumor-penetrating microparticles for intraperitoneal therapy of ovarian cancer.* Journal of Pharmacology and Experimental Therapeutics, 2008. **327**(3): p. 673-682.
98. Lu, Y., et al., *Folate receptor-targeted immunotherapy of cancer: mechanism and therapeutic potential.* Adv Drug Deliv Rev, 2004. **56**(8): p. 1161-76.
99. Zwicke, G.L., G.A. Mansoori, and C.J. Jeffery, *Utilizing the folate receptor for active targeting of cancer nanotherapeutics.* Nano Rev, 2012. **3**.
100. Kalli, K.R., et al., *Folate receptor alpha as a tumor target in epithelial ovarian cancer.* Gynecol Oncol, 2008. **108**(3): p. 619-26.
101. Qu, D., et al., *Formation mechanism and optimization of highly luminescent N-doped graphene quantum dots.* Scientific Reports, 2014. **4**: p. 5294.
102. Wang, F. and X. Liu, *Recent advances in the chemistry of lanthanide-doped upconversion nanocrystals.* Chemical Society Reviews, 2009. **38**(4): p. 976-989.
103. Li, T.S., T. Yawata, and K. Honke, *Efficient siRNA delivery and tumor accumulation mediated by ionically cross-linked folic acid-poly(ethylene glycol)-chitosan oligosaccharide lactate nanoparticles: for the potential targeted ovarian cancer gene therapy.* Eur J Pharm Sci, 2014. **52**: p. 48-61.

104. Teo, P.Y., et al., *Ovarian cancer immunotherapy using PD-L1 siRNA targeted delivery from folic acid-functionalized polyethylenimine: strategies to enhance T cell killing.* Adv Healthc Mater, 2015. **4**(8): p. 1180-9.

105. Tong, L., et al., *Folic acid-coupled nano-paclitaxel liposome reverses drug resistance in SKOV3/TAX ovarian cancer cells.* Anticancer Drugs, 2014. **25**(3): p. 244-54.

106. Allen, M.J., V.C. Tung, and R.B. Kaner, *Honeycomb carbon: a review of graphene.* Chemical reviews, 2009. **110**(1): p. 132-145.

107. Choi, W., et al., *Synthesis of graphene and its applications: a review.* Critical Reviews in Solid State and Materials Sciences, 2010. **35**(1).

108. Jia, X., et al., *Graphene edges: a review of their fabrication and characterization.* Nanoscale, 2011. **3**(1): p. 86-95.

109. Geim, A.K., *Graphene: status and prospects.* science, 2009. **324**(5934): p. 1530-1534.

110. Sanchez, V.C., et al., *Biological interactions of graphene-family nanomaterials: an interdisciplinary review.* Chemical research in toxicology, 2011. **25**(1): p. 15-34.

111. Dreyer, D.R., et al., *The chemistry of graphene oxide.* Chemical Society Reviews, 2010. **39**(1): p. 228-240.

112. Zhu, Y., et al., *Graphene and graphene oxide: synthesis, properties, and applications.* Advanced materials, 2010. **22**(35): p. 3906-3924.

113. Marcano, D.C., et al., *Improved synthesis of graphene oxide.* ACS nano, 2010. **4**(8): p. 4806-4814.

114. Wang, Y., et al., *Graphene and graphene oxide: biofunctionalization and applications in biotechnology.* Trends in biotechnology, 2011. **29**(5): p. 205-212.

115. Yan, X., X. Cui, and L.-s. Li, *Synthesis of large, stable colloidal graphene quantum dots with tunable size.* Journal of the American Chemical Society, 2010. **132**(17): p. 5944-5945.

116. Zhang, Z., K. Chang, and F. Peeters, *Tuning of energy levels and optical properties of graphene quantum dots.* Physical Review B, 2008. **77**(23): p. 235411.

117. Chen, M.L., et al., *Conjugation of quantum dots with graphene for fluorescence imaging of live cells.* Analyst, 2011. **136**(20): p. 4277-83.

118. Kim, S., et al., *Anomalous behaviors of visible luminescence from graphene quantum dots: interplay between size and shape.* ACS nano, 2012. **6**(9): p. 8203-8208.

119. Shen, J., et al., *Graphene quantum dots: emergent nanolights for bioimaging, sensors, catalysis and photovoltaic devices.* Chemical Communications, 2012. **48**(31): p. 3686-3699.

120. Shen, H., et al., *Biomedical applications of graphene.* Theranostics, 2012. **2**(3): p. 283.

121. Zhu, S., et al., *Strongly green-photoluminescent graphene quantum dots for bioimaging applications.* Chem. Commun., 2011. **47**(24): p. 6858-6860.

122. Zhang, L., et al., *Functional graphene oxide as a nanocarrier for controlled loading and targeted delivery of mixed anticancer drugs.* Small, 2010. **6**(4): p. 537-544.

123. Sun, X., et al., *Nano-graphene oxide for cellular imaging and drug delivery.* Nano research, 2008. **1**(3): p. 203-212.
124. Bao, H., et al., *Chitosan‐Functionalized Graphene Oxide as a Nanocarrier for Drug and Gene Delivery.* Small, 2011. **7**(11): p. 1569-1578.
125. Novoselov, K.S., et al., *A roadmap for graphene.* Nature, 2012. **490**(7419): p. 192-200.
126. Liu, J., L. Cui, and D. Losic, *Graphene and graphene oxide as new nanocarriers for drug delivery applications.* Acta biomaterialia, 2013. **9**(12): p. 9243-9257.
127. Gulbakan, B., et al., *A dual platform for selective analyte enrichment and ionization in mass spectrometry using aptamer-conjugated graphene oxide.* Journal of the American Chemical Society, 2010. **132**(49): p. 17408-17410.
128. Kim, H., et al., *Graphene oxide–polyethylenimine nanoconstruct as a gene delivery vector and bioimaging tool.* Bioconjugate chemistry, 2011. **22**(12): p. 2558-2567.
129. Björk, J., et al., *Adsorption of aromatic and anti-aromatic systems on graphene through* $\pi-\pi$ *stacking.* The Journal of Physical Chemistry Letters, 2010. **1**(23): p. 3407-3412.
130. Becerril, H.A., et al., *Evaluation of solution-processed reduced graphene oxide films as transparent conductors.* ACS nano, 2008. **2**(3): p. 463-470.
131. Zhang, M., et al., *Facile synthesis of water-soluble, highly fluorescent graphene quantum dots as a robust biological label for stem cells.* Journal of materials chemistry, 2012. **22**(15): p. 7461-7467.
132. Yang, H.-W., et al., *Gadolinium-functionalized nanographene oxide as a nanocarrier for combined drug and microRNA delivery and magnetic resonance imaging.* 2014.
133. Luo, S., et al., *A review of NIR dyes in cancer targeting and imaging.* Biomaterials, 2011. **32**(29): p. 7127-7138.
134. Li, J. and S.Q. Yao, *"Singapore Green": a new fluorescent dye for microarray and bioimaging applications.* Organic letters, 2008. **11**(2): p. 405-408.
135. Terai, T. and T. Nagano, *Fluorescent probes for bioimaging applications.* Current opinion in chemical biology, 2008. **12**(5): p. 515-521.
136. Alivisatos, A.P., W. Gu, and C. Larabell, *Quantum dots as cellular probes.* Annu. Rev. Biomed. Eng., 2005. **7**: p. 55-76.
137. Cao, L., et al., *Carbon dots for multiphoton bioimaging.* Journal of the American Chemical Society, 2007. **129**(37): p. 11318-11319.
138. Zrazhevskiy, P., M. Sena, and X. Gao, *Designing multifunctional quantum dots for bioimaging, detection, and drug delivery.* Chemical Society Reviews, 2010. **39**(11): p. 4326-4354.
139. Zhang, Y., et al., *Engineering lanthanide-based materials for nanomedicine.* Journal of Photochemistry and Photobiology C: Photochemistry Reviews, 2014. **20**: p. 71-96.
140. Wei, W., et al., *Cross relaxation induced pure red upconversion in activator-and sensitizer-rich lanthanide nanoparticles.* Chemistry of Materials, 2014. **26**(18): p. 5183-5186.

141. Zhou, J., Z. Liu, and F. Li, *Upconversion nanophosphors for small-animal imaging.* Chemical Society Reviews, 2012. **41**(3): p. 1323-1349.
142. Kim, J., et al., *Visualizing graphene based sheets by fluorescence quenching microscopy.* Journal of the American Chemical Society, 2009. **132**(1): p. 260-267.
143. Loh, K.P., et al., *Graphene oxide as a chemically tunable platform for optical applications.* Nature chemistry, 2010. **2**(12): p. 1015-1024.
144. Wei, G., et al., *Covalent modification of reduced graphene oxide by means of diazonium chemistry and use as a drug-delivery system.* Chemistry, 2012. **18**(46): p. 14708-16.
145. Liu, Y., C.-y. Liu, and Y. Liu, *Investigation on fluorescence quenching of dyes by graphite oxide and graphene.* Applied Surface Science, 2011. **257**(13): p. 5513-5518.
146. Some, S., et al., *Cancer therapy using ultrahigh hydrophobic drug-loaded graphene derivatives.* Scientific reports, 2014. **4**.
147. Zheng, X.T., et al., *Glowing graphene quantum dots and carbon dots: properties, syntheses, and biological applications.* Small, 2015. **11**(14): p. 1620-1636.
148. Liu, F., et al., *Facile Synthetic Method for Pristine Graphene Quantum Dots and Graphene Oxide Quantum Dots: Origin of Blue and Green Luminescence.* Advanced Materials, 2013. **25**(27): p. 3657-3662.
149. Luo, P., et al., *Aryl-modified graphene quantum dots with enhanced photoluminescence and improved pH tolerance.* Nanoscale, 2013. **5**(16): p. 7361-7367.
150. Xue, Q., et al., *Nearly monodisperse graphene quantum dots fabricated by amine-assisted cutting and ultrafiltration.* Nanoscale, 2013. **5**(24): p. 12098-12103.
151. Baker, S.N. and G.A. Baker, *Luminescent carbon nanodots: emergent nanolights.* Angewandte Chemie International Edition, 2010. **49**(38): p. 6726-6744.
152. Li, L., et al., *Focusing on luminescent graphene quantum dots: current status and future perspectives.* Nanoscale, 2013. **5**(10): p. 4015-4039.
153. Eda, G., et al., *Blue photoluminescence from chemically derived graphene oxide.* Advanced Materials, 2010. **22**(4): p. 505.
154. AlamáSk, M. and K. HwaáLim, *Revealing the tunable photoluminescence properties of graphene quantum dots.* Journal of Materials Chemistry C, 2014. **2**(34): p. 6954-6960.
155. Liu, R., et al., *Bottom-up fabrication of photoluminescent graphene quantum dots with uniform morphology.* Journal of the American Chemical Society, 2011. **133**(39): p. 15221-15223.
156. Teng, X., et al., *Lanthanide-Doped Na x ScF3+ x Nanocrystals: Crystal Structure Evolution and Multicolor Tuning.* Journal of the American Chemical Society, 2012. **134**(20): p. 8340-8343.
157. Chen, G., et al., *(α-NaYbF4: Tm3+)/CaF2 core/shell nanoparticles with efficient near-infrared to near-infrared upconversion for high-contrast deep tissue bioimaging.* ACS nano, 2012. **6**(9): p. 8280-8287.

158. Shen, J., et al., *Facile preparation and upconversion luminescence of graphene quantum dots.* Chem. Commun., 2011. **47**(9): p. 2580-2582.
159. Bacon, M., S.J. Bradley, and T. Nann, *Graphene quantum dots.* Particle & Particle Systems Characterization, 2014. **31**(4): p. 415-428.
160. Sk, M.A., et al., *Revealing the tunable photoluminescence properties of graphene quantum dots.* Journal of Materials Chemistry C, 2014. **2**(34): p. 6954-6960.
161. Shen, J.H., et al., *Facile preparation and upconversion luminescence of graphene quantum dots.* Chemical Communications, 2011. **47**(9): p. 2580-2582.
162. Dong, Y., et al., *Blue luminescent graphene quantum dots and graphene oxide prepared by tuning the carbonization degree of citric acid.* Carbon, 2012. **50**(12): p. 4738-4743.
163. Li, L.L., et al., *A Facile Microwave Avenue to Electrochemiluminescent Two‐Color Graphene Quantum Dots.* Advanced Functional Materials, 2012. **22**(14): p. 2971-2979.
164. Pan, D., et al., *Cutting sp 2 clusters in graphene sheets into colloidal graphene quantum dots with strong green fluorescence.* Journal of Materials Chemistry, 2012. **22**(8): p. 3314-3318.
165. Zhu, S., et al., *Surface Chemistry Routes to Modulate the Photoluminescence of Graphene Quantum Dots: From Fluorescence Mechanism to Up‐Conversion Bioimaging Applications.* Advanced Functional Materials, 2012. **22**(22): p. 4732-4740.
166. Wang, X., et al., *Multifunctional graphene quantum dots for simultaneous targeted cellular imaging and drug delivery.* Colloids and Surfaces B: Biointerfaces, 2014. **122**: p. 638-644.
167. Donoso, R., C. Cárdenas, and P. Fuentealba, *Article Previous Article Next Article Table of Contents Ab Initio Molecular Dynamics Study of Small Alkali Metal Clusters.* 2014.
168. Peng, J., et al., *Graphene quantum dots derived from carbon fibers.* Nano letters, 2012. **12**(2): p. 844-849.
169. Xu, M., et al., *Hydrothermal/solvothermal synthesis of graphene quantum dots and their biological applications.* Nano Biomed Eng, 2013. **5**: p. 65-71.
170. Sun, H., et al., *Graphene quantum dots-band-aids used for wound disinfection.* ACS nano, 2014. **8**(6): p. 6202-6210.
171. Ristic, B.Z., et al., *Photodynamic antibacterial effect of graphene quantum dots.* Biomaterials, 2014. **35**(15): p. 4428-4435.
172. Hu, T., et al., *Enzyme catalytic amplification of miRNA-155 detection with graphene quantum dot-based electrochemical biosensor.* Biosens Bioelectron, 2016. **77**: p. 451-6.
173. Hui, L., et al., *Antibacterial Property of Graphene Quantum Dots (Both Source Material and Bacterial Shape Matter).* ACS Appl Mater Interfaces, 2016. **8**(1): p. 20-5.
174. Ristic, B.Z., et al., *Photodynamic antibacterial effect of graphene quantum dots.* Biomaterials, 2014. **35**(15): p. 4428-35.
175. Qiu, J., et al., *Fluorescent graphene quantum dots as traceable, pH-sensitive drug delivery systems.* Int J Nanomedicine, 2015. **10**: p. 6709-24.

176. Wang, X., et al., *Multifunctional graphene quantum dots for simultaneous targeted cellular imaging and drug delivery.* Colloids Surf B Biointerfaces, 2014. **122**: p. 638-44.
177. Peng, J., et al., *Graphene quantum dots derived from carbon fibers.* Nano Lett, 2012. **12**(2): p. 844-9.
178. Ye, R., et al., *Coal as an abundant source of graphene quantum dots.* Nat Commun, 2013. **4**: p. 2943.
179. Zhou, Y., et al., *A novel composite of graphene quantum dots and molecularly imprinted polymer for fluorescent detection of paranitrophenol.* Biosens Bioelectron, 2014. **52**: p. 317-23.
180. Hilgenbrink, A.R. and P.S. Low, *Folate receptor-mediated drug targeting: from therapeutics to diagnostics.* J Pharm Sci, 2005. **94**(10): p. 2135-46.
181. Vergote, I.B., C. Marth, and R.L. Coleman, *Role of the folate receptor in ovarian cancer treatment: evidence, mechanism, and clinical implications.* Cancer Metastasis Rev, 2015. **34**(1): p. 41-52.
182. Walters, C.L., et al., *Folate and folate receptor alpha antagonists mechanism of action in ovarian cancer.* Gynecol Oncol, 2013. **131**(2): p. 493-8.
183. Basal, E., et al., *Functional folate receptor alpha is elevated in the blood of ovarian cancer patients.* PLoS One, 2009. **4**(7): p. e6292.
184. Kelemen, L.E., et al., *Multivitamin and alcohol intake and folate receptor alpha expression in ovarian cancer.* Cancer Epidemiol Biomarkers Prev, 2005. **14**(9): p. 2168-72.
185. Ward, C.M., *Folate-targeted non-viral DNA vectors for cancer gene therapy.* Curr Opin Mol Ther, 2000. **2**(2): p. 182-7.
186. Boca-Farcau, S., et al., *Folic acid-conjugated, SERS-labeled silver nanotriangles for multimodal detection and targeted photothermal treatment on human ovarian cancer cells.* Mol Pharm, 2014. **11**(2): p. 391-9.
187. Ferrero, J.M., et al., *Second-line chemotherapy with pegylated liposomal doxorubicin and carboplatin is highly effective in patients with advanced ovarian cancer in late relapse: a GINECO phase II trial.* Ann Oncol, 2007. **18**(2): p. 263-8.
188. A'Hern, R.P. and M.E. Gore, *Impact of doxorubicin on survival in advanced ovarian cancer.* J Clin Oncol, 1995. **13**(3): p. 726-32.
189. Doroshow, J.H., *Doxorubicin-induced cardiac toxicity.* N Engl J Med, 1991. **324**(12): p. 843-5.
190. Lenzhofer, R. and D. Magometschnigg, *[Doxorubicin-induced cardiomyopathy: hemodynamic studies for evaluating the limit of therapeutic risk].* Z Kardiol, 1983. **72**(5): p. 297-303.
191. Lenzhofer, R., *[Selective toxicity of cytostatic agents: studies on the cardiotoxicity of doxorubicin, its pathogenesis and contraindications].* Wien Klin Wochenschr Suppl, 1983. **144**: p. 3-31.

192. Octavia, Y., et al., *Doxorubicin-induced cardiomyopathy: from molecular mechanisms to therapeutic strategies.* J Mol Cell Cardiol, 2012. **52**(6): p. 1213-25.
193. Takemura, G. and H. Fujiwara, *Doxorubicin-induced cardiomyopathy from the cardiotoxic mechanisms to management.* Prog Cardiovasc Dis, 2007. **49**(5): p. 330-52.
194. Jeyaseelan, R., et al., *Molecular mechanisms of doxorubicin-induced cardiomyopathy. Selective suppression of Reiske iron-sulfur protein, ADP/ATP translocase, and phosphofructokinase genes is associated with ATP depletion in rat cardiomyocytes.* J Biol Chem, 1997. **272**(9): p. 5828-32.
195. Wu, C., et al., *Insight into the cellular internalization and cytotoxicity of graphene quantum dots.* Adv Healthc Mater, 2013. **2**(12): p. 1613-9.
196. Nurunnabi, M., et al., *In vivo biodistribution and toxicology of carboxylated graphene quantum dots.* ACS Nano, 2013. **7**(8): p. 6858-67.
197. Qin, Y., et al., *Graphene quantum dots induce apoptosis, autophagy, and inflammatory response via p38 mitogen-activated protein kinase and nuclear factor-kappaB mediated signaling pathways in activated THP-1 macrophages.* Toxicology, 2015. **327**: p. 62-76.
198. Dong, H., et al., *Multifunctional Poly(L-lactide)-Polyethylene Glycol-Grafted Graphene Quantum Dots for Intracellular MicroRNA Imaging and Combined Specific-Gene-Targeting Agents Delivery for Improved Therapeutics.* ACS Appl Mater Interfaces, 2015. **7**(20): p. 11015-23.
199. Abdullah Al, N., et al., *Target delivery and cell imaging using hyaluronic acid-functionalized graphene quantum dots.* Mol Pharm, 2013. **10**(10): p. 3736-44.
200. Qu, G., et al., *Cytotoxicity of quantum dots and graphene oxide to erythroid cells and macrophages.* Nanoscale Res Lett, 2013. **8**(1): p. 198.
201. Chong, Y., et al., *The in vitro and in vivo toxicity of graphene quantum dots.* Biomaterials, 2014. **35**(19): p. 5041-8.
202. Tang, L., et al., *Deep ultraviolet to near-infrared emission and photoresponse in layered N-doped graphene quantum dots.* ACS Nano, 2014. **8**(6): p. 6312-20.
203. Huan, J., et al., *Amplified solid-state electrochemiluminescence detection of cholesterol in near-infrared range based on CdTe quantum dots decorated multiwalled carbon nanotubes@reduced graphene oxide nanoribbons.* Biosens Bioelectron, 2015. **73**: p. 221-7.
204. Zhao, B., et al., *Sestrin2 protein positively regulates AKT enzyme signaling and survival in human squamous cell carcinoma and melanoma cells.* J Biol Chem, 2014. **289**(52): p. 35806-14.
205. Weitman, S.D., et al., *Cellular localization of the folate receptor: potential role in drug toxicity and folate homeostasis.* Cancer Res, 1992. **52**(23): p. 6708-11.
206. Boshnjaku, V., et al., *Nuclear localization of folate receptor alpha: a new role as a transcription factor.* Sci Rep, 2012. **2**: p. 980.

207. Derfus, A.M., W.C.W. Chan, and S.N. Bhatia, *Probing the cytotoxicity of semiconductor quantum dots.* Nano Letters, 2004. **4**(1): p. 11-18.
208. Yuan, X., et al., *Cellular distribution and cytotoxicity of graphene quantum dots with different functional groups.* Nanoscale Res Lett, 2014. **9**(1): p. 108.
209. Wang, Z.G., et al., *Toxicity of Graphene Quantum Dots in Zebrafish Embryo.* Biomed Environ Sci, 2015. **28**(5): p. 341-51.
210. Corsini, E., et al., *In vitro evaluation of the immunotoxic potential of perfluorinated compounds (PFCs).* Toxicol Appl Pharmacol, 2011. **250**(2): p. 108-16.
211. Gao, N., et al., *Steering carbon nanotubes to scavenger receptor recognition by nanotube surface chemistry modification partially alleviates NFkappaB activation and reduces its immunotoxicity.* ACS Nano, 2011. **5**(6): p. 4581-91.
212. Fu, P.P., et al., *Mechanisms of nanotoxicity: generation of reactive oxygen species.* J Food Drug Anal, 2014. **22**(1): p. 64-75.
213. Setyawati, M.I., et al., *The influence of lysosomal stability of silver nanomaterials on their toxicity to human cells.* Biomaterials, 2014. **35**(25): p. 6707-15.
214. Sharma, G., et al., *Iron oxide nanoparticle agglomeration influences dose rates and modulates oxidative stress-mediated dose-response profiles in vitro.* Nanotoxicology, 2014. **8**(6): p. 663-75.
215. Li, H., S. Horke, and U. Forstermann, *Oxidative stress in vascular disease and its pharmacological prevention.* Trends Pharmacol Sci, 2013. **34**(6): p. 313-9.
216. Arthur, J.S. and S.C. Ley, *Mitogen-activated protein kinases in innate immunity.* Nat Rev Immunol, 2013. **13**(9): p. 679-92.
217. Steinkamp, J.A., et al., *Phagocytosis: flow cytometric quantitation with fluorescent microspheres.* Science, 1982. **215**(4528): p. 64-6.
218. Shang, W., et al., *The uptake mechanism and biocompatibility of graphene quantum dots with human neural stem cells.* Nanoscale, 2014. **6**(11): p. 5799-806.
219. Nathan, C. and A. Cunningham-Bussel, *Beyond oxidative stress: an immunologist's guide to reactive oxygen species.* Nat Rev Immunol, 2013. **13**(5): p. 349-61.
220. Wagner, C., et al., *Comparative study of quercetin and its two glycoside derivatives quercitrin and rutin against methylmercury (MeHg)-induced ROS production in rat brain slices.* Arch Toxicol, 2010. **84**(2): p. 89-97.
221. Moghimi, S.M., A.C. Hunter, and J.C. Murray, *Nanomedicine: current status and future prospects.* FASEB J, 2005. **19**(3): p. 311-30.
222. Mao, H.Y., et al., *Graphene: promises, facts, opportunities, and challenges in nanomedicine.* Chem Rev, 2013. **113**(5): p. 3407-24.
223. Jiang, F., et al., *Eco-friendly synthesis of size-controllable amine-functionalized graphene quantum dots with antimycoplasma properties.* Nanoscale, 2013. **5**(3): p. 1137-42.
224. Wang, Z., et al., *Synthesis of strongly green-photoluminescent graphene quantum dots for drug carrier.* Colloids Surf B Biointerfaces, 2013. **112**: p. 192-6.

225. Zhan, L., et al., *Facile one-pot synthesis of folic acid-modified graphene to improve the performance of graphene-based sensing strategy.* J Colloid Interface Sci, 2014. **426**: p. 293-9.
226. Huang, P., et al., *Folic Acid-conjugated Graphene Oxide loaded with Photosensitizers for Targeting Photodynamic Therapy.* Theranostics, 2011. **1**: p. 240-50.
227. Doose, S., H. Neuweiler, and M. Sauer, *Fluorescence quenching by photoinduced electron transfer: a reporter for conformational dynamics of macromolecules.* Chemphyschem, 2009. **10**(9-10): p. 1389-98.
228. Dobretsov, G.E., T.I. Syrejschikova, and N.V. Smolina, *[On mechanisms of fluorescence quenching by water].* Biofizika, 2014. **59**(2): p. 231-7.
229. Mousa, S.A., et al., *Fluorescence quenching of protonated beta-carbolines in water and microemulsions: evidence for heavy-atom and electron-transfer mechanisms.* Photochem Photobiol Sci, 2013. **12**(9): p. 1606-14.
230. Mohan, P. and N. Rapoport, *Doxorubicin as a molecular nanotheranostic agent: effect of doxorubicin encapsulation in micelles or nanoemulsions on the ultrasound-mediated intracellular delivery and nuclear trafficking.* Mol Pharm, 2010. **7**(6): p. 1959-73.
231. Lenzhofer, R., et al., *[Pharmacokinetics and acute signs of cardiac toxicity during doxorubicin therapy].* Wien Klin Wochenschr, 1983. **95**(2): p. 52-5.
232. Lotem, M., et al., *Skin toxic effects of polyethylene glycol-coated liposomal doxorubicin.* Arch Dermatol, 2000. **136**(12): p. 1475-80.
233. Lyass, O., et al., *Correlation of toxicity with pharmacokinetics of pegylated liposomal doxorubicin (Doxil) in metastatic breast carcinoma.* Cancer, 2000. **89**(5): p. 1037-47.
234. Szebeni, J., et al., *Liposome-induced complement activation and related cardiopulmonary distress in pigs: factors promoting reactogenicity of Doxil and AmBisome.* Nanomedicine, 2012. **8**(2): p. 176-84.
235. Pelicano, H., D. Carney, and P. Huang, *ROS stress in cancer cells and therapeutic implications.* Drug Resist Updat, 2004. **7**(2): p. 97-110.
236. Simon, H.U., A. Haj-Yehia, and F. Levi-Schaffer, *Role of reactive oxygen species (ROS) in apoptosis induction.* Apoptosis, 2000. **5**(5): p. 415-8.
237. Maiuri, M.C., et al., *Self-eating and self-killing: crosstalk between autophagy and apoptosis.* Nat Rev Mol Cell Biol, 2007. **8**(9): p. 741-52.
238. Estaquier, J., et al., *The mitochondrial pathways of apoptosis.* Adv Exp Med Biol, 2012. **942**: p. 157-83.
239. Taylor, R.C., S.P. Cullen, and S.J. Martin, *Apoptosis: controlled demolition at the cellular level.* Nat Rev Mol Cell Biol, 2008. **9**(3): p. 231-41.
240. Mizushima, N. and B. Levine, *Autophagy in mammalian development and differentiation.* Nat Cell Biol, 2010. **12**(9): p. 823-30.

241. Green, D.R., L. Galluzzi, and G. Kroemer, *Mitochondria and the autophagy-inflammation-cell death axis in organismal aging.* Science, 2011. **333**(6046): p. 1109-12.

242. Mantawy, E.M., et al., *Insights antifibrotic mechanism of methyl palmitate: impact on nuclear factor kappa B and proinflammatory cytokines.* Toxicol Appl Pharmacol, 2012. **258**(1): p. 134-44.

243. Cao, Q., et al., *Nuclear factor-kappa beta regulates Notch signaling in production of proinflammatory cytokines and nitric oxide in murine BV-2 microglial cells.* Neuroscience, 2011. **192**: p. 140-54.

244. Antonelli, A., et al., *Cytokines (interferon-gamma and tumor necrosis factor-alpha)-induced nuclear factor-kappaB activation and chemokine (C-X-C motif) ligand 10 release in Graves disease and ophthalmopathy are modulated by pioglitazone.* Metabolism, 2011. **60**(2): p. 277-83.

245. Davies, C.M., et al., *Reactive nitrogen and oxygen species in interleukin-1-mediated DNA damage associated with osteoarthritis.* Osteoarthritis Cartilage, 2008. **16**(5): p. 624-30.

APPENDIX:

PERMISSION TO REPRINT

ELSEVIER LICENSE
TERMS AND CONDITIONS
Jun 14, 2016

This Agreement between yiru qin ("You") and Elsevier ("Elsevier") consists of your license details and the terms and conditions provided by Elsevier and Copyright Clearance Center.

License Number
3836720805072
License date
Mar 26, 2016
Licensed Content Publisher
Elsevier
Licensed Content Publication
Toxicology
Licensed Content Title
Graphene quantum dots induce apoptosis, autophagy, and inflammatory response via p38 mitogen-activated protein kinase and nuclear factor-κB mediated signaling pathways in activated THP-1 macrophages
Licensed Content Author
Yiru Qin,Zhi-Wei Zhou,Shu-Ting Pan,Zhi-Xu He,Xueji Zhang,Jia-Xuan Qiu,Wei Duan,Tianxin Yang,Shu-Feng Zhou
Licensed Content Date
2 January 2015
Licensed Content Volume Number
327
Licensed Content Issue Number
n/a
Start Page
62

End Page
76
Type of Use
reuse in a thesis/dissertation
Intended publisher of new work
other
Portion
full article
Format
electronic
Are you the author of this Elsevier article?
Yes
Will you be translating?
No
Order reference number
Title of your thesis/dissertation
Graphene Quantum Dots-Based Drug Delivery for Ovarian Cancer Therapy
Expected completion date
Jun 2016
Estimated size (number of pages)
100
Elsevier VAT number
GB 494 6272 12
Requestor Location
yiru qin
12901 Bruce B. Downs Blvd

TAMPA, FL 33613
United States
Attn: yiru qin
Billing Type
Invoice
Billing Address
yiru qin
12901 Bruce B. Downs Blvd

TAMPA, FL 33613

United States
Attn: yiru qin
Total
0.00 USD
Total
0.00 USD
Terms and Conditions
INTRODUCTION

1. The publisher for this copyrighted material is Elsevier. By clicking "accept" in connection with completing this licensing transaction, you agree that the following terms and conditions apply to this transaction (along with the Billing and Payment terms and conditions established by Copyright Clearance Center, Inc. ("CCC"), at the time that you opened your Rightslink account and that are available at any time at http://myaccount.copyright.com).

GENERAL TERMS

2. Elsevier hereby grants you permission to reproduce the aforementioned material subject to the terms and conditions indicated.

3. Acknowledgement: If any part of the material to be used (for example, figures) has appeared in our publication with credit or acknowledgement to another source, permission must also be sought from that source. If such permission is not obtained then that material may not be included in your publication/copies. Suitable acknowledgement to the source must be made, either as a footnote or in a reference list at the end of your publication, as follows:

"Reprinted from Publication title, Vol /edition number, Author(s), Title of article / title of chapter, Pages No., Copyright (Year), with permission from Elsevier [OR APPLICABLE SOCIETY COPYRIGHT OWNER]." Also Lancet special credit - "Reprinted from The Lancet, Vol. number, Author(s), Title of article, Pages No., Copyright (Year), with permission from Elsevier."

4. Reproduction of this material is confined to the purpose and/or media for which permission is hereby given.

5. Altering/Modifying Material: Not Permitted. However figures and illustrations may be altered/adapted minimally to serve your work. Any other abbreviations, additions, deletions and/or any other alterations shall be made only with prior written authorization of Elsevier Ltd. (Please contact Elsevier at permissions@elsevier.com)

6. If the permission fee for the requested use of our material is waived in this instance, please be advised that your future requests for Elsevier materials may attract a fee.

7. Reservation of Rights: Publisher reserves all rights not specifically granted in the combination of (i) the license details provided by you and accepted in the course of this licensing transaction, (ii) these terms and conditions and (iii) CCC's Billing and Payment terms and conditions.

8. License Contingent Upon Payment: While you may exercise the rights licensed immediately upon issuance of the license at the end of the licensing process for the transaction, provided that you have disclosed complete and accurate details of your proposed use, no license is finally

effective unless and until full payment is received from you (either by publisher or by CCC) as provided in CCC's Billing and Payment terms and conditions. If full payment is not received on a timely basis, then any license preliminarily granted shall be deemed automatically revoked and shall be void as if never granted. Further, in the event that you breach any of these terms and conditions or any of CCC's Billing and Payment terms and conditions, the license is automatically revoked and shall be void as if never granted. Use of materials as described in a revoked license, as well as any use of the materials beyond the scope of an unrevoked license, may constitute copyright infringement and publisher reserves the right to take any and all action to protect its copyright in the materials.

9. Warranties: Publisher makes no representations or warranties with respect to the licensed material.

10. Indemnity: You hereby indemnify and agree to hold harmless publisher and CCC, and their respective officers, directors, employees and agents, from and against any and all claims arising out of your use of the licensed material other than as specifically authorized pursuant to this license.

11. No Transfer of License: This license is personal to you and may not be sublicensed, assigned, or transferred by you to any other person without publisher's written permission.

12. No Amendment Except in Writing: This license may not be amended except in a writing signed by both parties (or, in the case of publisher, by CCC on publisher's behalf).

13. Objection to Contrary Terms: Publisher hereby objects to any terms contained in any purchase order, acknowledgment, check endorsement or other writing prepared by you, which terms are inconsistent with these terms and conditions or CCC's Billing and Payment terms and conditions. These terms and conditions, together with CCC's Billing and Payment terms and conditions (which are incorporated herein), comprise the entire agreement between you and publisher (and CCC) concerning this licensing transaction. In the event of any conflict between your obligations established by these terms and conditions and those established by CCC's Billing and Payment terms and conditions, these terms and conditions shall control.

14. Revocation: Elsevier or Copyright Clearance Center may deny the permissions described in this License at their sole discretion, for any reason or no reason, with a full refund payable to you. Notice of such denial will be made using the contact information provided by you. Failure to receive such notice will not alter or invalidate the denial. In no event will Elsevier or Copyright Clearance Center be responsible or liable for any costs, expenses or damage incurred by you as a result of a denial of your permission request, other than a refund of the amount(s) paid by you to Elsevier and/or Copyright Clearance Center for denied permissions.

LIMITED LICENSE

The following terms and conditions apply only to specific license types:

15. Translation: This permission is granted for non-exclusive world English rights only unless your license was granted for translation rights. If you licensed translation rights you may only translate this content into the languages you requested. A professional translator must perform all

translations and reproduce the content word for word preserving the integrity of the article.

16. Posting licensed content on any Website: The following terms and conditions apply as follows: Licensing material from an Elsevier journal: All content posted to the web site must maintain the copyright information line on the bottom of each image; A hyper-text must be included to the Homepage of the journal from which you are licensing at http://www.sciencedirect.com/science/journal/xxxxx or the Elsevier homepage for books at http://www.elsevier.com; Central Storage: This license does not include permission for a scanned version of the material to be stored in a central repository such as that provided by Heron/XanEdu.

Licensing material from an Elsevier book: A hyper-text link must be included to the Elsevier homepage at http://www.elsevier.com . All content posted to the web site must maintain the copyright information line on the bottom of each image.

Posting licensed content on Electronic reserve: In addition to the above the following clauses are applicable: The web site must be password-protected and made available only to bona fide students registered on a relevant course. This permission is granted for 1 year only. You may obtain a new license for future website posting.

17. For journal authors: the following clauses are applicable in addition to the above:

Preprints:

A preprint is an author's own write-up of research results and analysis, it has not been peer-reviewed, nor has it had any other value added to it by a publisher (such as formatting, copyright, technical enhancement etc.).

Authors can share their preprints anywhere at any time. Preprints should not be added to or enhanced in any way in order to appear more like, or to substitute for, the final versions of articles however authors can update their preprints on arXiv or RePEc with their Accepted Author Manuscript (see below).

If accepted for publication, we encourage authors to link from the preprint to their formal publication via its DOI. Millions of researchers have access to the formal publications on ScienceDirect, and so links will help users to find, access, cite and use the best available version. Please note that Cell Press, The Lancet and some society-owned have different preprint policies. Information on these policies is available on the journal homepage.

Accepted Author Manuscripts: An accepted author manuscript is the manuscript of an article that has been accepted for publication and which typically includes author-incorporated changes suggested during submission, peer review and editor-author communications.

Authors can share their accepted author manuscript:

- immediately

via their non-commercial person homepage or blog

by updating a preprint in arXiv or RePEc with the accepted manuscript

via their research institute or institutional repository for internal institutional uses or as part of an

invitation-only research collaboration work-group
directly by providing copies to their students or to research collaborators for their personal use
for private scholarly sharing as part of an invitation-only work group on commercial sites with which Elsevier has an agreement

- after the embargo period

via non-commercial hosting platforms such as their institutional repository
via commercial sites with which Elsevier has an agreement
In all cases accepted manuscripts should:

- link to the formal publication via its DOI
- bear a CC-BY-NC-ND license - this is easy to do
- if aggregated with other manuscripts, for example in a repository or other site, be shared in alignment with our hosting policy not be added to or enhanced in any way to appear more like, or to substitute for, the published journal article.

Published journal article (JPA): A published journal article (PJA) is the definitive final record of published research that appears or will appear in the journal and embodies all value-adding publishing activities including peer review co-ordination, copy-editing, formatting, (if relevant) pagination and online enrichment.

Policies for sharing publishing journal articles differ for subscription and gold open access articles:

Subscription Articles: If you are an author, please share a link to your article rather than the full-text. Millions of researchers have access to the formal publications on ScienceDirect, and so links will help your users to find, access, cite, and use the best available version.

Theses and dissertations which contain embedded PJAs as part of the formal submission can be posted publicly by the awarding institution with DOI links back to the formal publications on ScienceDirect.

If you are affiliated with a library that subscribes to ScienceDirect you have additional private sharing rights for others' research accessed under that agreement. This includes use for classroom teaching and internal training at the institution (including use in course packs and courseware programs), and inclusion of the article for grant funding purposes.

Gold Open Access Articles: May be shared according to the author-selected end-user license and should contain a CrossMark logo, the end user license, and a DOI link to the formal publication on ScienceDirect.

Please refer to Elsevier's posting policy for further information.

18. For book authors the following clauses are applicable in addition to the above: Authors are permitted to place a brief summary of their work online only. You are not allowed to download and post the published electronic version of your chapter, nor may you scan the printed edition to create an electronic version. Posting to a repository: Authors are permitted to post a summary of their chapter only in their institution's repository.

19. Thesis/Dissertation: If your license is for use in a thesis/dissertation your thesis may be

submitted to your institution in either print or electronic form. Should your thesis be published commercially, please reapply for permission. These requirements include permission for the Library and Archives of Canada to supply single copies, on demand, of the complete thesis and include permission for Proquest/UMI to supply single copies, on demand, of the complete thesis. Should your thesis be published commercially, please reapply for permission. Theses and dissertations which contain embedded PJAs as part of the formal submission can be posted publicly by the awarding institution with DOI links back to the formal publications on ScienceDirect.

Elsevier Open Access Terms and Conditions

You can publish open access with Elsevier in hundreds of open access journals or in nearly 2000 established subscription journals that support open access publishing. Permitted third party re-use of these open access articles is defined by the author's choice of Creative Commons user license. See our open access license policy for more information.

Terms & Conditions applicable to all Open Access articles published with Elsevier:

Any reuse of the article must not represent the author as endorsing the adaptation of the article nor should the article be modified in such a way as to damage the author's honour or reputation. If any changes have been made, such changes must be clearly indicated.

The author(s) must be appropriately credited and we ask that you include the end user license and a DOI link to the formal publication on ScienceDirect.

If any part of the material to be used (for example, figures) has appeared in our publication with credit or acknowledgement to another source it is the responsibility of the user to ensure their reuse complies with the terms and conditions determined by the rights holder.

Additional Terms & Conditions applicable to each Creative Commons user license:

CC BY: The CC-BY license allows users to copy, to create extracts, abstracts and new works from the Article, to alter and revise the Article and to make commercial use of the Article (including reuse and/or resale of the Article by commercial entities), provided the user gives appropriate credit (with a link to the formal publication through the relevant DOI), provides a link to the license, indicates if changes were made and the licensor is not represented as endorsing the use made of the work. The full details of the license are available at http://creativecommons.org/licenses/by/4.0.

CC BY NC SA: The CC BY-NC-SA license allows users to copy, to create extracts, abstracts and new works from the Article, to alter and revise the Article, provided this is not done for commercial purposes, and that the user gives appropriate credit (with a link to the formal publication through the relevant DOI), provides a link to the license, indicates if changes were made and the licensor is not represented as endorsing the use made of the work. Further, any new works must be made available on the same conditions. The full details of the license are available at http://creativecommons.org/licenses/by-nc-sa/4.0.

CC BY NC ND: The CC BY-NC-ND license allows users to copy and distribute the Article, provided this is not done for commercial purposes and further does not permit distribution of the Article if it is changed or edited in any way, and provided the user gives appropriate credit (with a link to the formal publication through the relevant DOI), provides a link to the license, and that the licensor is not represented as endorsing the use made of the work. The full details of the license are available at http://creativecommons.org/licenses/by-nc-nd/4.0. Any commercial reuse of Open Access articles published with a CC BY NC SA or CC BY NC ND license requires permission from Elsevier and will be subject to a fee.

Commercial reuse includes:

- Associating advertising with the full text of the Article
- Charging fees for document delivery or access
- Article aggregation
- Systematic distribution via e-mail lists or share buttons

Posting or linking by commercial companies for use by customers of those companies.

20. Other Conditions:

v1.8

Questions? customercare@copyright.com or +1-855-239-3415 (toll free in the US) or +1-978-646-2777.

ABOUT THE AUTHOR

Yiru Qin was born in Hunan, China. In 2006, she began her undergraduate studies in Beijing University of Chemical Technology, where she obtained her B.S. degree in Pharmaceutical Engineering. She continued her graduate studies in biomedical sciences at the University of South Florida (USF), where she earned a M.S. degree in 2014 and continued in the PhD program at USF.